POLITECNICO DI MILANO

School of Industrial and Information Engineering

Master's degree in

Materials Engineering and Nanotechnology

Chemistry, Materials and Chemical Engineering Department "Giulio Natta"

# Assessment and characterization of nanovectors based on poly(2-oxazoline) for Photodynamic Therapy

Supervisor: Prof. Francesca BALDELLI BOMBELLI

Co-supervisor: Prof. Barbara LONETTI, Prof. Anne-Françoise MINGOTAUD

Alice Tosi – 904754

Academic year 2020-2021

# Table of contents

# List of Figures

# List of Tables

# Abstract

Photodynamic therapy (PDT) is a clinically approved technique which uses light-absorbing compounds, the photosensitizers (PSs), to yield reactive oxygen species (ROS) upon irradiation, resulting in cell death. Irradiation is a topical stimulus, and PDT provides localized treatment, a highly desirable features for the therapy of many illnesses in dermatology, ophthalmology and oncology. Some imitations, however, prevent this therapeutic modality to reach its full potential: once administered intra-venously several PSs currently employed tend to aggregate decreasing treatment efficiency, their uncontrolled biodistribution, which can lead to cutaneous photosensitivity, constitutes another issue. One solution for these drawbacks consists in the encapsulation of the PS in nanovectors. Especially polymeric nanovectors are increasingly studied in this regard, offering both the possibility of passive targeting, for example exploiting the Enhanced Permeability and Retention (EPR) effect, or active targeting by functionalization with targeting moieties.

In this scenario, this research work aims to expand the study on poly(2-oxazoline), a polymer which is being investigated as a possible alternative to poly(ethylene glycol) (PEG) for the formation of self-assemblies to be used as nanovectors for PDT. The ability to form polymeric nanocarriers (micelles, vesicles, etc.) of a range of poly(2-oxaolines) was assessed varying methods of formations and conditions; characterization of the nano-objects was performed with dynamic light scattering (DLS), transmission electron microscopy (TEM) and cryogenic TEM. A preliminary protein corona analysis was carried out to investigate the formation of a protein corona on the nanovectors and the stability of the nano-systems in presence of biological fluid.

# Sommario

La terapia fotodinamica (PDT) è una tecnica clinica che utilizza composti fotoassorbenti, i photosensitizer (PS), per produrre specie reattive dell'ossigeno quando irradiati, con conseguente morte cellulare. L'irradiazione è uno stimolo topico e la PDT fornisce un trattamento localizzato, caratteristica altamente desiderabile per la terapia di molte malattie in dermatologia, oftalmologia e oncologia. Alcune limitazioni, tuttavia, impediscono a questa modalità terapeutica di raggiungere il suo pieno potenziale: una volta somministrati per via endovenosa diversi PS attualmente impiegati tendono ad aggregare diminuendo l'efficienza del trattamento, la loro biodistribuzione incontrollata, che può portare a fotosensibilità cutanea, costituisce un altro problema. Una soluzione a questi inconvenienti consiste nell'incapsulamento del PS in nanovettori. Soprattutto i nanovettori polimerici sono sempre più studiati in quest'ottica, dato che offrono sia la possibilità di targeting passivo, ad esempio sfruttando l'effetto di aumento della permeabilità e della ritenzione (Enhanced Permeability and Retention, EPR), sia il targeting attivo mediante funzionalizzazione con unità di targeting.

In questo scenario, questo lavoro di ricerca si propone di ampliare lo studio sulla poli(2-ossazolina), un polimero studiato come possibile alternativa al poli(etilenglicole) (PEG) per la formazione di self-assembly da utilizzare come nanovettori per PDT. La capacità di formare nanovettori polimerici (micelle, vescicole, ecc.) di una gamma di poli(2-ossazoline) è stata valutata con diversi metodi di formazione delle self-assembly e in diverse condizioni; la caratterizzazione dei nano-oggetti è stata eseguita con diffusione dinamica della luce (DLS), microscopia elettronica a trasmissione (TEM) e TEM criogenico. È stata condotta un'analisi preliminare sulla corona proteica per indagare la formazione di questa sui nanovettori e la stabilità dei nano-sistemi in presenza di fluido biologico.

# 1. Introduction

## 1.1 Photodynamic therapy

Photodynamic therapy (PDT) is an established therapeutic modality for patients with non-melanoma skin cancers, actinic keratoses, several other dermatologic conditions, and age-related macular degeneration. It also holds clinical approval for the palliative and curative treatment of bladder, esophageal, lung, cervical, endobronchial and brain cancer [1-5]. Despite the broad field of application, PDT remains still underutilized and its clinical potential has yet to be fulfilled.

PDT is based on three essential components: a light-absorbing compound, the photosensitizer (PS), light, and oxygen [3]. The PS is applied topically for cutaneous conditions, while visceral tumours require intravenous or oral administration [1]; if the PS is delivered systemically, it is allowed to circulate for a suitable time interval, during which it selectively accumulates in the malignant tissue [Figure 1.1]. Once tumour loci are irradiated with light at appropriate wavelength (600-800 nm), excitation of the PS occurs producing a reaction with the oxygen present in the cells, this generates reactive oxygen species (ROS), which have a cytotoxic effect leading to cell death through different pathways. The mechanisms include apoptosis (programmed cell death), necrosis (unregulated cellular breakdown), and macroautophagy (degradation of cellular components by lysosomes) [3,6].

Another possible biological effect is the damage to tumour vasculature: many PSs induce vascular constriction and thrombus formation, which suppress the source of oxygen and nutrients to the neoplasm. Beside direct effects, PDT often causes a potent immune response, which has the capacity of significantly enhancing its antitumour impact [3,4,6].

The relative contribution of these mechanisms depends on many variables, including type and dose of PS, tumour oxygen concentration, the time between administration and light exposure, and total light dose and its fluence rate [3].

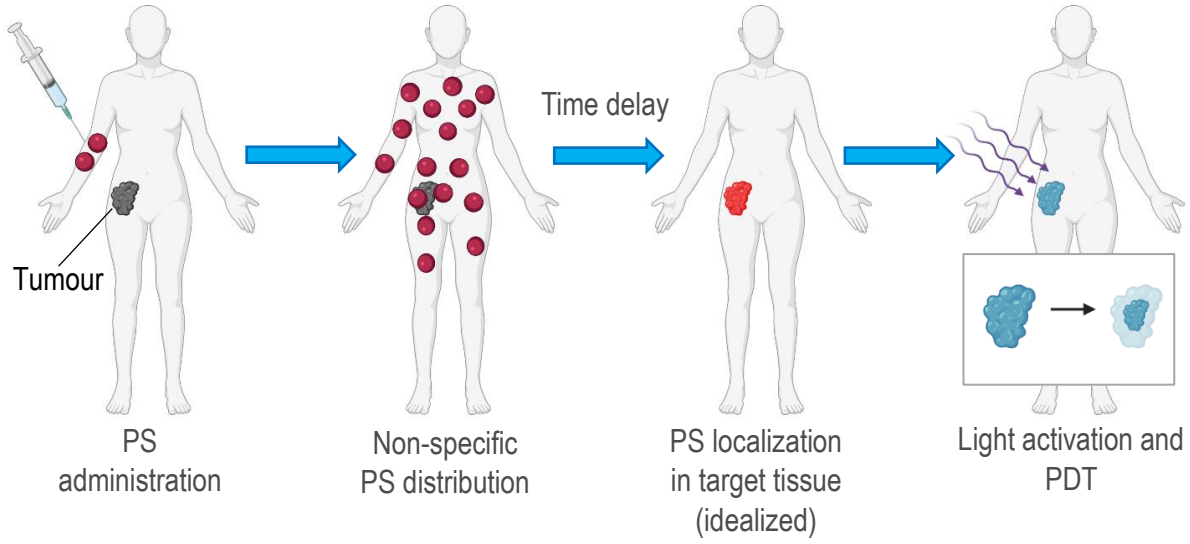


***Figure 1.1*** | *Schematic representation of the sequence of administration, localization, and light activation of the PS for PDT.*

PSs are classified in three categories according to their chronological order of development and conceptual approaches:

1° generation – It includes hematoporphyrin derivative (HpD), a complex natural mixture of porphyrins, and its purified form porfimer sodium (Photofrin®). Even though porfimer sodium is still widely employed, its clinical use is severely limited by intrinsic drawbacks such as poor chemical purity, relatively low absorption, and long half-life and intense accumulation in the skin, responsible for prolonged skin photosensitivity.

2° generation: They are synthetic compounds that present high absorption in the visible-near infrared region, high ROS yield, and a more predictable dose-response relation with respect to 1° generation formulas, because they are not mixtures. They include or are originated from porphyrins, bactereochlorins, phthalocyanines, chlorins, benzoporphyrins,

curcumin, methylene blue derivatives, and others. Only a few of them have been approved for clinical treatment, but many are on trials.

3° generation: This class of PSs is now being developed and is an area of active research. They are characterized by conjugation of second-generation compounds with targeting moieties (e.g. amino acids, peptides, carbohydrates, antibody, etc.) or by encapsulation into carriers, in order to improve accumulation at the targeted tumour site [3,7-9].

Various light sources have been utilized to perform PDT, comprising daylight, lasers, incandescent light, and light-emitting diodes [1]; as a matter of fact virtually, any light source may be used in PDT [9]. However, the need to select the required wavelength for a specific PS and to ease dosimetry calculations, lead to an abandonment of conventional lamps. The choice of a light source depends on the cost and the availability of the technical tool, but also on the characteristics of the cancerous lesion (tissue feature, size, location and accessibility) and the type of PS (spectrum of absorption and administration modality) [3]. Red and infrared radiations penetrate more deeply through tissue, and specifically the range between 600 and 800 nm is known as the "therapeutic window". Shorter wavelength have lower penetration capacity, while longer ones may not have enough power to generate ROS [1,9].

A complex dosimetry influences the clinical efficacy of PDT: total light dose, light exposure time, and light delivery mode (single vs fractionated or even metronomic) [3].

PDT is highly appealing in clinical practice for several reasons:

- its minimally invasive nature,
- the localized therapeutic effect based on selective accumulation of PS and specific light irradiation,
- its low systemic toxicity,
- limited side effects,

- no compromission of future treatment options for patients with residual or recurrent disease,
- the possibility of combination with other therapeutic modalities [3,5,6].

Combining PDT with established anticancer therapies, namely ionizing radiation and/or chemotherapy, represent a promising foundation for new treatment options, especially since PDT does not have the limitation of dose-limiting toxicity of either these techniques. Some chemotherapy drugs can act both as a PS and a cytotoxic agent, enhancing the antitumour effect, but mainly decreasing the risk of severe side effects with the reduction of the required chemotherapy dosage. Correspondingly, certain PSs could act as radiosensitizers in the combination with ionizing radiation [6].

Furthermore, there has been great interest in intensifying the potential immune response of PDT by joint administration of various immunostimulants: the target is to induce immunogenic cell death (ICD) which triggers the response of the innate and adaptive immune system. If ICD is obtained in vitro, the subsequent transplantation in the patient of the malignant cells means that the host is provided with protection against tumour cells of the same strain, thus acting as a cancer vaccine [6].

For example, in some studies in vitro and in vivo PDT was successfully combined with radiation, chemotherapy, immune-modulating agents, and receptors-targeted agents for the treatment of breast cancer [1]; the results showed synergistic effects proving the promising prospects of new treatments with PDT.

Regarding the possible side effects of PDT, sensitivity, swelling, burning sensation, taste alterations, ulcerations, loss of local sensation, erythema, sterile pustules, dyspigmentation, hyperpigmentation, and hair loss have been reported, but often with low magnitude and occasional occurrence [9,10].

### 1.1.1 Photosensitisation mechanisms

PSs promote the transfer of light energy to the cellular environment: when in the ground non-excited state ($S_0$) they absorb photons shifting to an electronically excited singlet state ($S_1$), the energy then can be dissipated by thermal decay or emission of fluorescence. Alternatively, the PS shifts to an excited triplet state ($T_1$) via intersystem crossing; this state is less unstable and it can transfer a hydrogen atom or an electron to biomolecules, disperse its energy by emission of phosphorescence or generate radicals with molecular oxygen ($O_2$) to form ROS [Figure 1.2] [3,4]. Two different photodynamic reactions can be promoted:

Type I – From the interactions with cellular substrates, ions are formed and they react with $O_2$ leading to products such as the superoxide anion ($O_2^{\bullet -}$), the hydroxyl radical ($OH^{\bullet}$) and hydrogen peroxide ($H_2O_2$).

Type II – The transfer of energy between the excited PS and $O_2$ is direct generating singlet oxygen ($^1O_2$), which is non-radical but highly reactive [4,9].

It is generally accepted that $^1O_2$-mediated photodynamic mechanism of cytotoxicity is the primary responsible for cell death, however the supplemental role of $H_2O_2$, $OH^{\bullet}$ and $O_2^{\bullet -}$ could be relevant, particularly under hypoxic conditions [4,11].

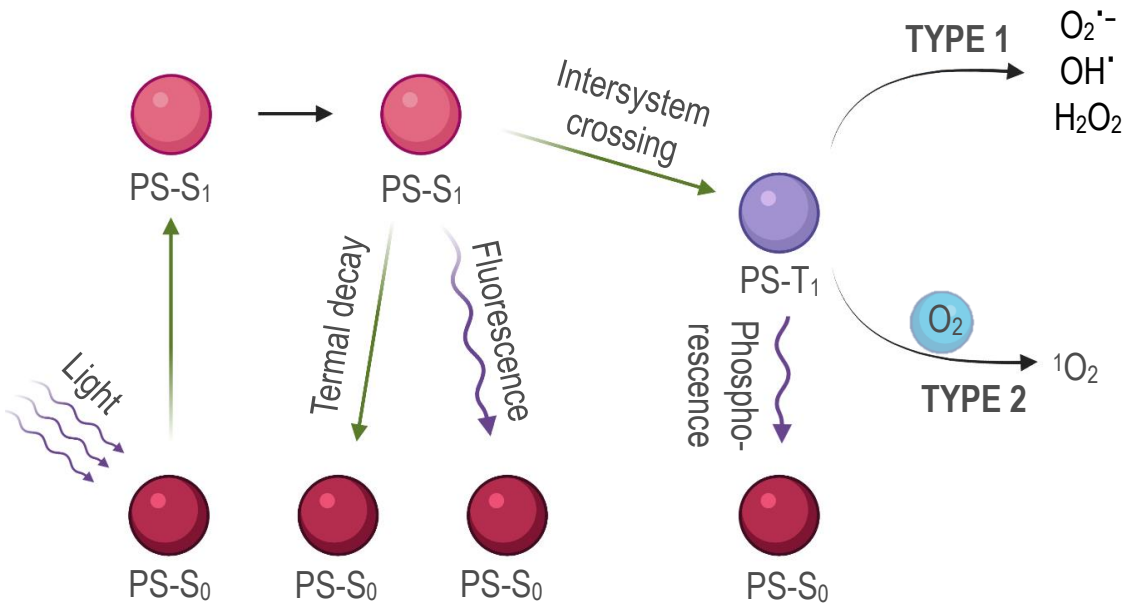


***Figure 1.2*** | *Schematic of the photophysical and photochemical basis of PDT.*

## 1.1.2 Photodynamic therapy and Imagining

Another noteworthy feature of PSs is their possible use as imagining agents in addition to being therapeutic ones for PDT. As mentioned before, upon excitation with appropriate wavelength, the electronic excitation of the molecules of PS can result in the emission of fluorescence from the relaxation of the excited singlet state back to the ground state. Since the PSs have the tendency to preferentially accumulate in neoplastic tissue, this phenomenon can be exploited for the selective visualization of tumours by utilizing fluorescence contrast to define the boundaries between healthy and cancerous tissue [11]. The shared excitation pathway for $^1O_2$ generation and fluorescence emission marks PSs as intrinsically theranostic [5]. The potential of PS fluorescence detection lies in diagnosis, therapy monitoring and guidance of surgery or other therapies. Moreover, it does not preclude the conjunct use of other contrast agents, exogenous or endogenous [11].

This practice, often termed photodynamic diagnosis (PDD) in the literature, is currently used for malignant gynecologic disease, and it has also been utilized for bladder cancer, gastrointestinal malignancy, malignant intrathoracic lesions and various carcinomas [2]. While most case reports of clinical applications show the positive contribution of both PDT and PDD to cancer treatment and diagnosis, other modalities are still preferred and other studies are needed to advance their therapeutical and diagnostic use.

### 1.1.3 Limitations of Photodynamic therapy

Despite the significant appetibility of PDT, owing to the high selectivity, which prevents the adverse effects associated with conventional therapies, and the fact that it does not confer tumour resistance, its widespread use is limited and there is a scarcity of randomized clinical trials in the literature [1]. PDT presents, in fact, some limitations, which are difficult to resolve since they pertain different aspects of its working mechanisms.

The main weakness of PDT is the PS, the success of the treatment ,in fact, depends on the $^1O_2$ yield, the molecule stability and the distribution of the therapeutic agent [7,8]. Many of the current PSs share the same disadvantages, namely the tendency to aggregate, which results in short triplet state lifetimes, hence a decreased $^1O_2$ yield and a lower efficiency [8]. An expanded aromatic ring is present in the structure of most compounds of the first and the second generation, aiming to absorb longer wavelength lights, but conversely decreasing their solubility in water and affecting one of the fundamental features for biomedical applications [7].

Other drawbacks of first-generation PSs are the prolonged patient photosensitivity, due to long elimination half-life and poor clearance, low absorption properties in the therapeutic range and lack of specificity [3,7].

The aim of the research on second-generation PS was to increase the solubility in biological media and triple the quantum yield; most experimental work focused on the modification and optimization of old-style PSs, so structures based on porphyrin, and though some encouraging results were obtained, the rational design of novel PSs with desirable properties remains a challenging task [8].

Alongside the synthesis of new types of molecules, efforts to improve the target distribution of PSs have been made [7,8]. While a number of hypotheses has been proposed [9], the mechanism that govern the preferential accumulation of PSs in atypical cells is still not well understood, hindering the optimization of delivery to the target tissues. Studies show that the high accumulation of PS in neoplastic lesions *in vitro* does not translate into an ideal outcome *in vivo* [11]. It has been observed that the accumulation of PSs in tumour cells increases with the hydrophobicity of the compound [4], this in turn hinders its ability to travel through the blood stream without damage, clumping or degradation [12].

Another key drawback of PDT is associated with its oxygen- dependent nature: since most existing PDT systems depend on the type II pathway, the treatment involves a dramatic consumption of $O_2$, the concentration of which, however, varies within the cancerous tissues, particularly in solid tumours. The interior regions of some solid neoplasms have very low levels of $O_2$, due to the proliferation of cancer cells and insufficient blood supply, and the efficiency of all clinically used PSs diminishes in the absence of oxygen [11,13].

Among the multiple routes researchers are investigating to overcome the limitations of PDT, the nanomedicine approach seems to be the most promising: different nanostructures could be used to improve the photophysical properties of PSs in aqueous media, and to actively or passively target the desired cancer sites [3,8]. The use of nanocarriers could also allow the implementation of combination therapy, for example by co-delivering a PS and a hypoxia-responsive anticancer drug, or of theranostic methods, by encapsulating a fluorescent dye together with the therapeutic agent [13].

## 1.2 Nanomedicine

Nanomedicine is the application of nanotechnology and nanoscience to the prevention and the treatment of human diseases. Nanotechnology concerns the understanding and control of matter in the 1-100 nm dimension range; there is, however, a lack of consensus on a clear description of nanotechnology, particularly applied to the medical field. Consequently, this means that a univocal definition of nanomedicine still escapes international regulatory agencies. A common denominator is the use of precisely engineered materials at the nanometric scale with the aim of developing novel therapeutic and diagnostic modalities [14-16].

Nanomedicine promises to revolutionise healthcare and medicine through transformative new diagnostic and therapeutic tools that can deliver cost-effective care for existing and new diseases, while potentially reducing side-effects [17].

Research has led to the design of nanotherapeutics with characteristics that differ from those of conventional medicines depending on their physicochemical properties (e.g. particle surface, size and chemical composition). Among these desirable characteristics, therapeutic nanosystems exhibit efficient transport through fine capillary blood vessels and lymphatic endothelium, longer circulation duration and blood concentration, higher binding capacity to biomolecules, higher accumulation in target tissues, and reduced immune response. These allow more specific drug targeting and delivery, greater safety and biocompatibility, faster development of new medicines with wide therapeutic ranges, and improvement of in-vivo pharmacokinetic properties [18].

Nanomedicine formulations have also been more and more exploited for imagining applications and theranostic approaches: nanomaterials with an intrinsic abilities of being utilized for imagining purpose have been developed and, on the other hand, drug delivery nano-systems have been co-loaded both with drugs and contrast agents [19].

The current lack of regulation and standards for nanomedicines in manufacturing practices, quality control, safety, and efficacy evaluation is a barrier to a successful clinical translation process; nonetheless in the last decade, many nanotherapeutics have been developed and commercially applied in clinical and non-clinical areas, others are presently being investigated in clinical trials, and academical research is thriving. Further advances and deeper understanding are needed, beside the establishment of regulatory definitions of key terms and of collective evaluation processes, but nanomedicine still offer huge opportunities and represents an important step for the upgrading of traditional pharmaceuticals [15,18,20].

### 1.2.1 Multifunctional properties of nanomedicine

The advantages of nanomedicine with respect to conventional therapeutic modalities are numerous and diverse, due to the possibility of designing treatment and imagining modalities with multiple functional elements.

*Solubilization and sustained drug release* – The addition of materials to allow drug solubilization is the simples and most intuitive form of multifunctionality. This approach could also offer a safer alternative to harmful formulations.
Another considerable feature is the high loading capacity, which enables a more specific drug dosage and reduces the exposure to excess materials that lack therapeutic efficacy. Sustained drug release is achieved and drug concentration is limited within the desired therapeutic window [15,16].

*Protection from degradation* – Some drugs are highly sensitive to enzymatic and mechanical degradation occurring in the bloodstream, in the extracellular space, and in lysosomes. Nanostructures can protect these therapeutic agents ensuring their stability and efficacy [16].

*Immunoevasion* – A critical limitation of several drugs and other bioactive agents is their easy immunological recognition and fast clearance. Encapsulating them in nanoparticles does not always solve this problem, however, by modifying the surface of the nanosystem with antifouling polymers, self-peptides, and cell coatings, it is possible to decrease nanoparticle uptake by the immune system [15,16].

*Mass transport characteristics* – The circulatory system of the body is usually exploited fro the delivery of intravenous and oral drugs, which compose the largest part of therapeutic agents. The molecules of these drugs are often smaller than 1 nm, so they efficiently diffuse throughout most tissues regardless of organ-specific vasculature mechanics. This widespread diffusion leads to exposure of the diseased cells to the drugs but imposes attentive dose adjustments to limit the damage to healthy cells, ultimately compromising the efficacy of the treatment.
Nanotherapeutic are much more dependent on vasculature properties for their transport in the body, and this dependence can be exploited to design tissue-specific delivery. In particular, transport oncophysics takes advantage of the unique characteristics of cancer blood vessels to increase drug accumulation in tumours [16].

Other possibilities of exploiting multifunctionality include the easy implementation of combination therapy (for example by delivering several drugs with the same NP), the surface conjugation of molecular targeting ligands for selective delivery and the use of intrinsic electromagnetic properties of inorganic nanoparticles for novel treatments like heat-induced tumour ablation [16].

### 1.2.2 Types of carriers

Nanotherapeutics are classified based on the type of nanomaterial used in their formulation.

*Liposome-based* – They are commonly used as vehicles for drug delivery since they are constituted by a lipid bilayer membrane that encloses a hollow core, where drugs can be encapsulated. Given their amphiphilic nature, they can deliver both hydrophilic and hydrophobic drugs, which are protected by the surrounding biological environment, improving in this way drug stability and circulation half-life. Employing liposomes leads to increased pharmacological effect and reduced non-specific toxicity, due to their better pharmacokinetics and the greater accumulation at lesion sites than conventional drugs. The surface of these spherical vesicles can also be functionalised to design active targeting systems. Liposomes are commonly coated with inert and biocompatible polymers, such as polyethylene glycol (PEG), to prolong their circulation in the bloodstream, being easily recognized and eliminated by the reticuloendothelial system (RES) in vivo.

Other lipid nano-systems include emulsions, solid-lipid nanoparticle (NP), and lectin-modified solid lipids, which share the same ability to control the degradation and metabolism of the formulation and prolong systemic exposure as liposomes [14,15,18].

*Polymer- based* – In the same way as liposomes, polymers have been utilized as nanocarriers to deliver encapsulated drugs, differently, however, they are also able to deliver conjugated therapeutic or imagining agents. Polymers are highly versatile, structurally diverse, and easy to functionalise; they may be used to enhance treatment efficacy by improving drug stability, by conferring biodegradability, and by enabling controlled release via stimuli-responsive functionalization.

Polymeric nanotherapeutics display a wide array of architectures, depending on which their characteristics may differ substantially. The most studied are polymeric micelles, nanospheres, dendrimers, and polymer-drug conjugates.

Polymer-drug conjugated improve drug solubilization and circulation, solve the problem of avoiding rapid clearance and enzymatic degradation, and reduce the immune response [15,18].

Dendrimers are highly ordered, branched structures, repetitive layers originate radially from an initiator core and end in terminal group forming a tree architecture. They can carry bioactive compounds by covalent bond, by ionic interaction, or by adsorption in the internal space [21]. They can be associated with other polymers or targeting structures, conferring them selective delivery, high membrane permeability, controlled release ability, and solubility improvement [18].

Polymeric micelles are usually formulated with amphiphilic polymers and therefore they undergo self-assembly, forming NPs with a hydrophobic core and a hydrophilic surface. Like liposomes they are able to entrap poorly water-soluble drugs, while providing solubility in aqueous environment, it is possible to functionalize their surface to favour active targeting, and they are often PEGylated – associated with a PEG shell – to reduce the non-specific RES uptake [15,18].

The structure of polymeric micelles is sometimes more complex than that of surfactant micelles (pure hydrophobic core surrounded by hydrophobic layer), they may consist of nano-objects with a structured core, or may be more accurately described as simple polymeric nanoparticles [22].

*Drug nanocrystal* – Nanocrystallization is a promising solution to the issue of poorly soluble drugs with low bioavailability. Through both top-down and bottom-up approaches, this technique modulates drug size increasing its dissolution velocity and its saturation solubility. Moreover, drug nanocrystals show great adhesiveness to biological mucosa, prolonging drug residence time; not requiring the use of a carrier, the dosage range is wide and adjustable, with an enhanced drug loading capacity with respect to nanocarrier drugs [15].

*Protein-based* – The principle behind protein NPs is similar to the one behind polymeric nanocarriers, however, unlike synthetic polymers, recombinant proteins offer homogeneous size distribution and little batch-to-batch variations. Protein-based

therapeutics represent the ideal drug delivery system thanks to their biocompatibility, biodegradability, low toxicity, renewable sources, and low immunogenicity [15].

*Inorganic nanoparticles* – Inorganic NPs theoretically offer infinite possibilities to nanomedicine given their tuneable size, shape, and chemical composition. Several materials have been implemented to realize these NPs, including semiconductors, metals, metal oxides and lanthanide-doped objects. Aside therapeutics, inorganic NPs show great potential as imagining probes, given their magnetic and optical properties [15,19].

For our purpose, the focus of the following review will be on polymer-based therapeutics, in particular polymeric nanoparticles and micelles formed through self-assembly of amphiphilic polymers.

### 1.2.3 Targeting methods

Delivery mechanisms of nanomedicine can be divided into intracellular transport, intercellular transport, and other methods. However, the most common classification of delivery makes the distinction between active and passive targeting [15,18,23].

*Active targeting*

Nanocarriers are programmed to actively bind to specific cells by attaching targeting agents on their surface in the synthesis process. These agents can be antibodies, proteins, peptides, or polysaccharides, and they are ligands, molecules that selectively bind to specific receptors present on the cell surface. Ligand-receptors interactions allow the recognition of the nano-objects, and bound carriers can be internalized in the cell before drug release. Common ligands used for this aim are folic acid, RGD peptide and aptamers. High selectivity is needed, and the surface marker (antigen or receptor) should be mainly present on target cells with respect to normal cells to maximise specificity [18,23].

*Passive targeting*

Both intracellular and intercellular transport can be described as passive targeting, as they refer to cellular uptake of nanomedicine through mechanisms different from receptor—ligand recognition.

In intracellular transport, an increase of membrane permeability and/or opening of tight junctions is achieved through binding involving bioadhesive polymers or chelates. The bioadhesive delivery system adheres on biological substrates in general, while the special case of mucoadhesive systems are typically used for sustained administration of drug substances across biological barriers with overlying mucous [18,24].

Intercellular transport of nanoparticles may occur through multiple different entry routes, which can be categorized into two general groups: endocytosis-based uptake pathways and direct cellular entry. The size of nanomedicines strongly influences this type of delivery, in fact smaller particles facilitate cell permeation, and also it has been reported that cell the affinity of cell surface transporters to nanotherapeutics varies depending on the particle size [18,25].

The most studied and exploited mode of delivering nanocarriers is the preferential accumulation of nano-objects in pathological tissues such as tumours and inflamed tissues by the enhanced permeability and retention (EPR) effect. Tumours presents leaky vasculature and a dysfunctional lymphatic drainage, so a nanocarrier can extravasate into the tumour and is retained inside where it is allowed to release drugs in the vicinity of tumour cells. Inflamed tissues, instead, can release vasodilators and chemotactic factors that promote nanovectors uptake with an EPR-like effect.

The EPR effect depends on the tumour type and localization, it can vary widely even in the same tumour kind, and imposes limitations on the size of nanomedicines: some experiments suggest that the threshold size for extravasation into tumours is ~400 nm, but other studies reported the highest effectivity with particles of diameter <200 nm [15,18,23].

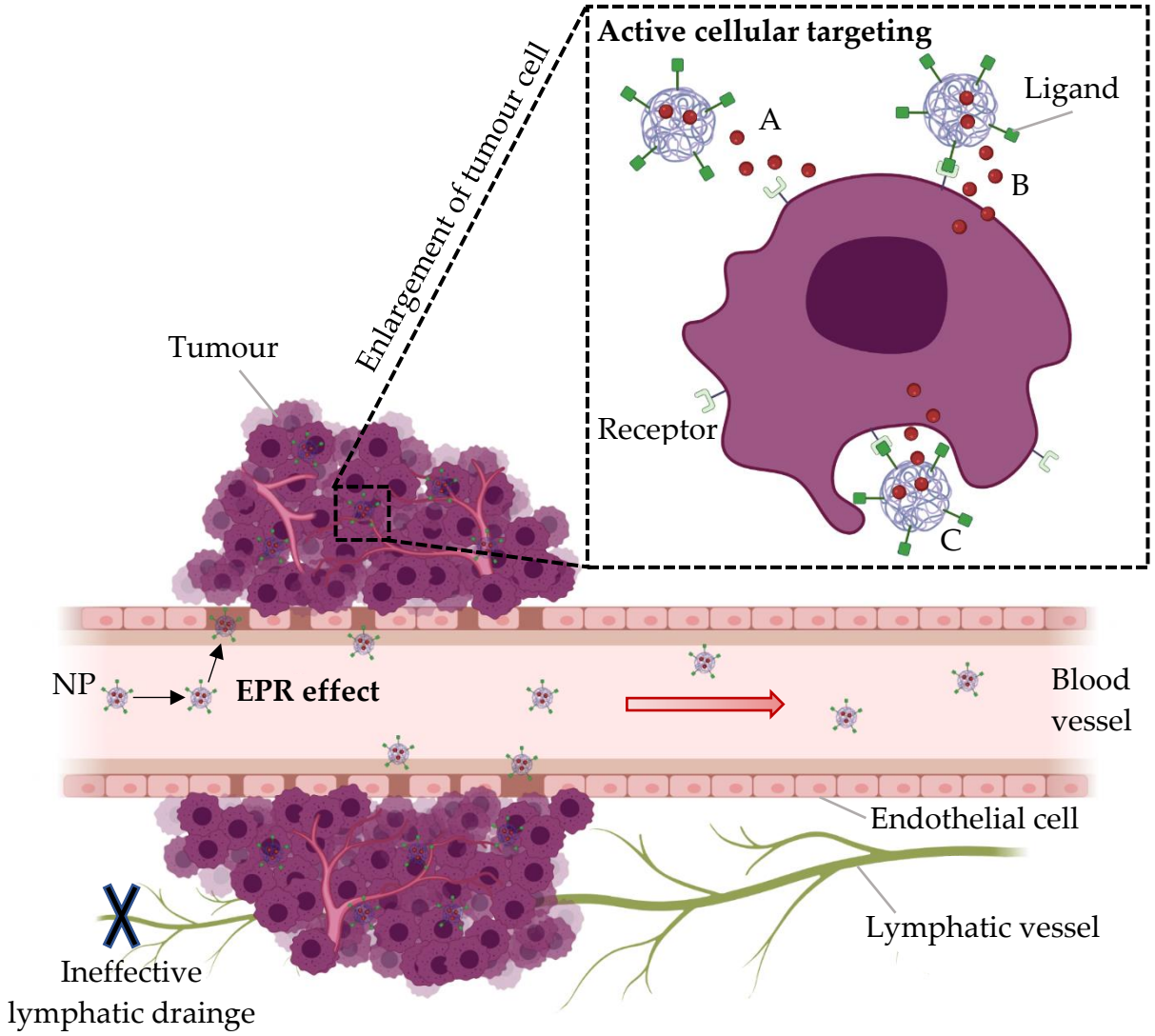


***Figure 1.3*** | *Schematic representation of different mechanisms by which nanocarriers can deliver therapeutic or imagining agents to tumours. Polymeric nanoparticles are shown as representative nanocarriers. Passive targeting is achieved by extravasation of NPs through increased permeability of the tumour vasculature and ineffective lymphatic drainage (EPR effect). Active targeting can be achieved by cell-specific recognition and binding promoted by ligands which the surface of NPs is functionalized with. The NPs (A) release their content in close vicinity of the targeted tumour cells, (B) attach to the cell acting as an extracellular depot with sustained therapeutic agent release, or (C) are internalized into the cell.*

Even though passive targeting approaches form the basis of clinical therapy, they suffer from several limitations, mainly stemming a considerable heterogeneity observed in

patients and the lack of control on the mechanisms of the process. By implementing active targeting on nanotherapeutics already exploiting passive delivery modalities, some of the drawback could be overcome and highly selective targeting may be achieved [15,16,23].

### 1.2.4 Characterization of the carriers

The gap between the advances made in research laboratories and the actual application of nanomedicine in clinically effective therapies has been called a "death valley" [26], where the enormous number of studies developing novel nanosystems translates in only a limited amount of approved therapeutics. Many challenges have been identified as bottlenecks, among them the complexity of a deep characterization and a still incomplete understanding of the interactions between nanomedicines and biological systems [26,27].

Nanosystems often present heterogenous physicochemical properties to a much greater extent than small-molecule compounds. Being aggregations of smaller materials, it is difficult to have a precise control on their exact dimensions and characteristics due to limitations in synthetic methods. An accurate design of the desired surface chemistry can be obtained either through high-cost synthetic routes (like photolithography), or by relying on the physicochemical properties of the parent compounds and associated reagents, which, however, could turn into an added difficulty. Polymers in particular possess inherent molecular weight polydispersity that likely transfers its properties to the nanocarriers [28].

Many characterization techniques have been applied directly from methods used for bulk materials or small-molecule systems, so without taking into account the unique properties and constraints of the nanoscale. Moreover, using conditions that do not simulate biological environment leaves the question of the stability and safety of nanotherapeutics once administered. It is necessary to design standardized processes and techniques for preclinical physicochemical characterization of nanoformulations to ensure consistency in

synthesis and better understanding and prediction their biodistribution, pharmacokinetic and safety profiles [27-29].

Nanomedicine characterization can be divided in three steps: first, an analytical characterization, to identify the materials they are composed of as well as develop eventual purification processes; second, a physicochemical characterization of the main parameters that will determine the performance of the nanomaterials *in vivo* (such as size, surface charge, morphology, surface chemistry, etc.); third, a study on their interaction with biological components [27].

As previously mentioned, there are no standards formally established in the scientific community for the physicochemical characterization of a nanomaterial, however an informal consensus agrees that nanotherapeutics should be characterized in terms of their size distribution, zeta potential, targeting/drug/imagining quantification, purity, stability, and batch-to-batch consistency. The wide range of techniques available for characterization includes dynamic light scattering (DLS), microscopy, spectroscopy, chromatography, and electrochemistry [26,28,29].

The size of a nanosystem is one of the most important parameters since it determines the cellular uptake mechanism and influences the immunogenicity. To accurately determine the range of sizes within the formulation and achieve a realistic and complete characterization, it is recommended to work with complementary methods: for example transmission electron microscopy (TEM) does not give accurate results, given that the measure should be done in aqueous solution (the physiological environment in which the NP will perform its function), so it has to be implemented together with DLS ,which allows to measure the hydrodynamic radius of the systems.

DLS has been considered to be the most suitable technique for size measurements of the nanocarriers, and it is attractive due to its relatively low price and its simplicity of use;

polydispersity (PDI) values obtained by DLS are also useful for representing the relative difference in size distribution in the case of multiple size population [28,29].

To increase the accuracy of size analysis and obtain more detailed information on shape and sample composition, the implementation of more advanced techniques is required. Size exclusion chromatography (SEC) is a valuable method to achieve size-based separation of NPs in complex samples. Asymmetrical Flow Field Fractionation (AF4) is able to separate macromolecules or particles over an even wider size range (1-1000 nm) than SEC, it has already been used with liposomes, polymeric NPs and metallic particles. Other techniques recognized by health agencies include electron microscopy, small angle X-ray scattering (SAXS), atomic force microscopy (AFM), and nanoparticle tracking analysis (NTA) [29].

The surface charge of the nanosystems is usually analysed by measuring the zeta-potential. The zeta potential is defined as the potential difference between the bulk solution (dispersing medium) and the surface of hydrodynamic shear (slipping plane), it is usually determined using zetasizers and the accuracy of the measure depends on the sample preparation and the employed procedures [28].

Size and surface charge are crucially important characteristics of the nanocarriers, often the characterization of nanomaterials is limited to measuring these two parameters, particularly in the case of monophasic multifunctional polymeric nanoparticles. However, due to the diversity of novel nanomaterials and consequently their complex interactions with biological systems, metrology must be expanded and customized [26,28]

Regarding the analysis of surface chemistry, nuclear magnetic resonance (NMR), absorption and fluorescence spectroscopy, together with various chromatographic methods are the conventional techniques used to quantify or at least confirm the presence of certain chemical groups on or in the surface of the nanomaterial. Also a wide range of microscopy instruments and methods are available for a detailed surface and internal analysis: AFM with automated ultramicrotomy, scanning tunnelling microscopy (STM),

environmental scanning electron microscopy (SEM), electron loss microscopy, Z-contrast TEM, and low voltage electron microscopy.

X-ray scattering methods give three-dimensional structural information for inorganic nanomaterials, like the degree of crystallinity and electronic band structure, and porosity. They have been also used in the characterization of the surface of lipid-polymeric NPs to individuate the distribution and position of the lipids on the particle surface.
Raman spectroscopy can be used in combination with microscopy, the unique spectra of nanomaterials allow the application of this technique for both molecular and full-particle characterization [28]

The design of efficient nanomedicines can not exclude a detailed study of their *in-vivo* behaviour, which is associated tightly with the protein corona effect.

### 1.2.5 Protein corona

The term "protein corona" (PC) refers to the well-known coating layer formed by biomolecules (sugar, lipids, proteins, etc.) that passivates the outer surface of nanomaterials shortly after systemic administration. This surface "biotransformation" alters the biological identity of the nanosystems changing their characteristics and ultimately affecting their cellular uptake, *in vivo* biodistribution, systemic toxicity, and potential therapeutic or diagnostic functionality [30,31].
The formation of a PC on nanomaterials is a dynamic and time-dependent process, in which the corona components vary with temperature, pH, and the locations of NPs during extracellular/intracellular travelling; it has been reported that also different diseases may lead to distinct PCs on the same type of nanosystem [32,33]. Protein binding (proteins are the main component of PCs) is energetically favoured since it minimizes free enthalpy,and it is mediated by Coulombic and van der Waals force, hydrogen bonding, and hydrophobic

interactions. The first adsorbed layer is a transient or "soft" corona which contains proteins of high abundance and lower affinity for the NP external chemistry; over time a "hard" corona coats the system with proteins of high affinity which may irreversibly bind to the NP surface [33,34].

The consequences of the formation of this "bio-nano interface" are multifold, influencing the transport mechanisms over biological barriers, blood coagulation and clearance, biodistribution, and cellular uptake of the nanotherapeutics [35]. The interaction between nanosystem and biological environment may also change: NP solubility may increase, biophysical processes of protein misfolding and aggregation may be triggered, an immune response may be provoked, and the functionalities present in or on the nanosystem may be masked and rendered ineffective [34].

The protein corona effect cannot be ignored when designing a novel nanomedicine.

One way to overcome it consist in covering the NP with an "anti-fouling" coating that offers non-specific resistance to protein absorption: the best-known developed polymer to this aim is poly(ethylene glycol), other examples are hydrophilic polycarbonates, hydroxypropyl methacrylamide and poly(propylene sulfoxide). These long-chain polymers impart steric stabilization to the nanosystem, and the high level of polymer hydration creates a barrier to protein absorption. Nanomaterials with low affinity for plasma proteins also have the peculiarity of preventing immune cell association, exhibiting what is known as "stealth effect" [31,35].

However, the effort to mitigate the complications caused by the protein absorption does not always lead to the best therapeutic outcome and completely resisting protein corona formation *in vivo* is ultimately difficult. It is increasingly agreed that controlling the protein corona rather than trying to eliminate it, would bring to more functional nanomedicine [31]. This process could be implemented by pre-coating the NPs with antibodies and plasma proteins in order to favour the absorption of types of proteins like dysopsonins, which

render the system invulnerable to immune surveillance. [31,35]. So, optimizing the physicochemical parameters of nanomedicines to manipulate and regulate indirectly the biological phenomena occurring once in biological environment becomes crucial for the final therapeutic and/or diagnostic efficacy [36].

After a careful characterization of the properties of the nanomaterials, a likewise attentive investigation of NP-protein interaction is to be performed. From microscopic screening methods to spectroscopic approaches, and from kinetic analysis to thermodynamic exploration, the selection of the proper characterization method depends on the specific NPs-protein system, and on its therapeutic or diagnostic aim [26,32].

The first factor to consider is the appropriate biological system: *in vitro*, *ex vivo* or *in vivo* systems have been used in literature depending on the research purpose. In *in vitro* investigations fetal bovine serum (FBS) is utilized since almost all cellular media contain FBS proteins regardless of cell species. For *ex vivo* methods the cellular medium changes depending on the exposure route (inhalation, intravenous injection, oral exposure, or others). Mice and rats are the common animal models used in *in vivo* experiments.

The conditions of incubation of nanomaterials with a certain biological fluid are expected to precisely mimic the real exposure scenarios, so a great attention is given to the tuning of several parameters, such as incubation temperature, plasma/NPs ratio and pH. In most studies NP-PC complexes are characterized under static conditions, in contrast to the highly dynamic blood system [32].

The nature of the interactions between nanomaterials and proteins can be studied *in situ* or *ex situ*, however *ex situ* tests were usually preferred in past studies given the limitation of the *in-situ* available techniques. NP-PC complexes are separated from the free biological fluid by centrifugation or chromatography, but cloud point extraction and capillary electrophoresis have also been used [37-39]. Size characterization of the complexes is implemented with the same techniques for the characterization of pristine nanomaterials

(DLS, NTA, SAXS, TEM, SEM, etc), while spectroscopic methods can be used for *in situ* monitoring, for example UV-vis absorption spectroscopy and fluorescence correlation spectroscopy (FCS).

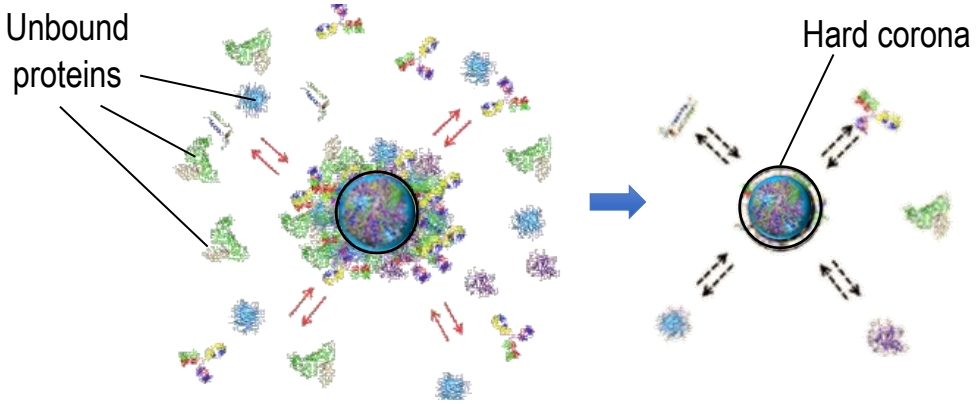


***Figure 1.4*** | *Schematic representation of the separation of the NPs-PC from the free biological fluid.*

The qualitative protein composition of PC can be identified by SDS-GEL electrophoresis, but identification of proteins requires liquid chromatography coupled with mass spectroscopy (LC-MS). X-ray crystallography and NMR are the most efficient methods for protein structural analysis, but they are not always feasible, spectroscopic methods (UV-vis spectroscopy, Fourier transform infrared spectroscopy, circular dichroism, etc.) can be used instead [26,32].

Techniques including isothermal titration calorimetry (ITC), surface plasmon resonance (SPR), quartz crystal microbalance (QCM), fluorescence-based spectroscopy and NMR could measure the thermodynamics and kinetics of association and dissociation between biomolecules and nanomaterials, but some experimental limitations at the nanoscale hamper their characterization ability; computational simulations can provide complementary insights to better understand the interaction sites, the driving forces and the conformational changes of NPs-PC complexes [32].

## 1.3 Photodynamic nanomedicine

The possible employment of nanomedicine in PDT has received increasing attention in recent years, since it could overcome most of the limitations of classic PS and expand the area of application of this therapeutic modality [40-42].

Nanomaterials could bestow numerous advantages to PDT depending on the type of vehicle and the mode of attachment or loading of the PS:

- The large surface to volume ratio could effectively increase the quantity of PS delivered to target cells.
- Nanocarriers may prevent premature release and potential inactivation of the PS, avoiding non-specific accumulation in healthy tissues.
- The problem of hydrophobic PSs could be circumvented by the amphiphilicity of the nanosystems, allowing unhindered travelling through the blood stream.
- The use of nanometric vehicles could allow the exploit of the EPR effect facilitating both the diffusion into and the retention within tumour tissues.
- Further surface modification of the vehicles with functional groups or targeting agents would be possible in order to change their biological and physical properties, thereby improving their biodistribution, pharmacokinetics, cell uptake, and targeting abilities.
- Nanocarriers could also be designed as multifunctional platforms to carry multiple components, such as imagining agents, chemotherapeutic drugs, targeting ligands, and "cloaking" agents (to avoid fast clearance by the immune system), ultimately building highly performing theranostic systems [43].

The nanomedicines investigated for the implement of nanomaterial-based PDT can be broadly classified in three categories depending on their function: carriers of PS, downconverting PSs, and energy transducers [42,43].

*Nanoparticles as delivery carriers of PS* – The encapsulation of PSs into nanovehicles is particularly appealing for a number of reasons other than overcoming PS hydrophobicity. Most organic PSs still suffer from photoinduced or enzymatic degradation, avoidable if contact with biological environment is mediated by a carrier [44]. Unlike chemotherapeutic drugs, for effective PDT the ideal dose is not necessarily the maximum number of PS that can be loaded in the carrier, which makes this technique more versatile. Moreover, the actual release of PS from the vehicle may not be required, since oxygen can easily diffuse within the nanosystem, interact with the photoactivated PS, and get converted into ROS, which can then diffuse back out [40].

Both biodegradable polymeric nanoparticles and non-biodegradable nanoparticles (ceramic or metal-based) have been studied to this end. Among the various nanoplatforms, polymeric micelles realized through the self-assembly of amphiphilic copolymers have elicited much interest, showing enhanced tumour accumulation, inhibition of tumour growth, and improved animal survival in various *in vivo* studies [45].

*Nanomaterials as downconverting PS* – Certain nanoscale structures have the ability to generate ROS, owing to their unique optical absorption properties, so they can behave as PSs by themselves. Among these structures there are fullerenes, titanium dioxide NPs, zinc oxide NPs, manganese dioxide nanosheets, transition metal dichalcogenide nanosheets, and black phosphorus [42,43].

*Nanosystems as energy transducers* – Some nanoparticles both act as carriers of the PS and actively participate in the energy transfer to the PS. Generally, they absorb energy from light, which is then transferred to the associated PS; this ability offers the possibility of indirectly activating the photosensitizing agent using light at wavelengths normally that it normally does not absorb. Some examples of these systems are semiconductor quantum dots, X-ray activatable NPs, two-photon absorbing NPs, and upconversion NPs, which

converts low energy light to high energy light through sequential excitation with multiple photons [43].

## 1.4 Aim of the project

The future of medicine can be changed by nanomedicine: using nanometric vectors to deliver the theranostic molecules to the desired site represents one of the main goals. For diseases such as cancer, it could overcome many major drawbacks of conventional treatments and revolutionise the entire field of studies [6]. Photodynamic therapy (PDT) is a therapeutic modality currently clinically used for the treatment of different types of tumours [1,3], it consists in the irradiation of the biological matter after the inoculation of a photosensitive species (the photosensitizer), which transfers its energy to oxygen, leading to formation of reactive oxygen species which are toxic to the local cancerous cells. Despite its promising features, PDT suffers today from several issues, the main one being an inadequate biodistribution of the photosensitizer (PS), leading to skin photosensitivity over several days. In previous studies carried out by the Laboratoire des Interactions Moléculaires et Réactivité Chimique et Photochimique (IMRCP) in Toulouse [46-49], it has been shown that encapsulating the PS in a polymeric nanovector strongly improves the PDT efficiency. The nanovectors were based on amphiphilic block copolymers, with a hydrophilic block constituted of poly(ethylene glycol) (PEG). In nanomedicine, the vast majority of the nano-objects also rely on this polymer to improve the circulation lifetime of the vectors *in vivo*, and to increase their stability and solubility, thus optimizing drug efficacy. However, after several decades of development and clinical use, PEG is still limited by multiple factors, and it faces emerging challenges destined to significantly impact its biomedical applications going forward [50]. For example, studies have been increasingly showing that upon several injections of PEG- based nanovectors, an immune response occurs, induced by the production of anti-PEG antibodies, leading to a rapid clearance of the vectors [50,51].

In collaboration with the the Département de Chimie Moléculaire et Macromoléculaire at the Institut Charles Gerhardt Montpellier (ICGM), the IMRCP lab has begun to assess a new type of vector to be used in PDT, based on poly(2-oxazoline); results have been encouraging suggesting that poly(2-oxazoline) could be a valid alterative to PEG in nanomedical applications [52]. This present thesis work is a follow-up study aimed to expand the research by assessing the ability of forming polymeric nanovectors (micelles or polymer vesicles) of a range of newly synthetised poly(2-oxazolines), considering the possible influence of molecular weight and composition. Different methods of formation of the nanovectors were employed varying the components in order to optimize the procedure. Characterization of the colloidal solutions was performed with dynamic light scattering (DLS), transmission electron microscopy (TEM) and cryo-TEM to investigate the size and morphology of the objects. Crosslinking the vectors by light, thanks to the presence of a photo-reactive group on the polymer chain, was also carried out. This process aims to provide more stability to the vectors and has previously shown to increase the efficiency of the vectors [47]. Crosslinking was assessed by proton nuclear magnetic resonance ($^1$H NMR) spectroscopy.

In collaboration with the SupraBioNanoLab (SBNLab) at Politecnico di Milano, preliminary studies on the protein corona formation on the nanovectors were carried out. The effect of proteins on the colloidal stability of the nanovectors dispersed in a biological environment (serum) was assessed by performing DLS, while centrifugation with sucrose cushion and ultracentrifugation with sucrose gradient were also used to isolate protein corona (PC) complexes. The qualitative composition of the PC associated to the nanovectors was obtained by SDS-GEL. The stability of the crosslinked and non-crosslinked nanovectors in biological environment was assessed with DLS analysis over a time interval of 24 hours.

# 2. Materials and Methods

## 2.1 General overview

The aim of the present thesis work is to assess a new type of vector, based on poly(2-oxazoline) for PDT.

The first part of the work was done at the Laboratoire des Interactions Moléculaires et Réactivité Chimique et Photochimique (IMRCP) in Toulouse with the team IDeAS in collaboration with the Centre de Microscopie Electronique Appliquée à la Biologie, Faculté de Médecine, in Toulouse, the Département de Chimie Moléculaire et Macromoléculaire at the Institut Charles Gerhardt Montpellier (ICGM), and Specific Polymers in Castries.

The ability of forming polymeric nanovectors (micelles or polymer vesicles) with a range of poly(2-oxazolines) was evaluated taking into account different molecular weight and composition and variating the method of formation. Characterization of the vectors was implemented in terms of size, size distribution and morphology: dynamic light scattering (DLS), transmission electron microscopy (TEM) and cryo-TEM were used. The ability of vector formation was investigated also in presence of a range of poly(ethyl methacrylates) functionalized with a photoreactive moiety, also present on the poly(2-oxazoline) chain. Photo-crosslinking was performed on these carriers to confer more stability to the vectors, and it was assessed by proton nuclear magnetic resonance ($^1$HNMR).

The second part of the work consisted in the study of protein corona formation on the nanocarriers. The NP-protein corona complexes were characterized physically and biologically with DLS and capillary electrophoresis. This part was carried out in the SupraBioNanoLab (SBNLab) at Politecnico di Milano.

## 2.2 Materials

The different poly(2-oxazolines) were synthesised at the ICGM lab [Figure 2.1], while Specific Polymers provided the various poly(ethyl methacrylates) [Figure 2.2]. These polymers were used as received and stored at ambient temperature protected from light. A poly(2-oxazoline) and a poly(methyl acrylate) previously used in another study [52] were also employed in the experiments; the poly(methyl acrylate) was stored in the fridge.

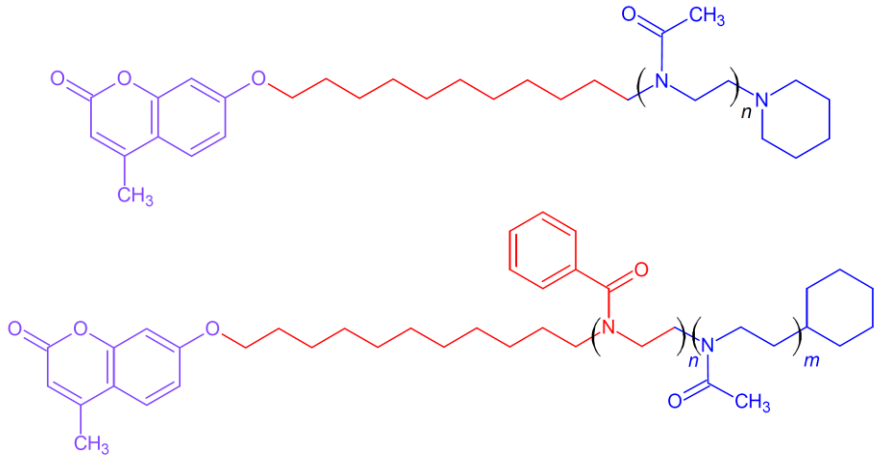

***Figure 2.1*** | *The chemical structure of the amphiphilic poly(2-oxazolines). In purple the photoreactive unit, in red the hydrophobic part and in blue the hydrophilic part.*

| Amphiphilic polymer | Designation | Molecular weight [g/mol] |
|---|---|---|
| $Coum - C_{11} - (MOx)_{15}$ | *CmPOx15* | 1615 |
| $Coum - C_{11} - (MOx)_{59}$ | *CmPOx59* | 5100 |
| $Coum - C_{11} - (PhOx)_{27} - b - (MOx)_{59}$ | *CmPhOx27:59* | 9700 |

***Table 2.1*** | *Theoretical molecular weight and degree of polymerization of the amphiphilic poly(2-oxazolines).*

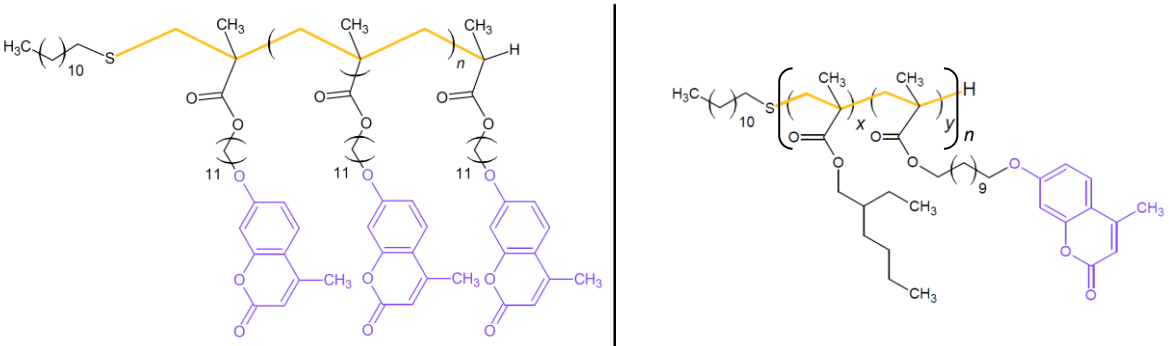

***Figure* 2.2** | *The chemical structures of the poly(methyl methacrylate) from the previous study (left), and of the different poly(ethyl acrylates) (right).*

| Stabilizing polymer | Designation | Degree of polymerization n | Molecular weight [g/mol] |
|---|---|---|---|
| $(MA - C_{11} - Coum)_{10}$ | *CmPMMA* | / | 4000 |
| $(MA - C_{11} - Coum)_{20} - b - (MA - Ethylhexyl)_{80}$ | *CmPMA20:80* | 27 | 6000 |
| $(MA - C_{11} - Coum)_{50} - b - (MA - Ethylhexyl)_{50}$ | *CmPMA50:50* | 20 | 6600 |
| $(MA - C_{11} - Coum)_{80} - b - (MA - Ethylhexyl)_{20}$ | *CmPMA80:20* | 18 | 6500 |

***Table* 2.2** | *Theoretical molecular weight and degree of polymerization of the stabilizing poly(alkyl methacrylates).*

Acetone, dichloromethane, *N,N*-dimethylformamide, tetrahydrofuran, methanol and chlorofom -used in self-assembly formation without further purification- were purchased from Sigma-Aldrich.

Sucrose, sodium chloride, potassium chloride, disodium hydrogen phosphate, potassium dihydrogenphosphate, Trizma® base, glycine, sodium dodecyl sulfate (SDS), N,N,N′,N′-tetramethylethylenediamine (Temed), ammonium persulfate (APS), Acrylamide/Bis-acrylamide (40% solution), hydrogen chloride, 2-mercaptoethanol, butanol, methanol and acetic acid– used for protein corona analyses without further purification – were purchased from Sigma-Aldrich.

For all manipulations done at IMRCP lab ultrapure water was obtained from an ELGA Purelab Flex system (resistivity higher than 18.2 MΩ cm) and was filtered using 0.2 μm RC

filters just before use. At the SBNlab ultrapure water was procured by the purification system provided by Simplicity® (18.2 MΩ cm).

## 2.3 Methods

### 2.3.1 Formation of the self-assemblies – Cosolvent method

For nanocarrier preparation the protocol of previous works was followed [48,52], this protocol could be viewed as a type of nanoprecipitation method of formation of the NPs [53]. The protocol followed for the formation of the self-assemblies with the two poly(2-methyl-oxazolines) consisted in five steps [Figure 2.3]:

1) Dissolution of the polymer (8 mg/ml) in filtered water (RC cut-off 0.2 μm);
2) Dissolution of the chosen poly(alkyl methacrylate) in acetone;
3) Dropwise addition of a small volume of the second solution – calculated to have a final desired ratio of 10% wt. of the poly(alkyl methacrylate) compared to the poly(2-methyl-oxazoline) – to the first solution under moderate stirring at room temperature;
4) Moderate stirring of the solution for 10 minutes;
5) The solution was left standing for 2 days to evaporate acetone.

Step 2 and 3 were skipped in case of analysis of the amphiphilic polymer alone.

In order to overcome an issue encountered during the previous research the solvent used for the dissolution of the stabilizing polymer was modified. In fact *CmPMMA* shows poor solubility in acetone, forming a rather turbid suspension with formation of a white precipitate observed on the bottom of the vial. Despite the obtained promising results using acetone, given by its easy elimination and low toxicity, the difficulty of knowing the real

concentration of *CmPMMA* in the final aqueous solution represents a limitation. Three alternative solvents were selected to substitute acetone: dichloromethane ($CH_2Cl_2$), *N,N*-dimethylformamide (DMF) and tetrahydrofuran (THF). All the other poly(methyl methacrylates) that were employed were soluble in acetone, except for *CmPMA80:20* which was solubilized in $CH_2Cl_2$ and DMF. *CmPMA20:80* and *CmPMA50:50* produced clear solutions indicating good solubility. *CmPMA80:20* resembled *CmPMMA*, forming turbid aqueous solutions when added after solubilization in both $CH_2Cl_2$ and DMF.

Depending on the organic solvent used for the self-assembly formation, the solution was left standing for a couple of days to let the solvent evaporate or dialysis was performed on a Mini Dialysis Kit (GE Healthcare Bio-Sciences) with 1kDA cut-off and 2 ml volume.

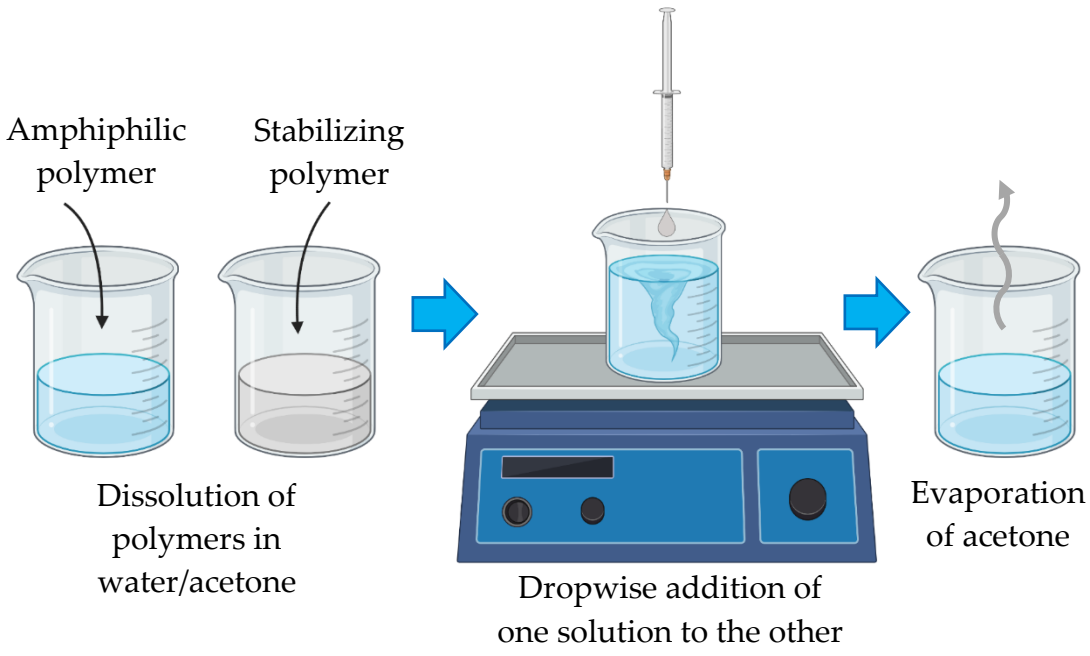


***Figure 2.3*** | *Schematic representation of the cosolvent method of formation of the self-assemblies.*

Regarding the third polymer studied, the addiction of phenyloxazoline to the chain increased the length of the hydrophobic alkyl part, making the copolymer insoluble in

water. The procedure of formation of the self-assemblies was slightly changed due to this reason:

1) Dissolution of the polymer (50 mg/ml) in acetone;
2) Dissolution of the chosen poly(alkyl methacrylate) in acetone;
3) Dropwise addition of both solutions, the volume of the second one calculated to have a final desired ratio of 10%wt. of the poly(alkyl methacrylate) compared to the poly(2-methyl-oxazoline), to 5 ml of filtered water (RC cut-off 0.2 μm) under moderate stirring at room temperature;
4) Moderate stirring of the solution for 30 minutes;
5) The solution was left standing for 2 days to evaporate acetone.

Step 2 and 3 were skipped in case of analysis of the amphiphilic polymer alone.

In this case the changes influenced by the use of other solvents ($CH_2Cl_2$ and DMF) were investigated both for the polymer alone and together with the stabilizing poly(alkyl methacrylate).

### 2.3.2 Formation of the self-assemblies – Film rehydration method

Given the solubility issues encountered using the cosolvent method, another procedure was tested for the formation of nanoparticles. The film rehydration method was previously used with copolymers of PEG [47] and consisted in 9 passages [Figure 2.4]:

1) Dissolution of the polymer (20 mg/ml) in methanol;
2) Dissolution of the chosen poly(alkyl methacrylate) in methanol/acetone;
3) Mixing of the solutions, the volume of the second one calculated to have a final desired ratio of 10% wt. of the poly(alkyl methacrylate) compared to the poly(2-methyl-oxazoline);

4) Evaporation of the solvent on rotary evaporator to form a uniform film for 1 hour;
5) Further drying under dynamic vacuum for 4 hours (at IMRCP lab the container was put into an oven connected to a vacuum pump, while at SBNLab the pump was directly connected to the container of the film);
6) Rehydration of the film (10 mg/ml) with filtered water;
7) Heating of the solution in oil bath at 65°C for 30 minutes;
8) Heating of the solution under sonication at 65°C for 1 hour;
9) Extrusion of the solution using a mini-extruding system from Polari Avanti Lipids with a polycarbonate membrane (cut-off of 0.2 and 0.1 μm) on a heating plate at around 50°C.

In the original protocol the polymer was dissolved in chloroform, but *CmPOx* didn't solubilize well. Solubility test were made with THF, $CH_2Cl_2$ and methanol, the last one being elected as the best choice; methanol was used also with *CmPhOx27:59*. For the two poly(alkyl methacryaltes) used for this method (*CmPMMA* and *CmPMA80:20*), methanol was also employed even though both polymers weren't satisfactorily solubilized.

The procedure was later optimized substituting methanol with chloroform for the amphiphilic polymer and with acetone for the poly(alkyl methacrylate), increasing the time of evaporation of the solvent on the rotary evaporator to 2 hours and decreasing the time of further drying of the film under vacuum to 3 hours.

The extrusion step was soon abandoned since it did not seem to impact on shape and size of the particles we were interested in; in some cases the process seemed to lower the PDI of the solution, probably due to the fact that it extruded large agglomerates present in suspension, however this was not controllable and the results weren't consistent between different samples.

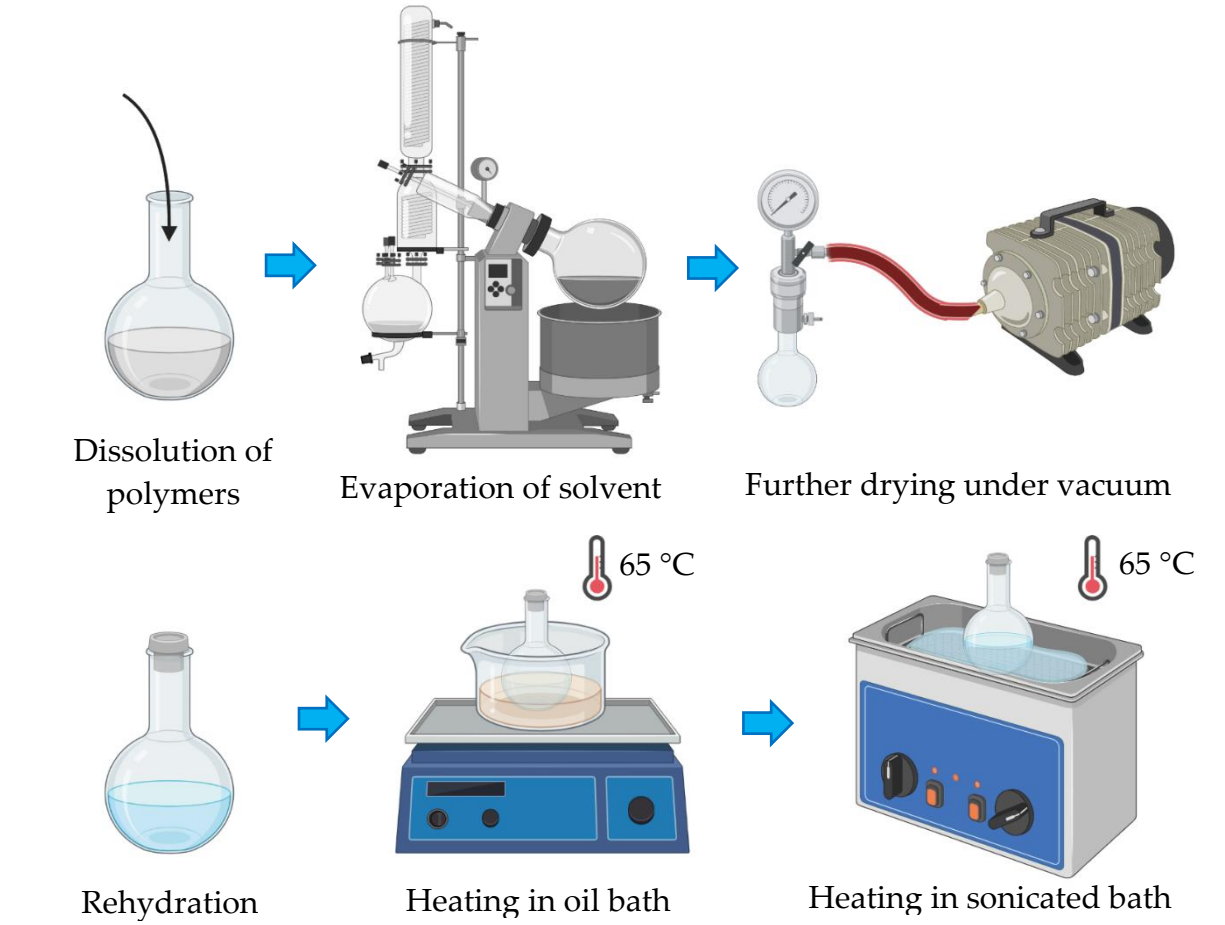


***Figure 2.4*** | *Schematic representation of the of the film rehydrationt method of formation of the self-assemblies (above). Picture of the mini-extruding system adapted from avantilipids.com (below).*

## 2.3.3 Crosslinking of the self-assemblies

All the polymers synthesised and analysed in this research work bear a photoreactive moiety on their chains, meaning coumarin. Numerous applications of coumarin have been described in biology and medicine as therapeutic agents (anti-HIV, antibacterial, antihyperproliferative, anticoagulant, anti-cancer) [54,55]. In our case coumarin was present to enable the UV light-induced dimerization of the groups present both on the chain of the amphiphilic polymer which forms the nano-vector and another polymer which ideally position itself inside the nano-object [Figure 2.5]; in this way the two polymers become crosslinked to each other stabilizing the system.

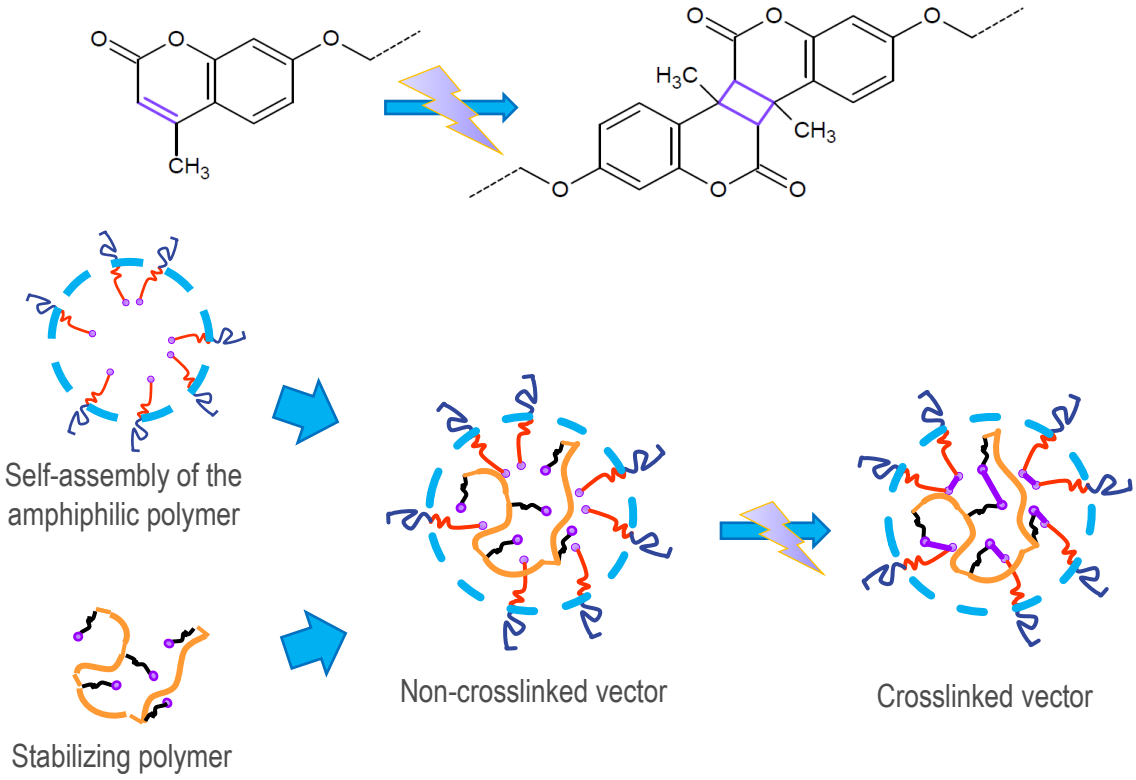


***Figure 2.5*** | *Photo-dimerization of coumarin (up). Process of formation of the nanovector and subsequent crosslinking: the purple dot indicates the photoreactive moiety, the red and blue lines represent respectively the hydrophobic and the hydrophilic part of the amphiphilic polymer.*

In the previous studies by the IMRCP lab [47,52], crosslinked vectors displayed higher PDT efficiency than non-crosslinked ones, so the photosensitive group was added to further examine the effect of crosslinking on this type of vector.

The same set-up [Figure 2.6] used for the previous study was employed for the crosslinking: a 5 mm NMR tube containing 2.2 mL of the self-assembly solution was placed for 7 hours between two UV lamps, Philips linear T5 8W, irradiation at 360 nm, lamp-tube distance 8 mm, total irradiance 1.0 mW/cm$^2$, measured using a HD9021 photometer obtained from Delta Ohm Inc. The time was increased to 14 hours for the polymer containing phenyloxazoline units.

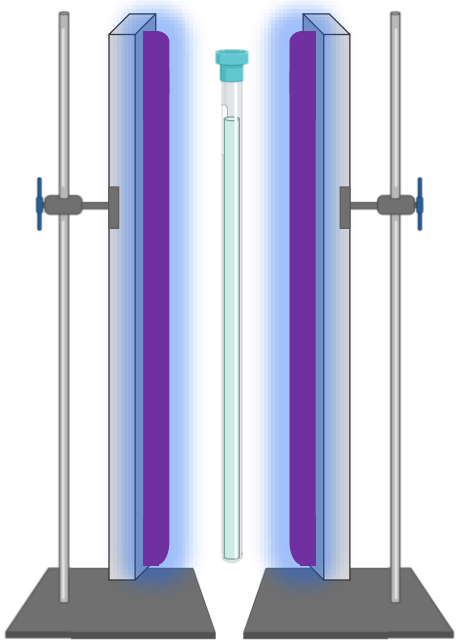

***Figure 2.6*** | *Scheme of the set-up used for crosslinking.*

### 2.3.4 Dynamic light scattering (DLS)

Dynamic Light Scattering, also known as Photon Correlation Spectroscopy (PCS), is a technique which measures the Brownian motion of particles in solution and relates this motion to their size distribution. Brownian motion theory, discovered by the botanist Brown in 1827 and theorized by Einstein in 1905, states that particles with nanometric size in a solution are in continuous thermally induced motion: these NPs are in constant collision with solvent molecules, therefore the generated random forces result into a random walk. The mobility or the diffusion in the solution highly depends on the particle size, the bigger the object, the smaller its mobility, so probing this mobility allows one to estimate the dimension pf the moving objects.

In a DLS experiment an incident monochromatic beam of light (laser) hits the sample and it is scattered in all directions depending on the size and the shape of the objects in solution. Scattering of light by particles can be distinguished into anisotropic Mie Scattering and isotropic Rayleigh Scattering. Mie scattering is angle dependent, the scattered light has different energy from the incident one, and it occurs when the size of the particles is higher than one tenth of the wavelength of the incident light. Rayleigh Scattering is angle independent, concerns particles with size smaller than one tenth of the incident wavelength, and scattered and incident light have equal energy [56].

When light hits, the continuous motion of particles causes multiple entrances and exits of particles from the observation zone, consequently the detected intensity of scattered light fluctuates over time and the fluctuations depends on the radius of the NPs [56-58].

Usually the instrument uses a digital autocorrelator which correlates the intensity fluctuations of scattered light over an interval of time in order to determine the rate of these fluctuations, in turn directly related to the diffusion behaviour of NPs. In this way we obtain the diffusion coefficient of our NPs which can be correlated to the hydrodynamic radius through the *Stokes-Einstein equation*:

$$D_0 = \frac{k_B T}{6\pi\eta R_H}$$

Where $D_0$ is the diffusion coefficient, $k_B$ is the Boltzmann constant, $T$ is the absolute temperature, $\eta$ is the viscosity of the solvent and $R_H$ is the hydrodynamic radius [56,58]. In particular, in order to extrapolate this information, DLS measures the normalised time correlation function $g^{(2)}(\tau)$ of the scattered light intensity $I$, which is a mathematical tool used to differentiate a random fluctuation of the signal from fluctuations due to the Brownian motion:

$$g^{(2)}(\tau) = \frac{\langle I(0) * I(\tau)\rangle}{\langle I(0)\rangle^2}$$

Where $\tau$ is the correlation delay time. The same can be expressed also in terms of the correlation function $g^{(1)}(\tau)$ of the scattered light field through the *Siegert relation*:

$$g^{(2)}(\tau) = 1 + \beta * \left[g^{(1)}(\tau)\right]^2$$

Where $\beta$ is the coherence factor, a parameter characteristic of the instrument.
In the case of equal-sized particles, $g^{(1)}(\tau)$ (or $g^{(2)}(\tau)$) can be expressed as a mono-exponential decreasing function:

$$g^{(1)}(\tau) = exp(-\Gamma * \tau)$$

From which one can extract a characteristic constant called the decay rate Γ. The decay rate is proportional to the translational diffusion coefficient:

$$\Gamma = D_0 * q^2$$

The scattering vector $q$ depends on the scattering angle $\theta$ through the following relation:

$$q = \frac{4\pi n}{\lambda} * \sin\left(\frac{\theta}{2}\right)$$

All the above-mentioned equations constitute the theory behind DLS technique and lead to the determination of the hydrodynamic size of the spherical NPs; in case of different shapes other equations are applied.

When the sample is polydispersed, difficulties arise since the autocorrelation function is a sum of decreasing exponentials with a series of decay rates, each one associated to a different size of particles.

$$g^{(1)}(\tau) = \int G(\Gamma) * exp(-\Gamma * \tau) d\Gamma$$

$G(\Gamma)$ is the normalized distribution of decay rates. Therefore, $g^{(1)}(\tau)$ resembles the Laplace transform of $G(\Gamma)$, which can be obtained by inverse transformation. This operation is not simple, three main ways are generally used to get $G(\Gamma)$:

1. The distribution function is approximated by a series, one generally uses the development of the function based on their cumulants.
2. The distribution function is described by a fixed number of exponentials corresponding to a pre-selected decay rate, then a minimization process is conducted leading to an estimation of the importance of each of each exponential. Among the most utilized methods there are CONTIN and the non-negative least square (NNLS) algorithms.
3. Finally, the distribution function may be assumed to be a given function and the problem is then to adjust this function in such way that the theoretical correlogram is close to the experimental one.

Other techniques implemented include exponential sampling, regularization, maximum entropy and maximum likelihood [56,59].

In our research work at the IMRCP lab, DLS was carried out on a Malvern (Orsay, France) Zetasizer NanoZS, equipped with a He-Ne laser with a wavelength of 633 nm and a

maximum intensity of 4 mW. The measurements were carried out at 25 °C with a warm-up time of 120 seconds and each measurement was the result of the average of three subsequent runs of 10 seconds each. Data were analysed using the general-purpose NNLS method and the apparent hydrodynamic radius was obtained from an intensity weighted and a number weighted fitting of the autocorrelation function.

All correlograms obtained by the instrument were also analysed using a custom-made program named STORMS in order to obtain a more precise characterization of the solutions [60]. This program has been designed at the IMRCP lab using Matlab and gives the opportunity to fit the autocorrelation functions using different sets of parameters. Data treatment going from correlograms to size results consists in three levels of choices: the first one to select the mathematical method which estimates the distribution of decay rates (therefore of the diffusion coefficients), the second one to choose a physical model describing the relationship between the diffusion coefficient and the geometry of the particles, and the final one to select a second physical model relating the scattering properties of the particles to their size. For each step, STORMS provides the choice of different parameters.

For our nano-objects, a NNLS fitting was used, a spherical shape was assumed for all objects, and two different scattering models were selected depending on the results obtained with the data analysis on the Malvern instrument: one model correspond to a mixture of micelles and vesicles (maximum micelle size fixed at a radius of 25 nm), while the other considers only full small spheres. Different sets of regularization parameter were used in order to obtain the less residuals possible: expansion was either 0 or 1, alpha was varied between 5 and 20, range was usually set at 2 and classes at 100. This treatment provided residuals lower than $5 \times 10^{-3}$ for all analyses.

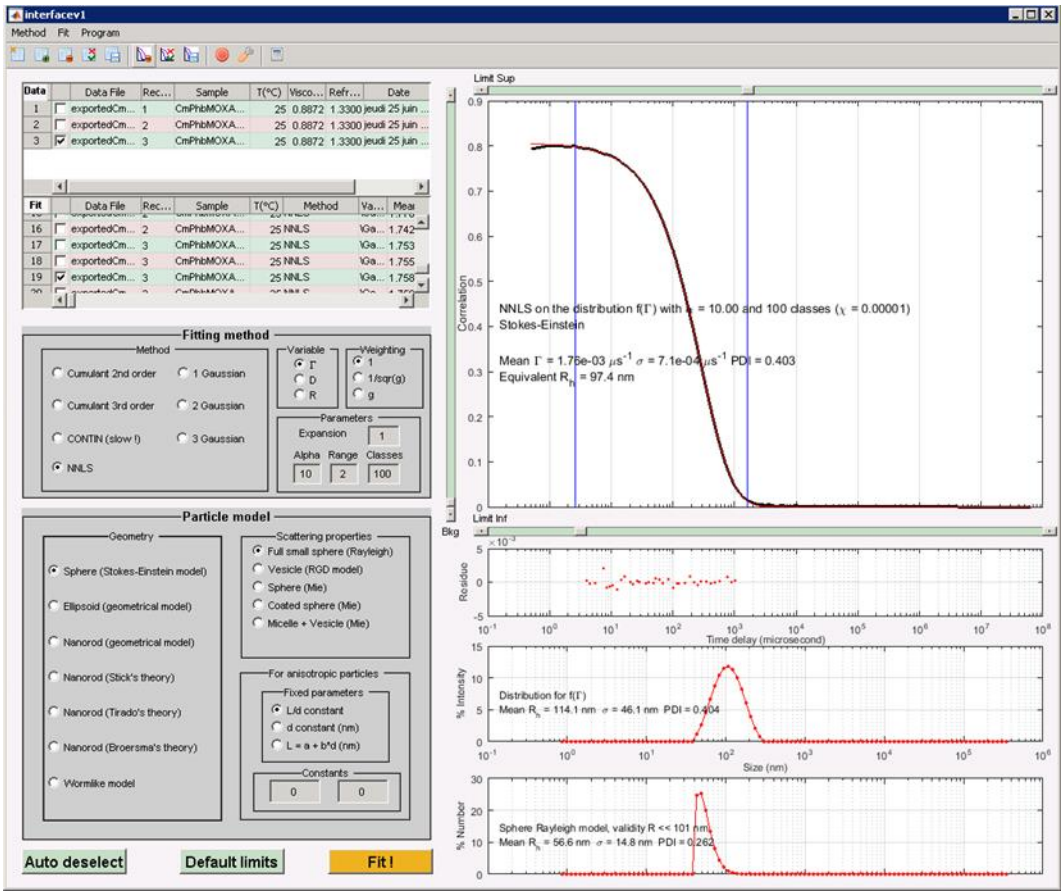


***Figure 2.7*** | *The main STORMS window in an example of analysis.*

In our research work at the SBNLab, multiangle DLS was performed on a ALV compact goniometer system, equipped with ALV-5000/EPP Correlator and special optical fiber detector, with He-Ne laser ($\lambda$ = 633 nm, 22 mW output power) as light source. The temperature was set at 25°C and controlled with a thermostatic bath. The volume used for the analysis was between 800 μl and 1 ml. DLS was measured at different scattering angles (70°, 90°, 110°, 130°). Each measure was the result of the average of three subsequent run of 10 seconds, with a threshold sensibility of 10%. Data analysis was done with ALV-Correlator software using CONTIN algorithm and the apparent hydrodynamic radius was obtained from an intensity weighted and a number weighted fitting of the autocorrelation function.

### 2.3.5 Transmission electron microscopy (TEM) and cryogenic transmission electron microscopy (cryo-TEM)

Transmission electron microscopy is a high magnification measurement technique able to produce images describing the structure and the morphology of materials at the nanometric scale, starting from a beam of electrons passing through the sample. Amplitude and phase variations in the transmitted beam give imaging contrast which depends on the sample thickness and on the sample material (heavier atoms scatter more electrons and therefore have a smaller electron mean free path than lighter atoms). TEM imaging has significantly higher resolution than light-based imaging techniques, because this technique uses electrons rather than light to illuminate the sample, and the wavelength of electrons is much shorter than that of light [61]. A common approach to increase contrast is the application of high-atomic-number stains (e.g. osmium tetroxide, ruthenium tetroxide, uranyl acetate, ammonium molybdate and phosphotungstic acid) which selectively bind to the grid (negative stanining) or to the particles (positive staining) [58].

TEM analyses were performed at the Centre de Microscopie Electronique Appliquée à la Biologie in Toulouse using a Hitachi HT7700 (Hitachi High Tech, Hitachinaka, Japan) microscope (accelerating voltage of 75 kV). Small amounts of aqueous samples were deposited onto a discharged copper grid (200 mesh) coated with a carbon membrane, left for 1–3 min depending on the solution, and gently dried with absorbing paper. A drop of uranyl acetate solution was deposited onto the grid for 10 seconds, and the grid was then dried under a lamp for at least 5 min. The process of preparation of the grids was performed by the technicians of the Centre, usually the day before the analysis of the samples.
At the SBNLab, TEM measurements were performed with Philips® CM200 Field Emission Gun with an electrons acceleration tension of 200 kV. The carbon coated copper grids (200

mesh) were prepared at the end of the procedure of formation of the self-assemblies, depositing 10-20 μl of solution and removing the excess with filter paper.
Several images were obtained for each sample, analysing different zones of the grids. A measurement of the mean size (as well as the standard deviation) was performed using the ImageJ software, considering between 200 and 300 nano-objects. Statistical analysis and plotting were performed using the Origin.Pro software.

Cryo-TEM is the most widely used technique to avoid sample dehydration before imagining by TEM, it allows the direct investigation of colloids in a frozen hydrated state, which is very close to their pristine state. This method provides a more precise assessment of size and shape than the one offered by conventional TEM [62]. In our research, cryo-TEM was done in collaboration with Dr. Stéphanie Balor, Microscopie Electronique Intégrative, Centre de Biologie Intégrative, Université Toulouse III Paul Sabatier, Toulouse, France.

### 2.3.6 Proton nuclear magnetic resonance ($^1$HNMR) spectroscopy

Nuclear Magnetic Resonance spectroscopy is a non-destructive analytical method used to determine the chemical structure and composition of almost any compounds exploiting the nuclear magnetic resonance property of some isotopes. Atoms with either atomic mass (A) or atomic number (Z) odd and atoms with both A and Z odd possess a non-null intrinsic angular momentum (called spin), when these isotopes are placed in an external static magnetic field the mean orientations and the energetic values of the dipole moment of the atoms will be affected. The dependence of the dipole moment $\mu$ on the spin $I$ is expressed in the following relation:

$$\mu = \gamma I = g\frac{q}{2m}I$$

Where $\gamma$ is the gyromagnetic ratio, defined as the ratio between magnetic moment and angular momentum, $g$ is the g-factor of the rotation, $q$ is the charge and $m$ is the mass of the atom.

The number of possible spin energetic states is equal to $(2I+1)$ so if $I$ is equal to ½, only two different orientations are possible: the atoms will orient parallelly or antiparallelly with respect to static magnetic field direction. These two states present an energy difference, which depend on the applied field and is usually in the radiofrequency (RF) range. During the analysis, the sample is placed inside the field of a large electromagnet and a RF field is applied. The magnetic field is increased and the excitation or "flipping" of the atoms from an orientation to the other is detected as an induced voltage, resulting from the absorption of energy from the RF field. An NMR spectrum is the plot of the induced voltage against the sweep of the field and from this spectrum the chemical structure of the sample can be deduced. The information is obtained from the value of the gyromagnetic ratio as well as the energy difference of the transitions, which are both depending on the element considered and on its chemical surrounding. In fact, the magnetic field experienced by the nucleus of the atoms in our sample is altered by the presence of electrons that can act as a "shield".

The most used isotopes in this analysis are $^{1}H$, $^{13}C$, $^{15}N$, $^{19}F$ and $^{31}P$. In the case of $^{1}$HNMR, considering any spectrum, the number of signal groups indicates the numbers of different proton environments, the chemical shift suggests the general environment of the protons (i.e. chemical bond), the multiplicity denotes how many protons are on adjacent atoms and the peak area represents the number of protons in each environment. Samples are dissolved in deuterated solvents which won't affect the spectrum except to provide a reference signal [63].

In our research project, we used $^{1}$HNMR spectra to verify the absence of residual solvent in the aqueous solutions of our self-assemblies prepared with cosolvent method and to

ascertain the occurrence of dimerization of the coumarin groups present on the polymeric chains. Samples were freeze-dried, dissolved in about 1 ml of deuterated chloroform, and inserted in 5mm NMR tubes; in same cases the sample were directly prepared in deuterated water to be directly analysed without drying. NMR spectra were recorded on 300 or 400 MHz Bruker spectrometers and consequently analysed with Bruker TopSpin software in France and MestreNova in Italy.

### 2.3.7 Protein corona analysis – centrifugation, gel electrophoresis, and stability analysis

The most widely used approach to simplify studies of protein–NP interactions in the body and the effects of the protein corona formation on the nano-objects is to expose NPs to biological fluids (e.g., human serum, human plasma, and fetal bovine serum) *in vitro*. Such *in vitro* studies are a convenient medium for preliminary studies on protein corona formation. [64]. Our aim was to investigate the presence of a definite protein corona to confirm the absorption of proteins and evaluate the possible change in size of the NPs.

Choosing a method for the isolation of particles with their corona proteins from a protein-rich matrix, for example a cell culture medium containing bovine serum, is a critical step. In fact, the separation has a major influence on the results and their interpretation, as it decides which proteins can be identified as part of the corona. False positive or false negative results may be obtained due to association or dissociation of proteins from the corona due to physical or chemical interactions occurring during the isolation and purification process. Considering the literature, isolation methods are not standardized and it remains unclear whether the most appropriate isolation strategy for the particular scenario investigated has been chosen based on in-depth pre-testing and procedure

optimization. Moreover, it should be taken into account that most model matrices reproduce the *in vivo* environment only to a limited degree [37].

*Centrifugation and ultracentrifugation*

In our research work we selected the most common method for separating particles and their protein corona from a matrix, meaning centrifugation and ultracentrifugation. Figure 2.8 summarizes the aspects to consider when setting up a centrifugation-based separation method. Given the preliminary nature of the study no optimization process was performed, basing the choice of the various parameters on previous literature [37-39].

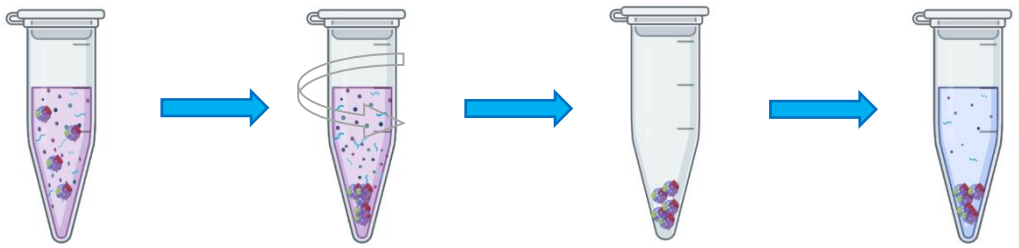

Parameters: particle species centrifugation speed number of washing steps
incubation medium centrifugation time buffer
incubation time centrifugation temperature
incubation temperature gradient

***Figure 2.8*** | *General workflow comprising repeated washing and centrifugation steps: preparation and incubation of the sample is followed by centrifugation, separation of pellet and supernatant solution and washing of the pellet (resuspension). Below is reported the selection of parameters to be considered when conducting centrifugation experiments for protein corona analysis.*

Once the solution is under centrifugation a particle is subject of three main forces: centrifugal, buoyant and frictional.

$$F_c = \rho_p V \omega^2 r$$

$$F_b = -\rho_f V \omega^2$$

$$F_f = fv$$

Where $\rho_p$ and $\rho_f$ are the densities of the particles and of the fluid, $V$ is the volume of the particle, $\omega$ the angular velocity, $r$ the distance between the particle and the axis of rotation, $f$ the frictional coefficient (dependent on size and shape of the particle) and $v$ the velocity of the particle. Particles with different shape and size move at different velocities, but when the forces are balanced ( $F_c + F_b = F_f$), they will sediment with a constant velocity:

$$v = \frac{V(\rho_p - \rho_f)\omega^2 r}{f}$$

A variation to classic centrifugation methods consists in the use of sucrose cushions, useful to reduce the interaction time between NPs and media: unbound proteins are kept separated and agglomerates tend to float above the cushion. The sucrose cushion can be used either as a homogeneous sucrose solution with a defined concentration or as a gradient; the latter alternative allows the gathering of different fractions of NP-corona complexes; which can be analysed separately.

For low-density particles, ultracentrifugation in combination with a sucrose cushion is the method of choice. Ultracentrifugation can spin to as much as 150000 rotations per minute (rpm) (equivalent to 1000000×g), and it can be divided into analytical and preparative ultracentrifugation. Analytical ultracentrifugation allows monitoring concentration of the analyte in the sample in real time, providing data about sedimentation properties and size distribution. Preparative or sequential centrifugation has been used to achieve a precise separation of particle-corona complexes [37,39].

Our samples were diluted 1:2 (final concentration 1.25 mg/ml) in filtered phosphate buffered saline (PBS) (RC 0.2 μm) with 10% of fetal bovine serum (FBS), then incubated for 1 hour at 37°C and 95% relative humidity (RH) [37]. This first step was common for all the analyses on the protein corona. The samples were added to a 0.7 M sucrose cushion

solution, which was then centrifuged for 30 minutes at 18000×g and 4 °C and washing with filtered PBS; centrifugation and washing were both repeated 3 times [38]. DLS analysis was performed both on resuspended samples and the supernatant solutions to verify the presence of NPs complexes.

Ultracentrifugation with sucrose gradient was performed by Dr. Beatrice Lucia Bona at the laboratories of IRCCS (Institutes for comprehensive cancer patient care and research) Humanitas Cancer Center. Centrifugation polypropylene tubes (Beckman Coulter) of 13 ml were prepared carefully layering 1 ml solutions of sucrose in water from the most to the less concentrated one; starting from a stock sucrose solution of 30% wt, other 10 solutions were obtained through different dilutions; the tube containing sucrose density gradient was left to equilibrate overnight to create a continuum gradient.

Before centrifugation, 0.7 ml of the polymer NP dispersion was added to the tube on the top of the gradient. Ultracentrifugation was performed for 1 hour at 60000×g and 20 °C. Once finished, aliquots of 1 ml were carefully collected from the top to the bottom of the tube. Dialysis was performed on all the layers with pieces of Spectra/Por® 6 Dialysis Membrane, pre-wetted RC tubing (MWCO 2 kD) closed with zip-ties to remove sucrose. They were left overnight at 4°C.

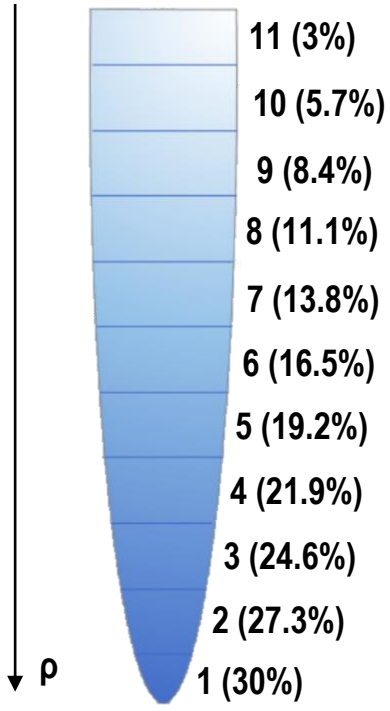


***Figure 2.9*** | *Representation of the tube containing a sucrose gradient divided into layers of different densities. From the bottom with the highest density up to the top where the least dense layer.*

*Gel electrophoresis*

Electrophoresis is used to separate proteins and nucleic acids from a mixture based on their molecular weight. In particular, SDS-PAGE (sodium dodecyl sulphate–polyacrylamide gel electrophoresis) is a discontinuous electrophoretic procedure developed by Ulrich K. Laemmli, which is commonly used as a method to separate proteins with molecular masses between 5 and 250 kDa. The combination of SDS and polyacrylamide gel eliminates the influence of structure and charge, such that the proteins are solely separated on the basis of different molecular weights. Protein elution and separation via SDS-PAGE allows the direct visualization and qualitative comparison of stained protein patterns [38,65,66]. In our research work, electrophoresis was performed on a BioRad Mini-PROTEAN® Tetra system following the protocol presented in figure 2.10. A Precision Plus Protein™ Standard All Blue purchased from BioRad was used as protein marker for the electrophoresis.

**Stacking Buffer (4X):** 1 l

- 60.5 g TRIZMA BASE®
- 4 g SDS
- Set pH = 6.8 with pure HCl

**Running Buffer (4X):** 1 l

- 182 g TRIZMA BASE®
- 4 g SDS
- Set pH = 8.8 with pure HCl

**Cathode Buffer (Tris-Glycine pH 8.3):** 1 l

- 1.5 g TRIZMA BASE®
- 14.3 g Glycine
- 1 g SDS

**Anode buffer (Tris-HCl, pH 8.8):** 1l (5X)

- 227 g TRIZMA BASE®
- Set pH = 8.8 with pure HCl (about 40 ml)

**Solution to prevent bubbles in the gel:**

- Water + Butanol (1:1)

**Running gel 12%**

- 1.5 ml Acrylamide/Bis-acrylamide (40%)
- 1.25 ml Running Buffer 4X
- 2.24 ml water
- 10 µl APS
- 8 µl Temed

**Stacking gel:**

- 200 µl Acrylamide/Bis-acrylamide (40%)
- 500 µl Stacking Buffer 4X
- 1.29 ml water
- 8 µl APS
- 4 µl Temed

PREPARATION OF THE GEL

Put two glass slide (1 mm) on the support.
Prepare the running gel.
Pour the gel between the slides in order to fill up to ¾ of their height.
Add the solution to prevent bubbles.
Leave to polymerize about 30 minutes.
Eliminate the solution and wash with water.
Dab the cavity between the slides with filter paper to remove water.

Prepare the stacking gel.
Pour the stacking gel between the slides.
Insert the comb for the formation of the wells.
Leave to polymerize about 1 hour and a half.

PREPARATION OF THE SAMPLES

5 µl of mercaptoethanol were added to 15 µl of sample.
Put at 99°C for 5 minutes.

LOADING OF THE SAMPLES

Remove the slides from the support and put in the support
of the electrophoretic cell.
Pour cathode buffer in the central part of the cell until it overflows.
Remove the comb.
Load the samples in the wells. Load 4 µl of protein marker in the first one.
Pour 500 ml of anode buffer (100 ml of buffer 5X + 400 ml of water)
in the external part of the electrophoretic cell.

ELECTROPHORETIC RUN

Connect the cell to power.

- 50 V for 20 minutes
- 100 V for 40 minutes
- 150 V for 4 hours (or 200 V to force the electrophoretic run)

Remove the gel from the slides and proceed with staining.

***Figure 2.10*** | *Protocol of gel electrophoresis.*

Beforehand the samples were concentrated from 1 ml to 20 µl using Corning® Spin-X® UF concentrators, 100K MWCO purchased from Sigma-Aldrich.

The gels were consequently stained with 2D-Silver Stain Reagent II purchased from Cosmo Bio Co.,Ltd following the procedure provided by the company.

*Stability analysis*

The formation of a protein corona can cause a critical issue, meaning particle destabilization, which completely undermines the effectiveness in nanomedicine. Hence, estimating the colloidal stability of polymeric NPs in biological environments is fundamental for an optimal design and to clarify the fate of these devices after administration [67,68]. In our work, the stability of the objects was evaluated by DLS analysis registering the change of the hydrodynamic radius of the NPs in a solution of PBS (dilution 1:2) in presence of 10%FBS. After the incubation step, DLS analysis was performed after 1 hour, 4 hours and 24 hours maintaining the sample at 37°C and RH = 95%.

# 3. Experimental results

## 3.1 Introduction

As explained above, the aim of this projects was the development and assessment of new nanovectors for PDT based on poly(2-oxazoline). In the first part of the work the procedure for the formation of the nano-objects ideated in the previous study [52] was optimized and a different procedure was tested for the newly synthesized polymers. Once formed, the NPs were characterised with DLS and TEM, investigating the differences in size, size distribution and morphology depending on numerous factors: molecular weight and composition of the poly(2-oxazoline), molecular weight and composition of the stabilizing poly(alkyl methacrylate), method of formation and solvent used. The stability of the nano-objects over about a month from the formation was also measured with DLS and TEM. Cryo-TEM images were obtained for the more promising formulations.

Crosslinking was performed on both polymers together with a different stabilizing poly(alkyl methacrylate), but the process was not further optimized.

In the second part, one poly(2-oxazoline) and one poly(alkyl methacrylate) were selected to carry out protein corona analysis. Firstly, one formulation procedure was selected and optimized to replicate the same results obtained in both laboratories. Then, changes in the NP size and size distribution in presence of a biological fluid were evaluated isolating the PC complexes through different techniques (centrifugation, ultracentrifugation and gel electrophoresis). Stability of both crosslinked and non-crosslinked nanovectors was also assessed.

## 3.2 Nanoparticle formation and characterization

The nanovectors are formed by an amphiphilic poly(2-oxazoline) which spontaneously self-assembles in water. For each of the three poly(2-oxazolines) studied, two different methods of formation were employed: cosolvent method and film rehydration method. In agreement with previous studies [47,52], a second polymer was also added to the formulations: ideally this poly(alkyl methacrylate) is encased by the self-assemblies (see Figure 2.3) during formation and, once irradiated with UV-light, allows the crosslinking of the nanovectors.

In the next pages, the results obtained with cosolvent method are reported first, followed by the ones of film rehydration method; for both methods the analyses of the two amphiphilic polymers containing only methyloxazoline (*Coum* – $C_{11}$ – $(MOx)_n$) are presented before the ones of the polymer containing the additional hydrophobic block of phenyloxazoline (*Coum* – $C_{11}$ – $(PhOx)_{27}$ – *b* – $(MOx)_{59}$).

### 3.2.1 Cosolvent method

As reported before, the protocol of this method was implemented with different solvents, mainly to solve the issue of poor solubility of *CmPMMA* in acetone, but also to study the influence of the solvent on dimension and shape of the self-assemblies. The selected alternatives were dichloromethane ($CH_2Cl_2$), *N*,*N*-dimethylformamide (DMF) and tetrahydrofuran (THF). *CmPMMA* showed good solubility in all three, forming clear solutions. Upon dropwise addition of dissolved *CmPMMA* to water or the aqueous solution of the amphiphilic polymer, the latter turned increasingly more turbid, however, none of the formulations presented precipitate or visible aggregates in suspension. Being not miscible with water, $CH_2Cl_2$ separated on the surface of the solution; the analyses confirmed the formation of self-assemblies, but it has to be taken into consideration that the results

refer to the solution under the layer of $CH_2Cl_2$ on the surface. Moreover, for the systems prepared with *Coum – $C_{11}$ – (PhOx)$_{27}$ – b – (MOx)$_{59}$* the formation of white precipitate was observed after about a day. THF and DMF were miscible with water, but presented the drawback of requiring dialysis to eliminate the solvent: up to five days were needed in spite of the small volume present. The solutions were analysed both with DLS and TEM and the results were compared to the ones obtained with acetone. The absence of solvent in the final solution was confirmed by $^1$HNMR analysis.

Table 3.1 is a summary of all the combination of amphiphilic polymers, stabilizing poly(methyl methacrylates) and solvents.

| **Amphiphilic polymer** | **Stabilizing polymer** | **Solvent used** | | | |
|---|---|---|---|---|---|
| | | **Acetone** | **$CH_2Cl_2$** | **DMF** | **THF** |
| *CmPOx15* | *CmPMMA* | √ | √ | √ | √ |
| *CmPOx59* | - | - | - | - | - |
| | *CmPMMA* | √ | - | - | - |
| | *CmPMA20:80* | √ | - | - | - |
| | *CmPMA50:50* | √ | - | - | - |
| | *CmPMA80:20* | - | √ | √ | - |
| *CmPhOx27:59* | - | √ | √ | √ | - |
| | *CmPMMA* | - | √ | √ | - |
| | *CmPMA20:80* | √ | - | - | - |
| | *CmPMA50:50* | √ | - | - | - |

***Table 3.1*** | *Summary of the solvents used with the different polymers.*

*Coum – $C_{11}$ – $(MOx)_n$*

The two poly(2-methyl-oxazolines) which were investigated presented the same structure and composition, with different degree of polymerization and molecular weight [Figure 3.1].

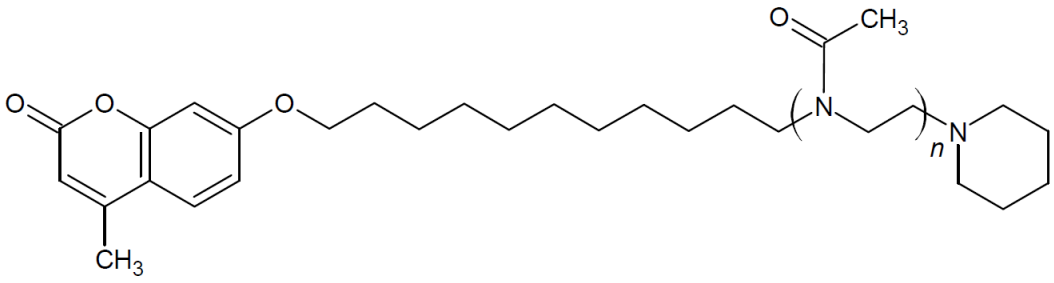


***Figure 3.1*** | *The chemical structure of the amphiphilic poly(2-methyl-oxazolines) "CmPOxn".*

Since no conspicuous difference was observed in the analyses of both poly(2-methyl-oxazolines) using the same stabilizing polymer and the same solvent, the results are presented together. The pictures of the DLS and TEM results presented in the following paragraphs belong to *CmPOx59/CmPMMA* systems, all the others are reported in the appendixes.

***CmPOx59 alone***

The poly(2-methyl-oxazoline) synthesised by the ICGM lab (*CmPOx59*) forms self-assemblies by direct dissolution in filtered water. DLS results [Figure 3.2] suggested the presence of multiple populations, but only the presence of a population of size around 10 nm was registered in TEM images [Figure 3.3]. This is the most abundant population as suggested by the values of the number weighted hydrodynamic radius [Table 3.2].

***CmPOxn/stabilizing polymer***

The systems of poly(2-oxazoline) together with *CmPMMA* prepared with acetone were similar to the ones without stabilizing polymer in the TEM images [Figure 3.3] while DLS

analyses registered a population of quite larger size [Figure 3.2 and Table 3.2]. Also these results are consistent with previously obtained ones [52], since DLS is much sensitive to the presence of even a small number of big size objects.

The alternative solvents influenced the size of the self-assemblies [Table 3.2]. The comparison between correlation functions obtained with DLS analysis varying the solvent while preparing *CmPOx15*/*CmPMMA* systems is reported in figure 3.4.

THF was used only in the case of *CmPOx15*/*CmPMMA*: it seemed to lead to the formation of highly disperse nano-objects with the presence of very big aggregates [Figure A.1 in Appendix A and Table 3.2] and it was comparable to DMF in toxicity and mean of elimination.

For both *CmPOx*, samples prepared with $CH_2Cl_2$ were quite polydisperse (see PDI from DLS measurements in Table 3.2 and Figure 3.2 and A.1) and presented rather big agglomerates (~1 μm) together with smaller nano-objects, probably the most abundant population, which is thw only one observed in TEM with a mean size around 10 nm. The results obtained with DMF were the most promising ones given low PDI in comparison with the other solvents [Table 3.2]. The size of the nano-objects in the TEM images [Figure B.1 and 3.3] was quite larger (up to 100 nm) with a wide distribution. A second population of smaller size (~5 nm) seemed to be present in the TEM images of the samples of *CmPOx59*/*CmPMMA*, but not in the TEM images of *CmPOx15*/*CmPMMA* [Figure 3.3]. It is important to underline that the presence of different sizes of self-assemblies is a feature of interest, in fact some mixtures of nanovectors were found to have comparable or even higher PDT efficiency compared to monomorphous systems [48].

In the case of *CmPOx59*, *CmPMMA* was replaced by the new poly(ethylhexil methacrylates) synthesized by Specific Polymers [Figure B.2], *CmPMA20:80* and *CmPMA50:50* seemed to slightly increase the dimensions of the bigger nano-objects in solution. Once again, the most abundant population is poorly visible in DLS, but it is observed in the dry state of TEM

[Figure B.2 and Table 3.2] and the stabilizing polymer containing more coumarin units seems to induce formation of bigger nano-objects (20 nm versus 13 nm). Regarding *CmPMA80:20*, the dispersity of the nano-objects was clearly influenced as before by the use of the solvents $CH_2Cl_2$ and DMF in the formulation [Figures A.2, B.2 and Table 3.2].

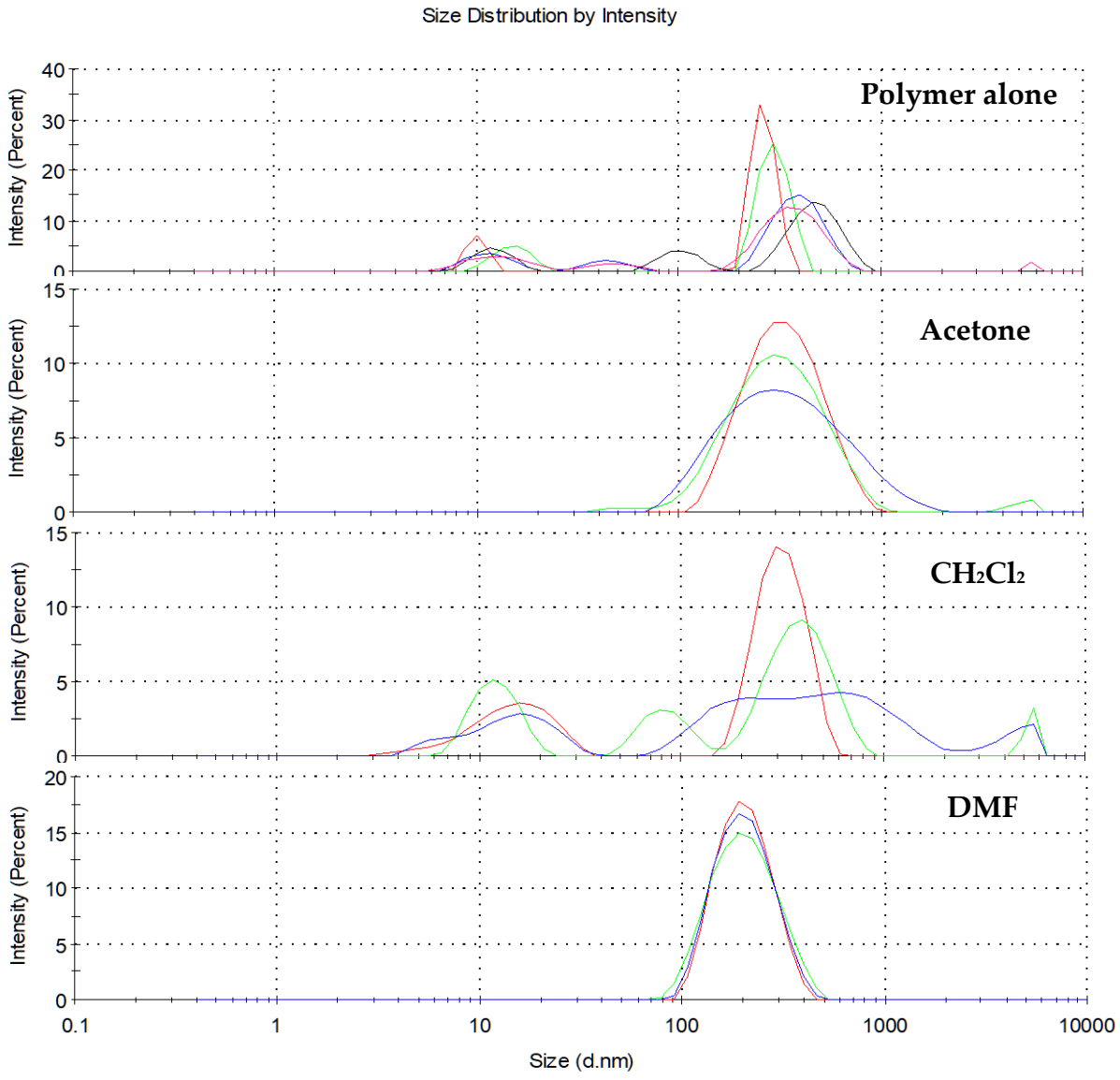


***Figure 3.2*** | *Intensity-weighted size distribution for CmPOx59 and CmPOx59/CmPMMA self-assemblies prepared with different solvents.*

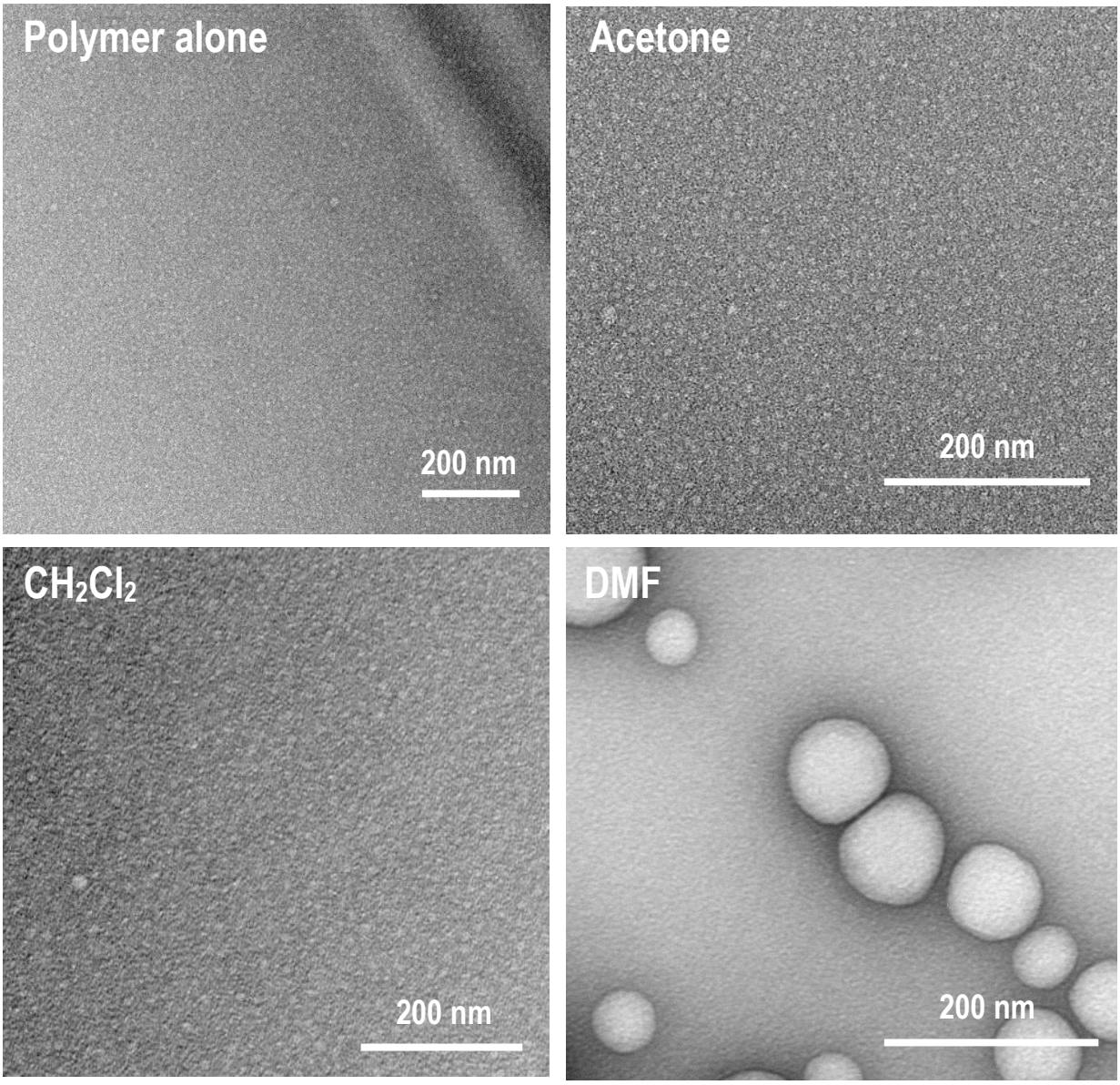


***Figure 3.3*** | *TEM images of the solutions of CmPOx59 alone (up left), of CmPOx59/CmPMMA prepared with acetone (up right), of CmPOx59/CmPMMA prepared with $CH_2Cl_2$ (bottom left) and of CmPOx59/CmPMMA prepared with DMF (bottom right).*

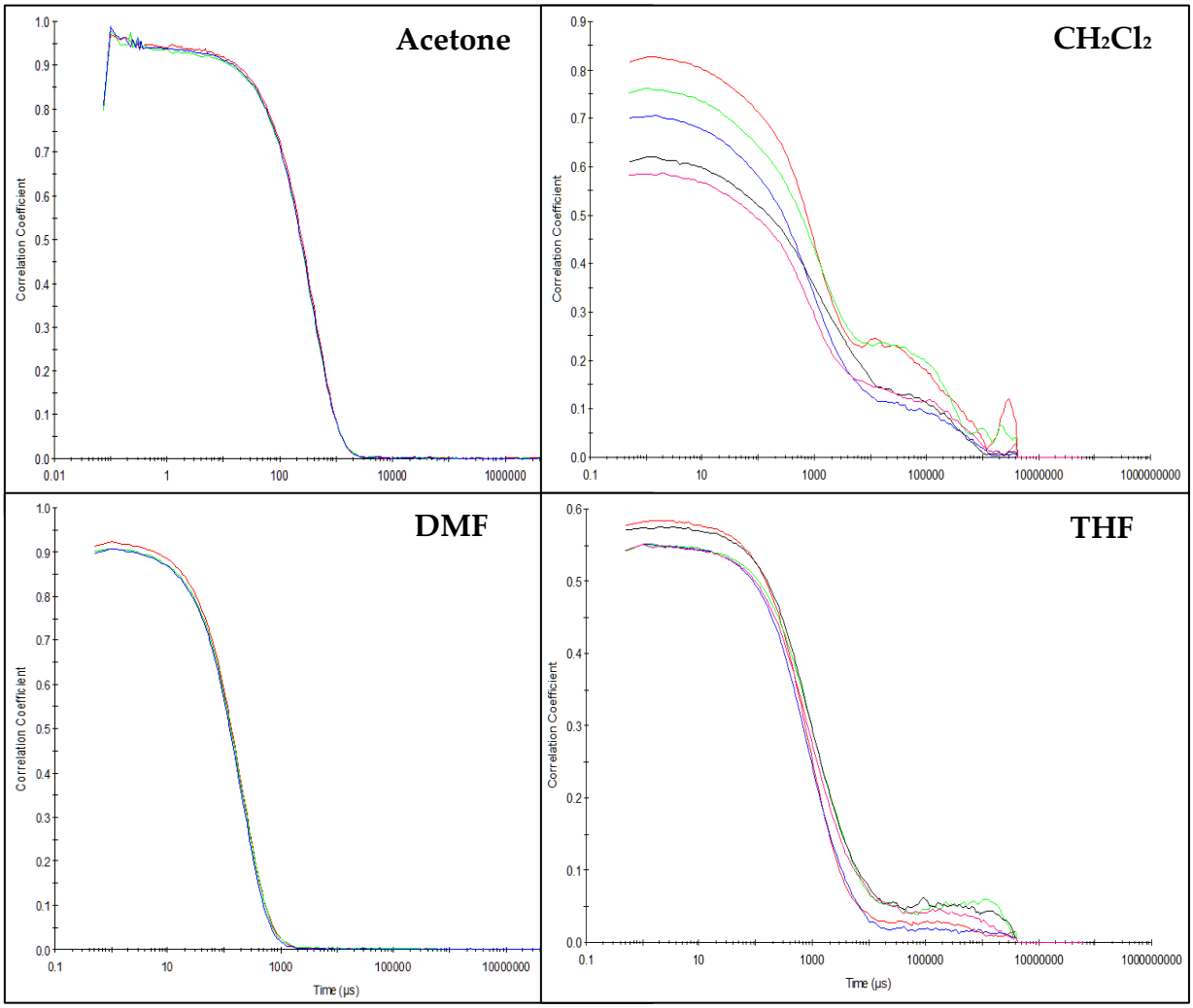


***Figure 3.4*** | *Comparison of the correlation functions between the four solvents for CmPOx15/CmPMMA systems. Different colours indicate different runs, which was increased from 3 to 5 in case of unconventional shape of the curve.*

| | | DLS | | | | TEM |
|---|---|---|---|---|---|---|
| | | **Size [nm] int** | **PDI** | **Size [nm] num** | **PDI** | **Size [nm]** |
| *CmPOx59* alone | - | 610 | 1.35 | 18 | 0.16 | 10 ± 2 |
| *CmPOx15/ CmPMMA* | **Acetone** | 340 | 0.36 | 180 | 0.25 | 15 ± 4 |
| | **$CH_2Cl_2$** | 1026 | 2.65 | 11 | 0.25 | 23 ± 5 |
| | **DMF** | 165 | 0.35 | 97 | 0.24 | 44 ± 25 |
| | **THF** | 938 | 1.56 | 265 | 0.45 | 10 ± 4 |
| *CmPOx59/ CmPMMA* | **Acetone** | 330 | 0.43 | 180 | 0.35 | 9 ± 2 |
| | **$CH_2Cl_2$** | 28/496 | 1.56 | 12 | 0.18 | 7 ± 1 |
| | **DMF** | 202 | 0.25 | 147 | 0.21 | 5 ± 1/ 83 ± 30 |
| *CmPOx59/ CmPMA20:80* | **Acetone** | 722/828 | 0.45 | 120/305 | 0.40 | 13 ± 2 |
| *CmPOx59/ CmPMA50:50* | **Acetone** | 592 | 0.51 | 276 | 0.35 | 28 ± 5 |
| *CmPOx59/ CmPMA80:20* | **$CH_2Cl_2$** | 24/793 | 1.78 | 10 | 0.28 | 12 ± 2 |
| | **DMF** | 349 | 0.40 | 195 | 0.25 | 11 ± 2/ 300 ± 86 |

***Table 3.2*** | *Characterization of CmPOx15/CmPMMA, CmPOx59 alone and CmPOx59/stabilizing polymer self-assemblies: mean hydrodynamic diameter and PDI (intensity weighted in the third and fourth column, number weighted on the fifth and sixth column)) from DLS analysis, mean diameter from TEM analysis.*

*Coum – $C_{11}$ – $(PhOx)_{27}$ – b – $(MOx)_{59}$*

The other poly(2-oxazoline) synthesized at ICGM lab and analysed in this research work included a long chain of phenyloxazoline units [Figure 3.5].

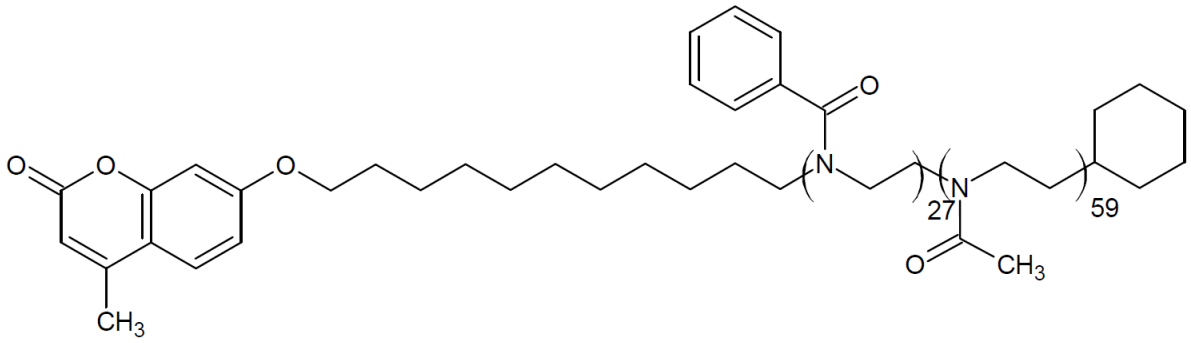


***Figure 3.5*** | *The chemical structure of the amphiphilic poly(2-phenyl-2-methyloxazoline) "CmPhOx27:59".*

The pictures of the DLS and TEM results presented in the following paragraphs belong to *CmPhOx27:59* systems, all the others are reported in the appendixes.

***CmPhOx27:59 alone***

The polymer seemed to solubilize in all the three solvents utilized, however, the slightly turbid appearance of the preparation, especially in the case of acetone, suggests the formation of a suspension rather than a solution. White precipitate at the end of the process was observed only in the case of $CH_2Cl_2$.

DLS measurements [Figure 3.6 and Table 3.3] reported the presence of a population of size around 100 nm and of another of slightly smaller size only in the case of $CH_2Cl_2$ (about 30 nm). As in the case of *CmPOx* described above, samples prepared $CH_2Cl_2$ appeared to be more polydisperse, while the ones formulated with DMF registered a slight decrease in the intensity weighted dimensions. These results were mirrored in the TEM images [Figure 3.7]: the presence of a wide array of objects was observed in the respective TEM images of the samples solubilized in $CH_2Cl_2$ and in DMF, but no evidently distinct populations could

be detected. The change of solvent also imparted a modification of the morphology of the self-assemblies, which did not resemble anymore sphere-like particles. This is particularly true for $CH_2Cl_2$ where worm-like objects have been observed. In the case of acetone preparation, two populations are clearly present, definitely smaller than those observed in DLS measurements.

The solution of *CmPhOx27:59* alone prepared with acetone was also analysed with cryo-TEM by Dr. Stéphanie Balor at the laboratory of Microscopie Electronique Intégrative, Centre de Biologie Intégrative, Université Toulouse III Paul Sabatier in Toulouse. These images [Figure 3.8] showed a wide and diverse distribution of nano-objects with dimensions similar to the population of larger size present in TEM images and quite consistent with the values measured with DLS. The average measured size was 40 ± 17 nm.

***CmPhOx27:59/stabilizing polymer***

Adding *CmPMMA*, the use of $CH_2Cl_2$ entailed the previously reported issue of miscibility, very polydisperse nano-objects and appearance of precipitate, and in the TEM images [Table 3.3 and Figure B.3] two distinct populations (much smaller in size) were detected. Both the formulation based on acetone and DMF produced comparable results to the ones obtained without *CmPMMA*, detecting only a very small increase in DLS size [Figure A.3 and Table 3.3]. TEM images show the presence of two distinct populations, similar to the ones observed with $CH_2Cl_2$. The solution of *CmPhOx27:59*/*CmPMMA* prepared with acetone was also analysed with cryo-TEM: in presence of *CmPMMA* there appeared to be a more distinctive difference between a smaller and a bigger population [Figure 3.8], the first of size lower than 50 nm, while the second quite larger. The average measured size was 28 ± 23 nm.

With the addition of *CmPMA20:80* and *CmPMA50:50*, DLS results didn't change drastically with respect to the *CmPhOx27:59*/*CmPMMA* self-assemblies. The sizes measured on TEM

pictures, instead were definitely larger, and in the case of the poly(ethylhexyl methacrylate) containing more coumarin units only the bigger population was detected [Figure B.3].

Differently from *CmPOx59*, in this case the use of differing stabilizing polymers influenced the morphology of the nano-objects, worm-like self-assemblies seemed to be present, at least in the dry state analysed with TEM.

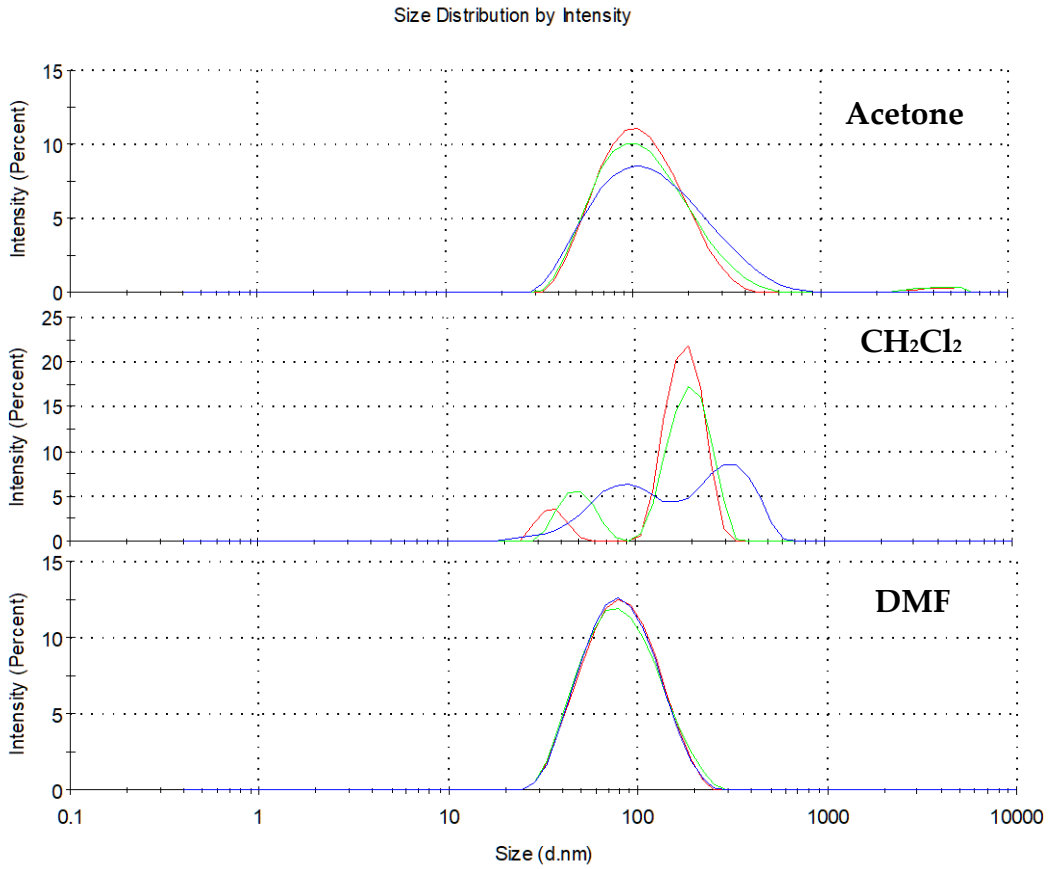


***Figure 3.6*** | *Intensity-weighted size distribution for CmPhOx27:59 self-assemblies prepared with different solvents.*

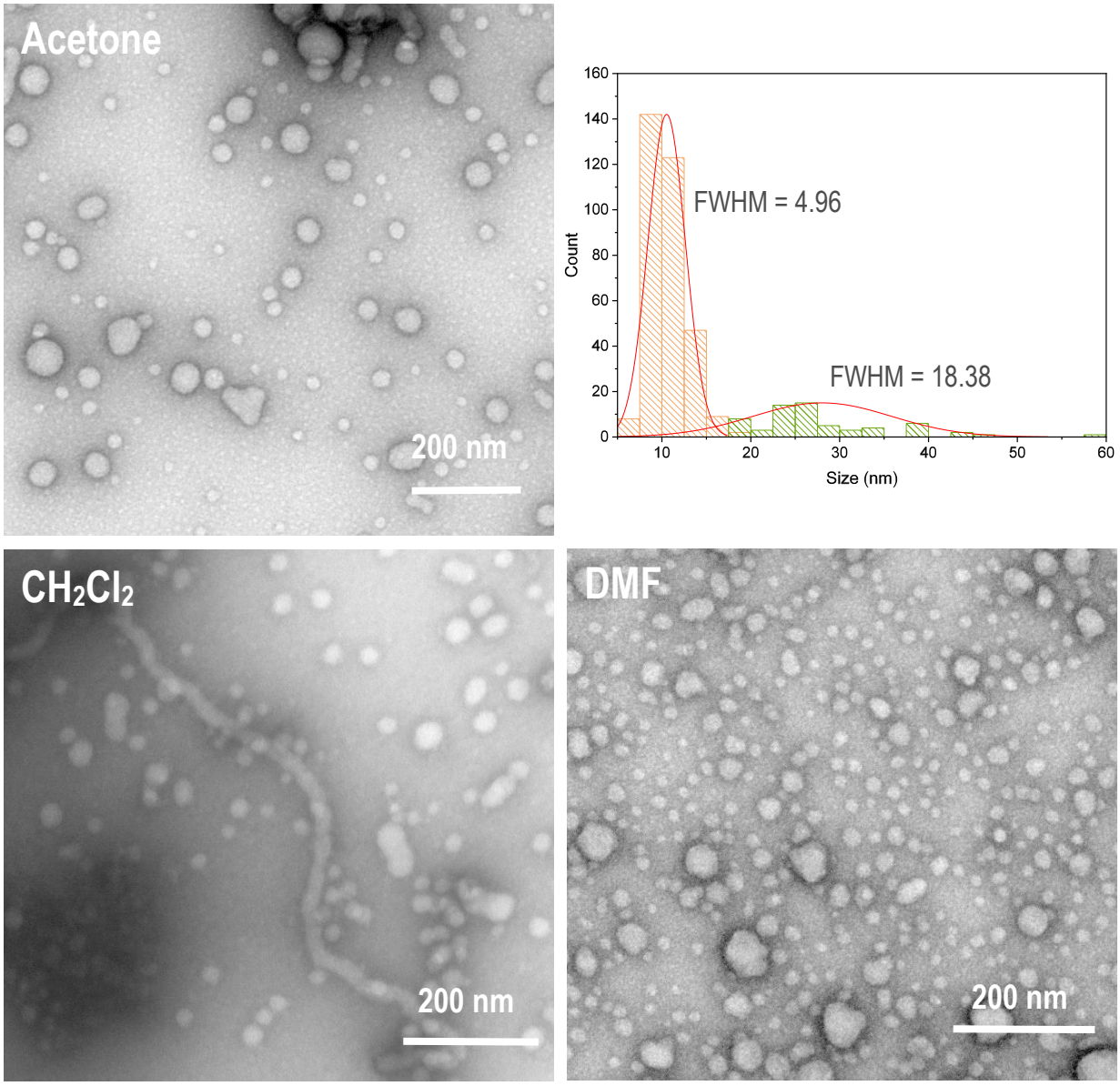


***Figure 3.7*** | *TEM images of the solutions of CmPhOx27:59 prepared with acetone (up left), with $CH_2Cl_2$ (bottom left) and with DMF (bottom right). On the up right a typical statistical analysis of the size distribution of a solution of CmPhOx27:59 prepared with acetone. FWGH stands for Full Width Half Maximum.*

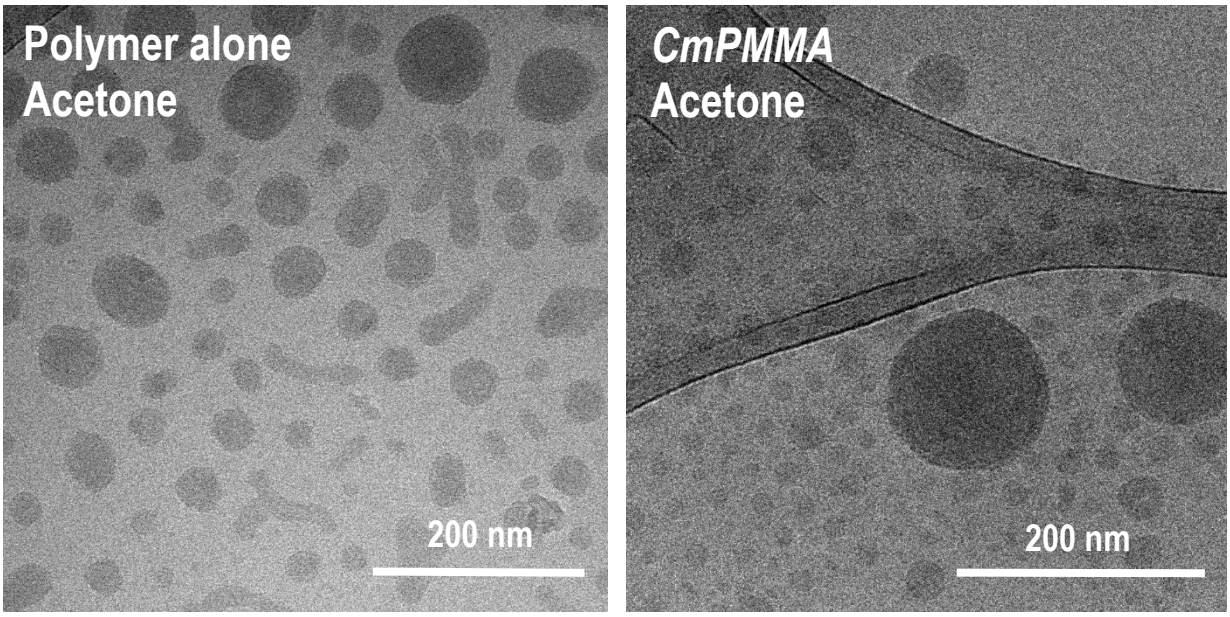


***Figure 3.8*** | *Cryo-TEM image of the solution of CmPhOx27:59 (left), CmPhOx27:59/CmPMMA (right) both prepared with acetone cosolvent method.*

| | | DLS | | | | TEM |
|---|---|---|---|---|---|---|
| | | **Size [nm] int** | **PDI** | **Size [nm] num** | **PDI** | **Size [nm]** |
| *CmPhOx27:59* alone | **Acetone** | 123 | 0.36 | 71 | 0.24 | 11 ± 3/ 29 ± 10 |
| | **$CH_2Cl_2$** | 510 | 1.83 | 50 | 0.30 | 25 ± 8 |
| | **DMF** | 80 | 0.31 | 50 | 0.24 | 19 ± 8 |
| *CmPhOx27:59/ CmPMMA* | **Acetone** | 209 | 0.29 | 115 | 0.33 | 10 ± 2/ 29 ± 7 |
| | **$CH_2Cl_2$** | 290 | 0.86 | 60 | 0.29 | 7 ± 2/ 25 ± 6 |
| | **DMF** | 175 | 0.32 | 110 | 0.24 | 8 ± 2/ 23 ± 6 |
| *CmPhOx27:59/ CmPMA20:80* | **Acetone** | 228 | 0.40 | 114 | 0.26 | 27 ± 6/ 56 ± 15 |
| *CmPhOx27:59/ CmPMA50:50* | **Acetone** | 252 | 0.28 | 115 | 0.41 | 23 ± 6 |

***Table 3.3*** | *Characterization of CmPhOx27:59, CmPhOx27:59/CmPMMA, CmPhOx27:59/CmPMA20:80 and CmPhOx27:59/CmPMA50:50 self-assemblies.*

### 3.2.2 Film rehydration method

The results reported in this section refer to the systems obtained using methanol in the procedure of preparation, the results given by employing chloroform and acetone are presented in the section of protein corona analysis.

#### *Coum – $C_{11}$ – $(MOx)_n$*

*CmPOx15* was tested together with *CmPMMA*, while *CmPOx59* was tested alone and together with *CmPMMA* and *CmPMA80:20*. As before the results for the systems in presence of stabilizing polymer are presented together for both poly(2-methyl-oxazolines).

***CmPOx59 alone***

For the polymer alone, DLS showed the presence of a predominant population of size between 10 and 20 nm, however, for this experiment the count rate was surprisingly low and analysis of the data with the STORMS software could not be implemented. TEM showed the clear presence of two populations of different size both with relatively narrow size distribution [Table 3.4]. It must be noted that this process produces less polydisperse solutions with less abundant big nano-objects than those obtained for the same polymer directly dispersed in water.

***CmPOxn/stabilizing polymer***

For *CmPOx15*/*CmPMMA* systems DLS results registered the presence of large nano-objects together with a population of size around 10 nm [Figure 3.9 and Table 3.4]. TEM apparently confirmed the presence of this small population. The shape and appearance of the self-assemblies was comparable to the one obtained with the acetone cosolvent method [Figure 3.10].

The DLS results obtained with *CmPOx59* were consistent with each other whichever the stabilizing polymer used: polydisperse solutions presenting one population at about 10 nm together with bigger populations [Figure 3.9]. The small more abundant population was detected on TEM pictures [Figure 3.10]. A second population with few and quite far apart objects was observed with *CmPMMA*. This population was characterized by a much wider distribution with respect to the one observed in the absence of *CmPMMA*.

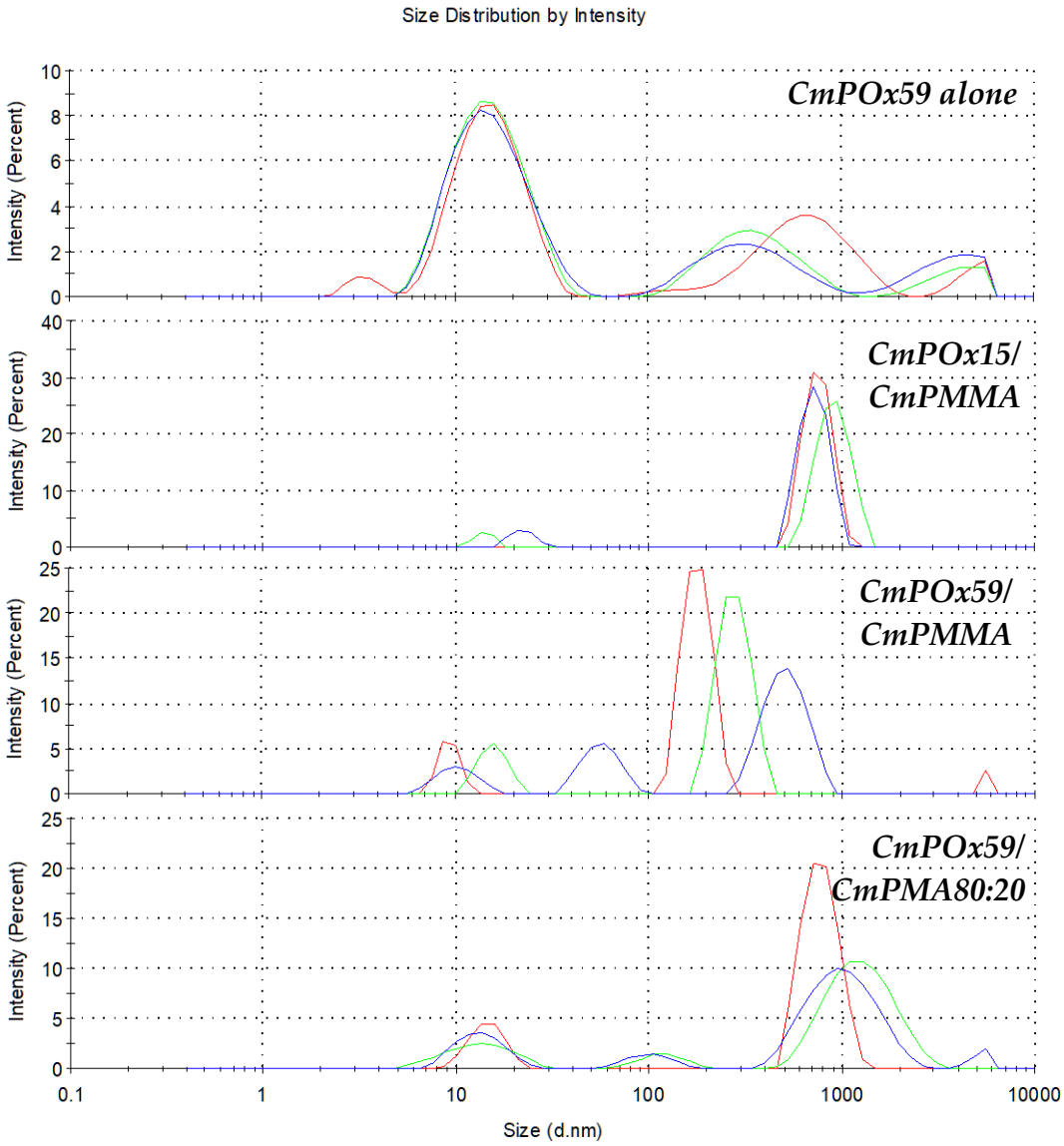


***Figure 3.9*** | *Intensity-weighted size distribution for CmPOx59, CmPOx15/CmPMMA, CmPOx59/CmPMMA and CmPOx59/CmPMA80:20 self-assemblies prepared with film rehydration method.*

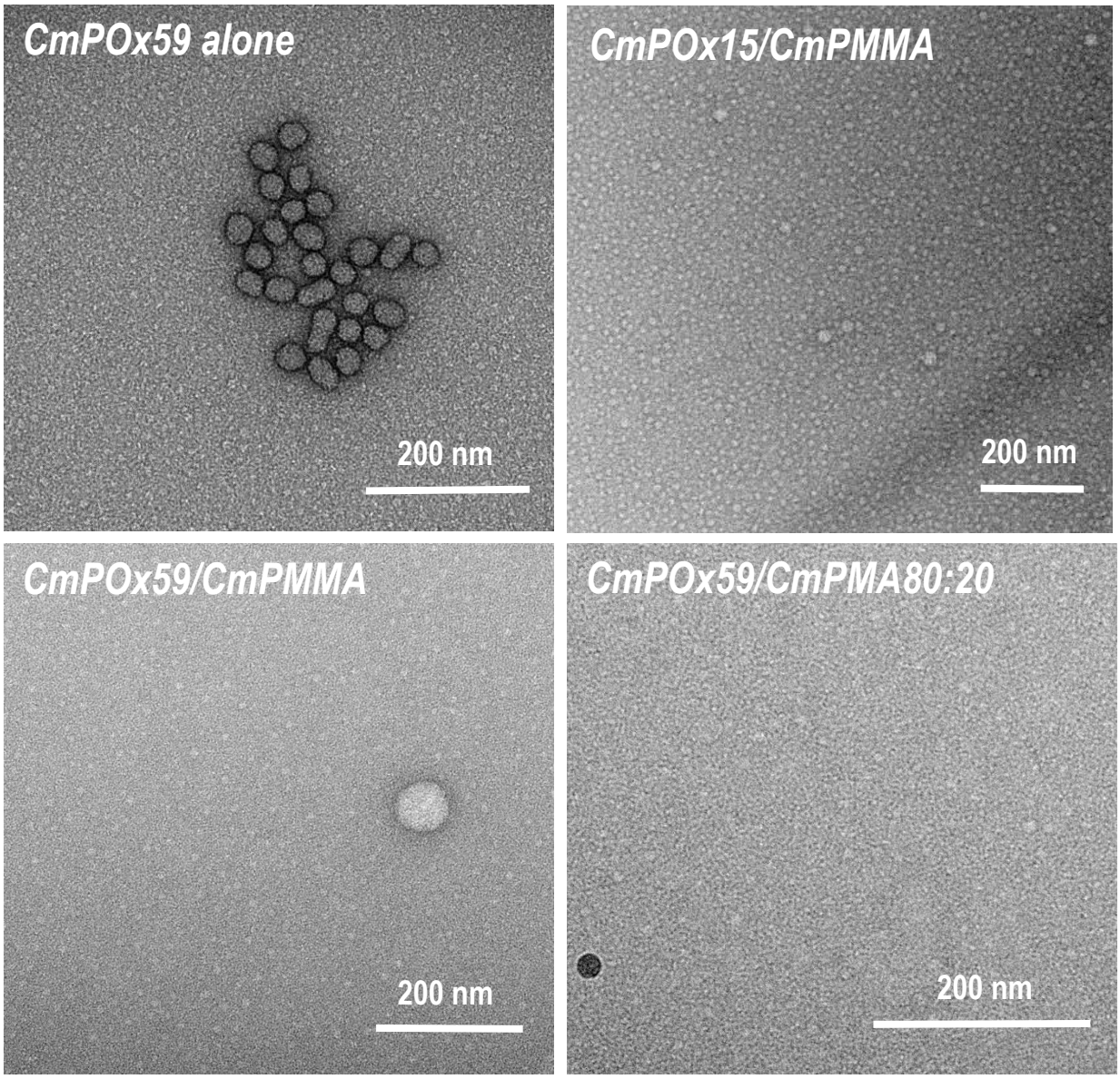


***Figure 3.10*** | *TEM images of the solutions of CmPOx59 alone (up left), of CmPOx15/CmPMMA (up right), of CmPOx59/CmPMMA (bottom left) and of CmPOx59/CmPMA80:20 (bottom right) prepared with film rehydration method.*

| | DLS | | | | TEM |
|---|---|---|---|---|---|
| | **Size [nm] int** | **PDI** | **Size [nm] num** | **PDI** | **Size [nm]** |
| *CmPOx59* alone | 16/388[a] | 0.47[a] | 8[a] | 0.45[a] | 8 ± 2/ 28 ± 4 |
| *CmPOx15/ CmPMMA* | 760 | 2.62 | 14 | 0.24 | 12 ± 3 |
| *CmPOx59/ CmPMMA* | 420 | 0.94 | 10 | 0.27 | 11 ± 2/ 68 ± 31 |
| *CmPOx59/ CmPMA80:20* [b] | 809 | 0.92 | 13 | 0.26 | 10 ± 2 |

***Table 3.4*** | *Characterization of CmPOx59 alone, CmPOx15/CmPMMA, CmPOx59/CmPMMA and CmPOx59/CmPMA80:20 self-assemblies.* [a]*Data not analysed with STORMS.* [b]*Extrusion step was not performed.*

$Coum - C_{11} - (PhOx)_{27} - b - (MOx)_{59}$

*CmPhOx27:59* was used to form self-assemblies by film rehydration method utilizing the polymer alone and with *CmPMMA* and *CmPMA80:20*.

***CmPhOx27:59 alone***

After the first heating step the solution is clear but wormlike agglomerates are present. After sonication the solution is turbid and the agglomerates are still present; they are no longer observable after extrusion.

DLS and TEM results with *CmPhOx27:59* resembles the ones obtained with *CmPOx59*, with a generally lower PDI [Figure 3.11 and Table 3.5]. The same clearly distinct populations were detected on TEM images [Figure 3.12]. Cryo-TEM was also used to study the solution of *CmPhOx27:*59 alone. Only one population of nano-objects was detected on the images [Figure 3.12], the size distribution was quite narrow (27 ± 4 nm) and the size resembled the

one of the larger population observed in TEM images, this could mean that the presence of smaller objects in TEM images is an artifact of the analysis.

### *CmPhOx27:59/stabilizing polymer*

The addition of *CmPMMA*, differently from the other amphiphilic polymer, seemed to not influence the results of the analyses with respect to the polymer alone [Figure 3.11 and B.3]. Using *CmPMA80:20*, big agglomerates were observed together with the two populations [Figure 3.11]. In the case of this amphiphilic polymer, the method of formation of the nano-assemblies seems to have the most prominent effect on their size and distribution.

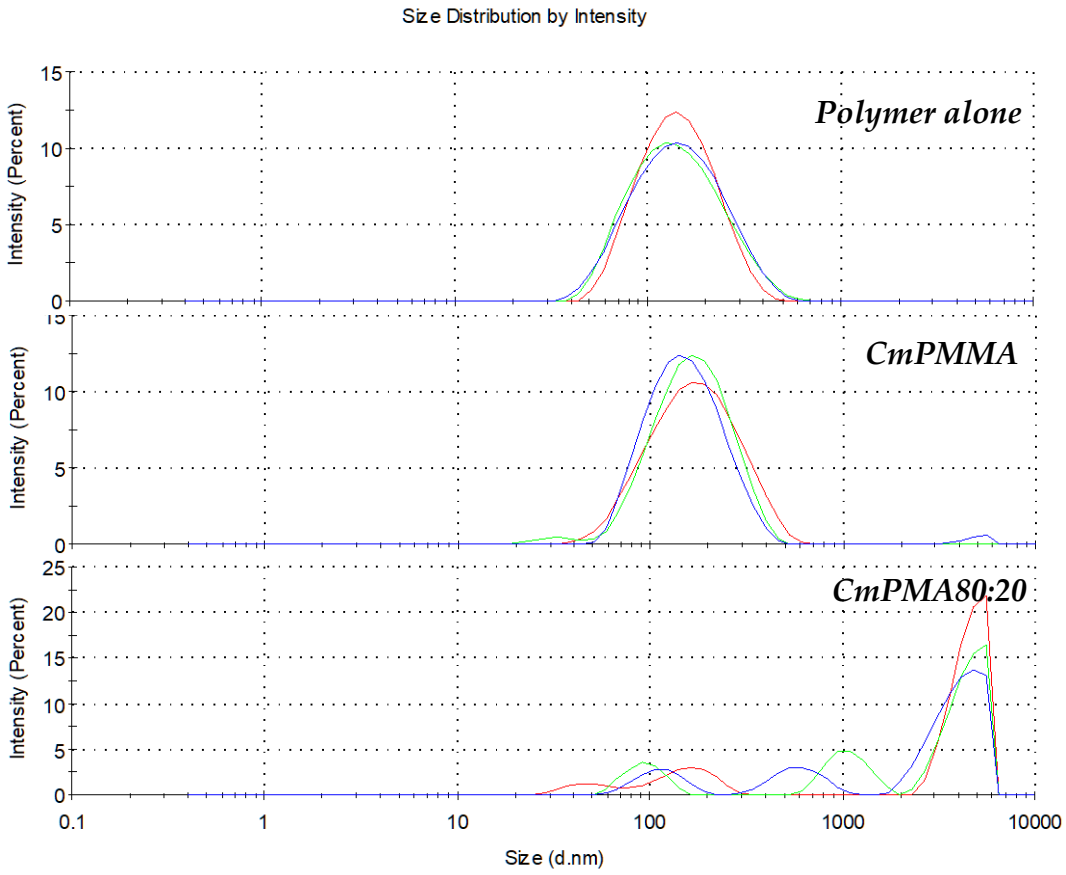


***Figure 3.11*** | *Intensity-weighted size distribution for CmPhOx27:59, CmPhOx27:59/CmPMMA and CmPhOx27:59/CmPMA80:20 self-assemblies prepared with film rehydration method.*

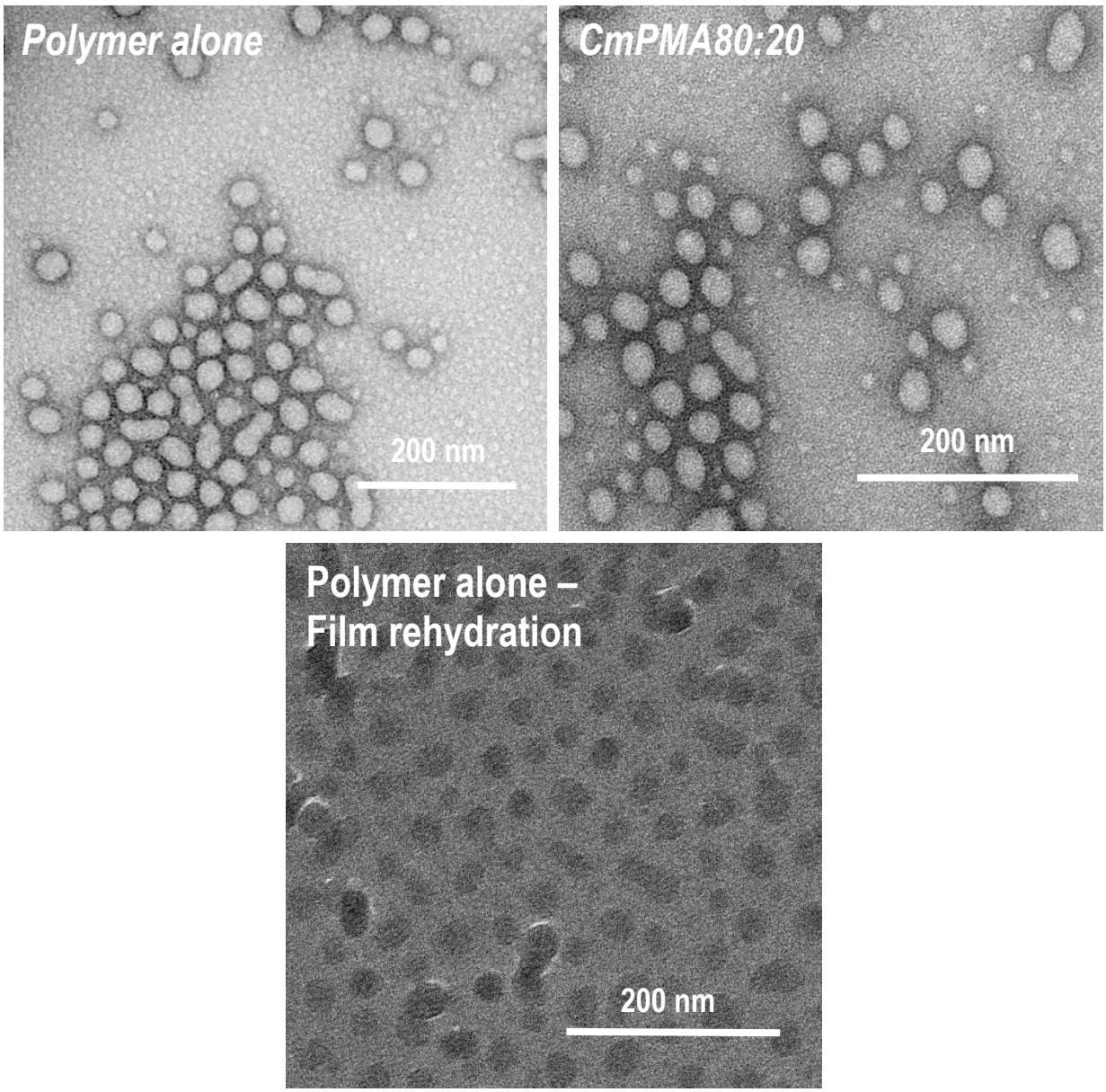


***Figure 3.12*** | *TEM images of the solutions of CmPhOx27:59 alone (up left) and of CmPhOx27:59/CmPMA80:20 (up right) prepared with film rehydration method. Cryo-TEM image of the solution of CmPhOx27:59 alone prepared with film rehydration method (bottom).*

| | DLS | | | | TEM |
|---|---|---|---|---|---|
| | **Size [nm] int** | **PDI** | **Size [nm] num** | **PDI** | **Size [nm]** |
| *CmPhOx27:59* alone | 145 | 0.36 | 82 | 0.25 | 10 ± 2/ 34 ± 5 |
| *CmPhOx27:59/ CmPMMA* | 162 | 0.36 | 89 | 0.25 | 11 ± 2/ 34 ± 4 |
| *CmPhOx27:59/ CmPMA80:20* [(a)] | 3911 | 1.04 | 10 | 0.15 | 11 ± 2/ 30 ± 4 |

***Table 3.5*** | *Characterization of CmPhOx27:59 alone, CmPhOx27:59/CmPMMA and CmPhOx27:59/CmPMA80:20 self-assemblies.* [(a)]*Extrusion step was not performed.*

## 3.2.3 Comparison between the methods of formation

In the case of *CmPOxn* with stabilizing polymer, the solutions obtained with film rehydration method were in general more polydisperse, except for the ones prepared with cosolvent method using $CH_2Cl_2$. The average-intensity size is quite higher for the film rehydration method, but the population of diameter around 10 nm observed in TEM images is confirmed by the number average analysis, unlike for the cosolvent method. For cosolvent method, the solvent clearly influences the size of the objects and the polydispersity of the solutions, while further analyses are needed to evaluate the influence of changing the stabilizing poly(alkyl methacrylate).

For *CmPhOx27:59* the results were more homogenous between the distinct methods and less sensitive to solvent change. The average-intensity size and polydispersity index were lower and less variable, and two populations were clearly present in all TEM images.

In several cases, the presence of big objects (up to 1 μm) was evidenced by DLS, they could be small aggregates or another less abundant population. Their nature was not investigated, additional studies are necessary to get further details. For example, analysing the effect of the concentration of the polymers on the size and polydispersity of the nano-objects.

## 3.3 Crosslinking of the nanoparticles

Crosslinking was performed on *CmPOx15*/*CmPMMA* and *CmPhOx27:59*/*CmPMA50:50* self-assemblies. The occurred dimerization of coumarin was confirmed by the right shift of the peaks of interests in the $^{1}$HNMR spectrum [Figure 3.13]. The nano-objects formed by *CmPOx15*/*CmPMMA* were characterized with DLS and TEM and the results were coherent with the ones obtained in the previous study [52], showing that nor the size distribution or the shape of the self-assemblies is modified after crosslinking (results not reported).

The crosslinking of *CmPhOx27:59*/*CmPMA50:50* systems was carried out at the IMRCP lab in Toulouse by Dr. Orélia Cerlati. The process required at least 12 hours for a complete dimerization, indicated by the shift of the same peaks present in the other spectra. Reproducing of the process at the SBNLab in Milan was attempted with the use of a photoreactor, employing the same type of lamps but with the distance between the sample and the lamps increased to 3 cm. This attempt failed since crosslinking was not observed even after 14 hours. No further attempts were made.

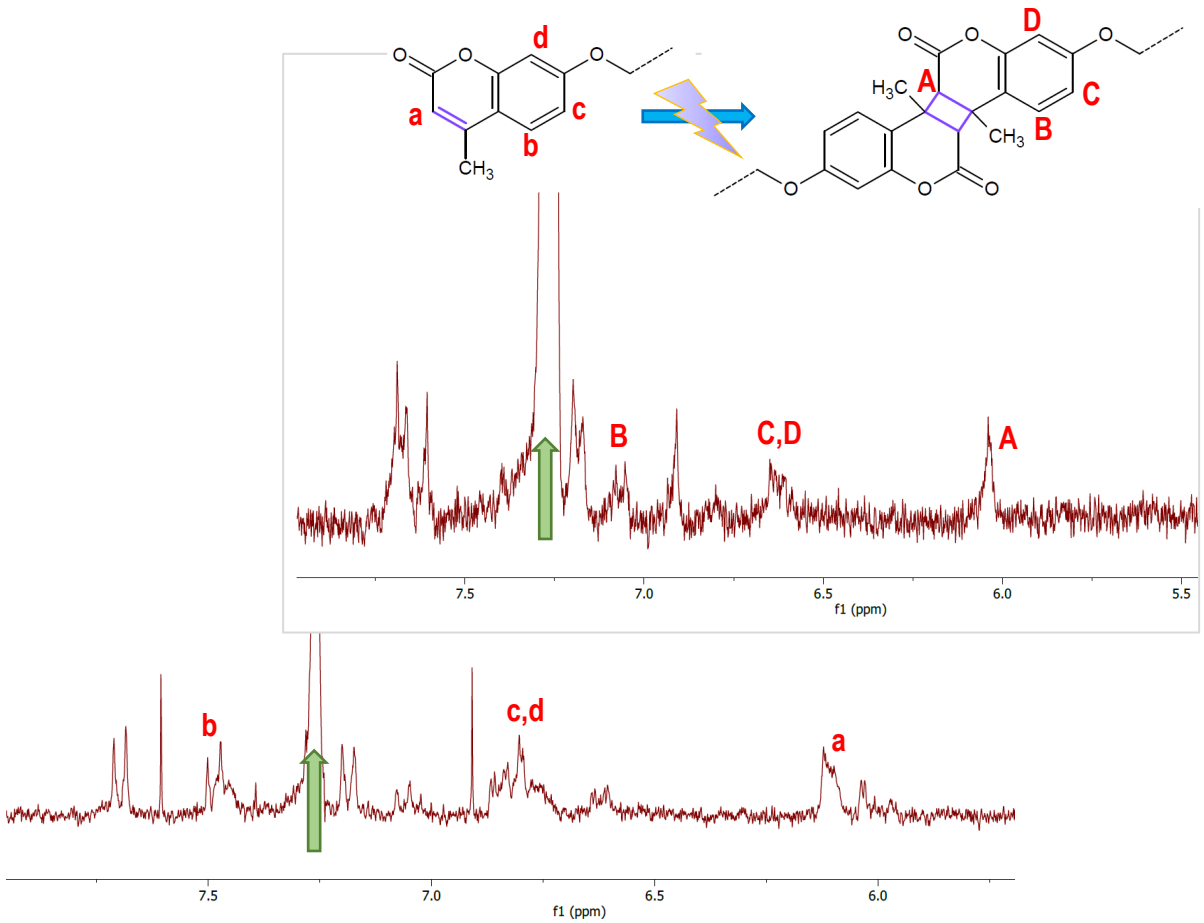


***Figure 3.13*** | *[1]HNMR of CmPOx15/CmPMMA self-assemblies before (bottom) and after (up) crosslinking. Coumarin cycloaddition is reported above. The green arrows indicate the reference solvent chloroform-d.*

## 3.4 Selection of the polymers for protein corona analysis

The results obtained with *CmPhOx27:59* were deemed the most relevant for our study given the presence of narrow multiple populations with in general a lower PDI with respect to the ones achieved with *CmPOx* systems. Further analyses are needed to better understand the morphology of the nano-objects and define their size in solution, however the influence of the composition of the amphiphilic polymer on the formation of the self-assemblies is clear: increasing the length of the hydrophobic part seems to allow the formation of larger self-assemblies together with the smaller ones already observed [52]. These systems were less sensitive to the choice of formation method and stabilizing polymer.

The features of the nano-objects were affected by the formation method, chosen solvent and chosen stabilizing polymer. In general, the film rehydration method seemed to be least influenced by the choice of constituents of the formulation. Regarding the cosolvent method, the alternative solvents tried out in this research didn't offer any advantage to the procedure, but they produced issues not present with acetone.

*CmPhOx27:59*/*CmPMA50:50* systems were selected to carry out protein corona analyses.

## 3.5 Protein corona analysis

### 3.5.1 Characterization of the self-assemblies

We started trying to reproduce the same procedure of the cosolvent method at the SBNLab. However, the solubility of *CmPhOx27:59* in acetone seemed to have decreased, a white precipitate was observable in the vial right after the end of the preparation of the solution in water. Heating and sonicating the solution helped the dissolution, but the precipitate reappeared soon after ceasing heating. Since the same hindrance was observed by our collaborators at the IMRCP lab, it was hypothesised that the polymers underwent some changes, maybe absorption of water. The conservation of the polymer was changed from ambient temperature to at about 4°C inside a fridge and in a container under vacuum.
To avoid solubility issues, the protein corona analyses were carried out only on self-assemblies prepared with the film rehydration method. The final concentration of the solution was decreased to 2.5 mg/ml and acetone was used to solubilize *CmPMA50:50*. The extrusion step was not performed. The objects were characterized in absence and in presence of biological fluid.

For simplicity only intensity-weighted average size distribution measured at 90° are reported. Differently from before, the size consists in the radius and not the diameter of the objects. The value of the hydrodynamic radius (only intensity-weighted) obtained from fitting of the correlation function was doubled for a better comparison with the TEM value and previous analyses.

***Pristine nanocarriers***

The solution was turbid and white precipitate was observed some time after the end of the formation procedure. DLS measurements showed the presence of a population around 50

nm and another around 200 nm together with larger aggregates [Figure 3.14 and Table 3.6]. TEM analysis was carried out with the assistance of Dr. Andrea Pizzi; the pictures exhibit only one population similar to the smaller one detected with DLS [Figure 3.15].

In collaboration with IMRCP lab the procedure was optimized substituting methanol with chloroform and acetone, increasing the time of evaporation of the solvent on the rotary evaporator to 2 hours and decreasing the time of further drying of the film under vacuum to 3 hours. However, also in this case white precipitate was observed in solution after some time. DLS confirmed the presence of large aggregates in suspension, and the same two populations detected before [Figure A.4]. TEM was not performed. The results were comparable with the ones obtained by our collaborators at the IMRCP lab.

Since stability analysis (see later) confirmed the stability of non-crosslinked self-assemblies in presence of biological fluid, the nano-objects were also prepared and characterized in absence of the stabilizing polymer. No precipitate was observed and only a population of size around 60 nm seemed to be present [Figure A.5 and Table 3.6], suggesting that the larger "population" observed with *CmPMA50:50* could be aggregates. The results were different from the ones obtained in Toulouse using methanol in the procedure, indicating that the solvent may influence the size the of nano-objects also in this method.

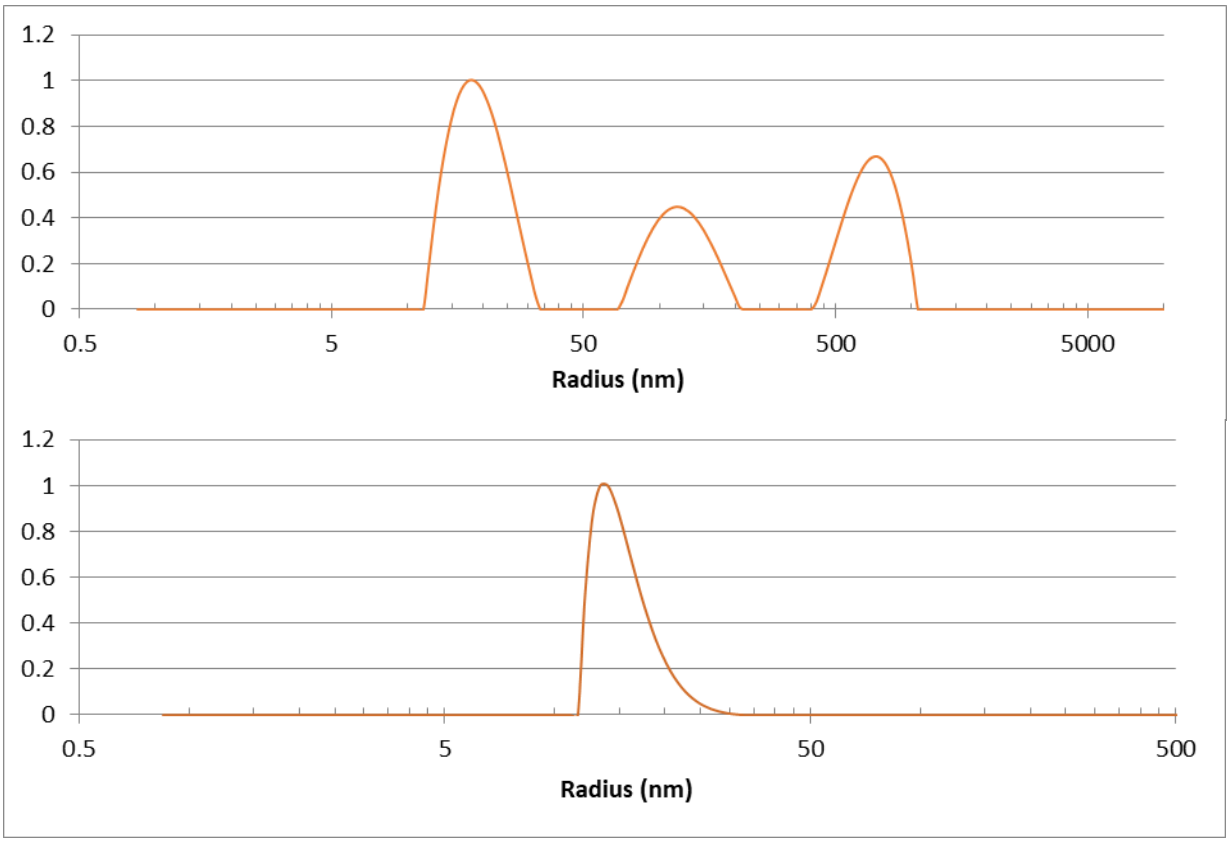


***Figure 3.14*** | *Intensity-weighted (above) and number-weighted (below) size distribution for CmPhOx27:59/CmPMA50:50 self-assemblies prepared with film rehydration method using methanol.*

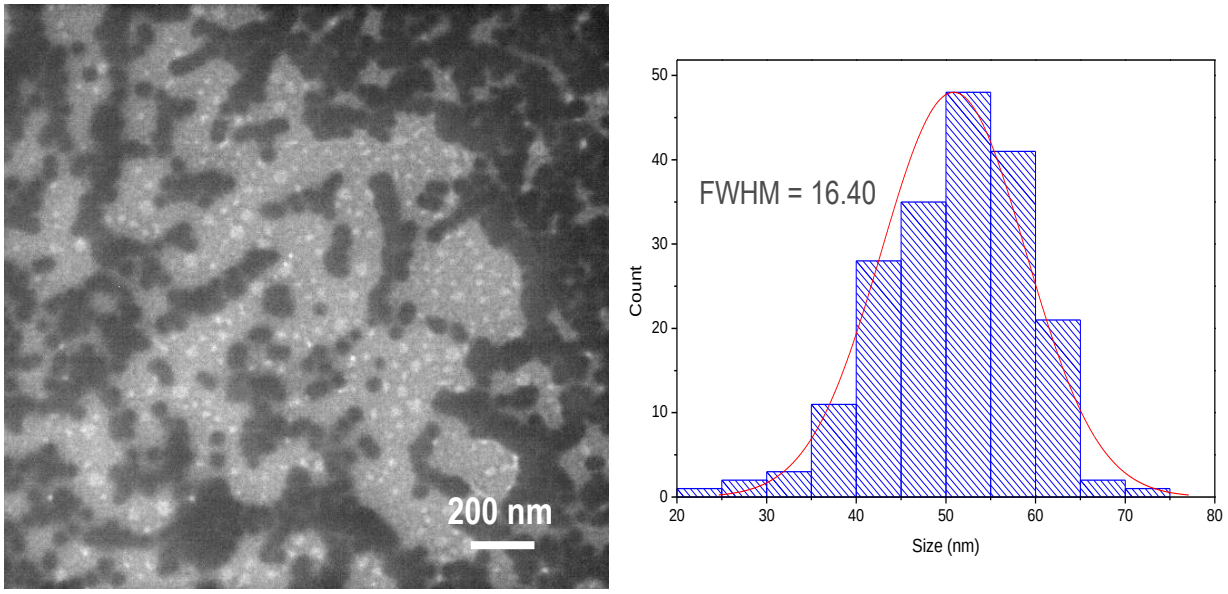


***Figure 3.15*** | *TEM images of the solution of CmPhOx27:59/CmPMA50:50 prepared using methanol (left) and statistical analysis of the size distribution (right).*

| | | DLS | | TEM |
|---|---|---|---|---|
| | | **Size [nm] int** | **PDI** | **Size [nm]** |
| *CmPhOx27:59/ CmPMA50:50* | **Methanol** | 151 | 0.45 | 55 ± 5 |
| | **Chloroform** | 149 | 0.50 | - |
| *CmPhOx27:59* | **Chloroform** | 60 | 0.15 | - |

***Table 3.6*** | *Characterization of CmPhOx27:59/CmPMA50:50 self-assemblies prepared with film rehydration method using chloroform.*

### *Nanocarriers in presence of FBS*

The non-crosslinked and crosslinked samples were supplied by our collaborators at the IMRCP lab. Both samples were diluted in PBS with 10% FBS and incubated for 1 hour.

Both samples showed no change in size and PDI after 1 hour of incubation in presence of FBS (only non-crosslinked results are reported) [Figure 3.16]. This is interesting, since it could suggest that the protein corona formed on the nano-systems is very thin or entirely absent, confirming the biofouling properties of poly(2-oxazolines) [69].

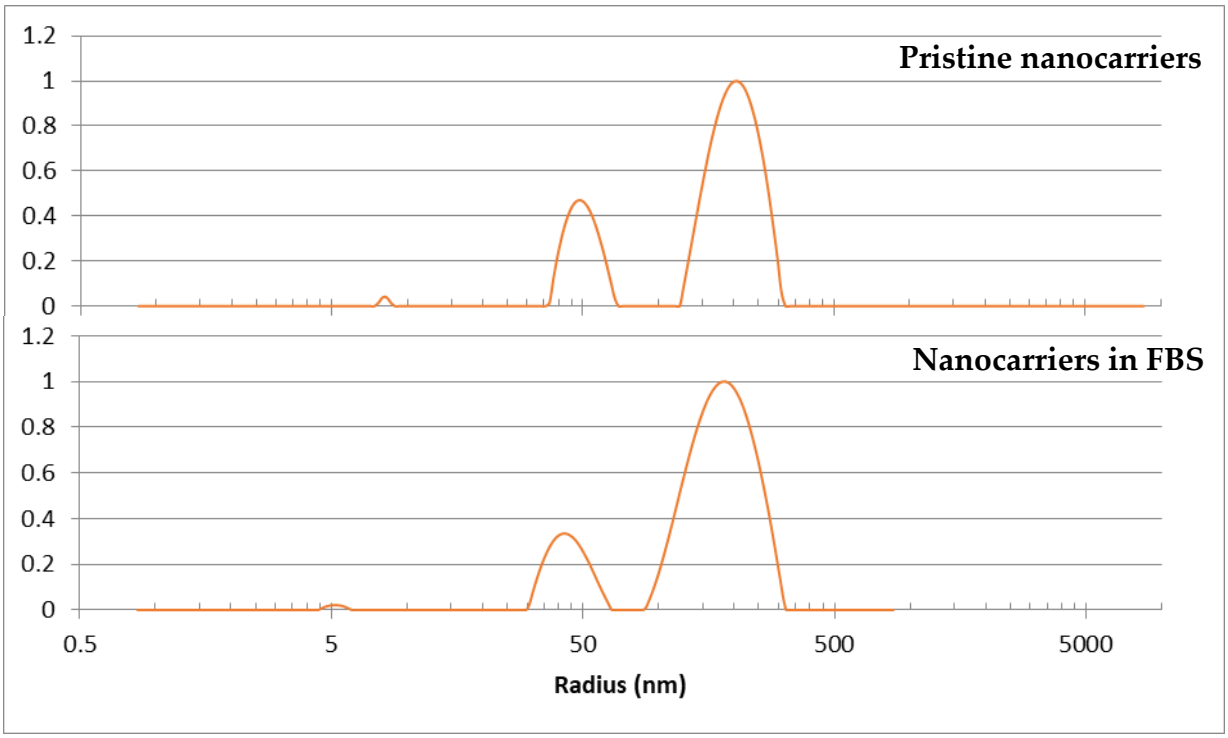


***Figure 3.16*** | *Intensity-weighted size distribution for CmPhOx27:59/CmPMA50:50 self-assemblies in aqueous solution (above) and diluted with PBS in presence of FBS (below).*

### 3.5.2 Stability analysis

A non-crosslinked sample and a crosslinked one were prepared and charcaterized as fresh and incubated in the biological medium for 1 hour. After incubation, the samples were analysed by DLS after 1 hour, 4 hours and 24 hours. The dispersions were kept at 37°C and RH = 95% (same conditions of the incubation period).

No change was observed in 24 hours: both samples showed a good colloidal stability passing (only non-crosslinked results are reported) [Figure 3.17]. This represents a promising result since it suggests that the nanocarriers are stable in the biological environment. Further analyses are needed to confirm these results and test for how much time the self-assemblies remain unchanged.

Since stability analysis confirmed a good stability of non-crosslinked self-assemblies, ultracentrifugation and respective gel electrophoresis was performed on systems formed only by the amphiphilic polymers *CmPhOx27:59*.

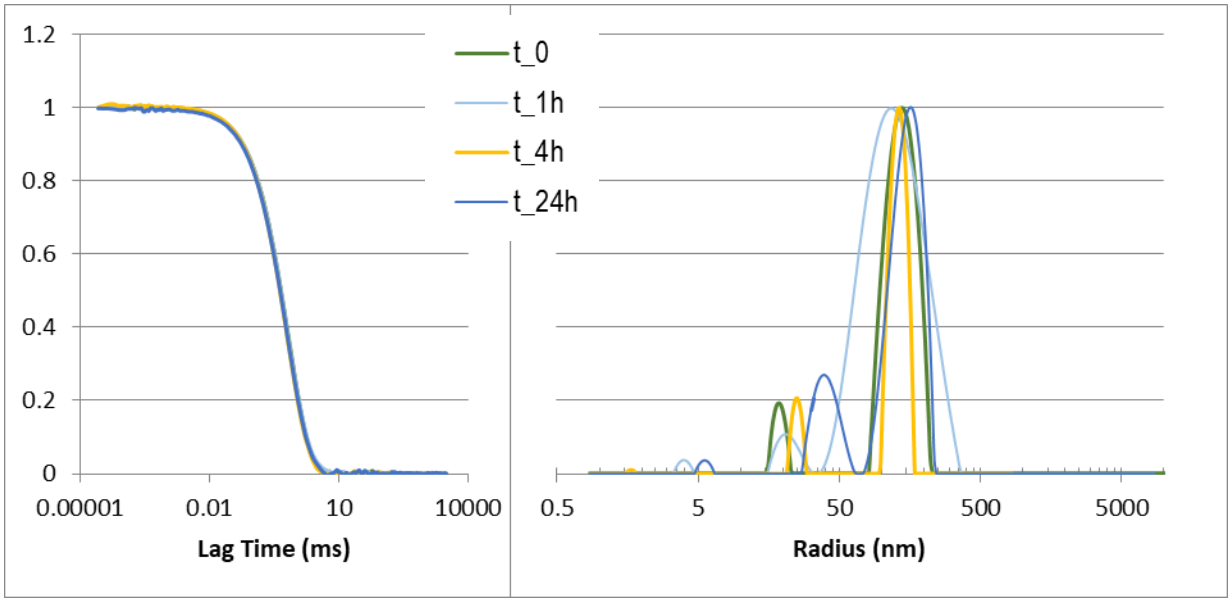


***Figure 3.17*** | *Time evolution of correlation function and intensity-weighted size distribution for CmPhOx27:59/CmPMA50:50 self-assemblies in presence of FBS.*

### 3.5.3 Isolation of the protein corona - carrier complexes

In order to isolate the protein corona – carrier complexes from unbound proteins present in solution, centrifugation with sucrose cushion and ultracentrifugation with sucrose cushion gradient were performed. Gel electrophoresis was carried out on supernatant solutions and resuspended dispersions from the obtained pellets for the centrifugation experiments with sucrose cushion, and on all the layers of the sucrose gradient obtained with ultracentrifugation.

***Sucrose cushion centrifugation***

The centrifugation was performed on both non-crosslinked and crosslinked samples (DLS results are not reported). After incubation both were transferred into 2 ml Eppendorf tubes with the same amount of 0.7 M sucrose cushion solution and centrifugated for three times. A pellet was observed for each centrifugation step; DLS analysis on the resuspended pellet solutions confirmed the isolation of NPs. DLS analysis on the supernatant solutions showed the presence of NPs even after three centrifugation cycles, meaning that a satisfying isolation of the corona-carrier complexes was not achieved in these conditions [Figure 3.18]. The low density of our particles or the lack of formation of a rich corona could be possible explanations for these results [39]; optimization of the process according to the properties of the objects is required to further the analysis.

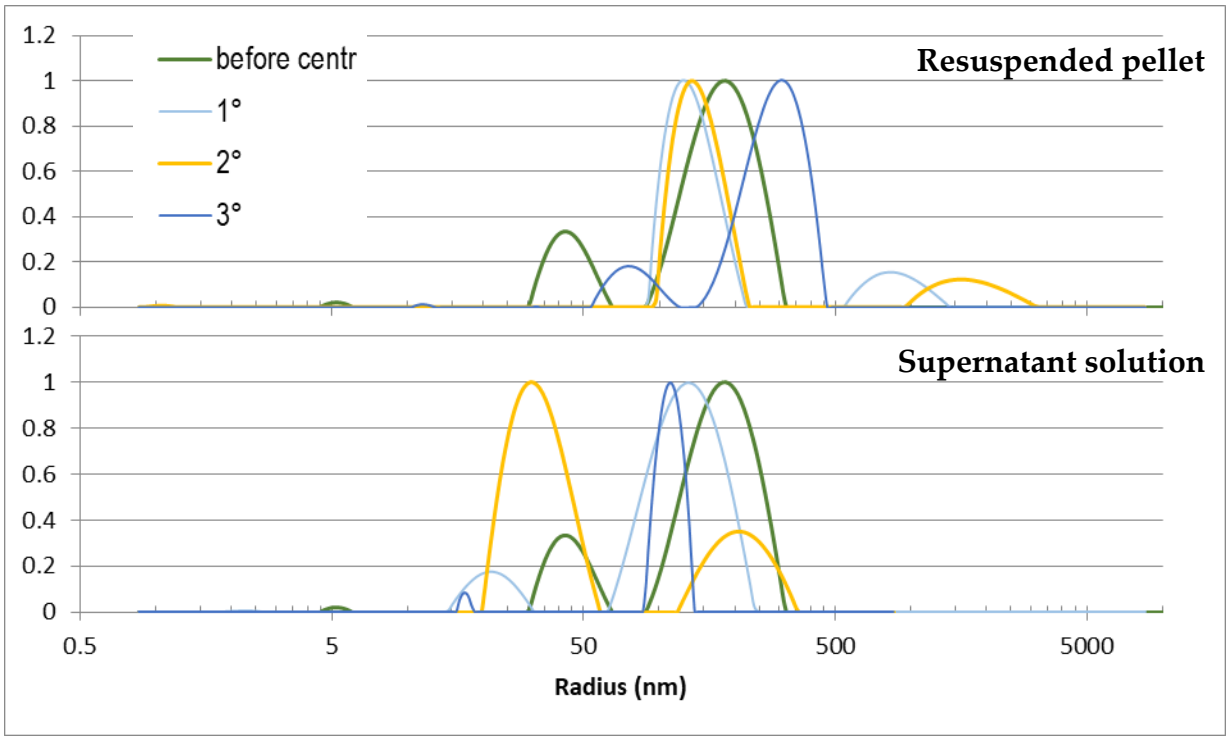


***Figure 3.18*** | *Comparison of intensity-weighted size distribution for CmPhOx27:59/CmPMA50:50 self-assemblies in presence of FBS and sucrose cushion.*

### *Sucrose gradient ultracentrifugation*

The experiments were carried out on a sample prepared with *CmPhOx27:59* in PBS incubated in presence of 10% FBS, and on a control sample composed by PBS and 10% FBS without any NP dispersion to allow the comparison of the layers.

Ultracentrifugation experiment has been repeated only once and during dialysis we lost some samples probably due to unexpected leakage of the sample from the membrane tubes. Thus, we could only have a partial view on the samples and some preliminary considerations can be done. Sucrose layers at higher densities, 11 and 10, showed the presence of most proteins both in NP sample and control sample. In the NP sample, layer 9 showed the presence of objects of 60 nm, while the control did not show any in layer 9 [Figure 3.19]. Other systems around 200 nm seemed to be present between layer 6 and 3.

These results should be considered together with the ones obtained with gel electrophoresis.

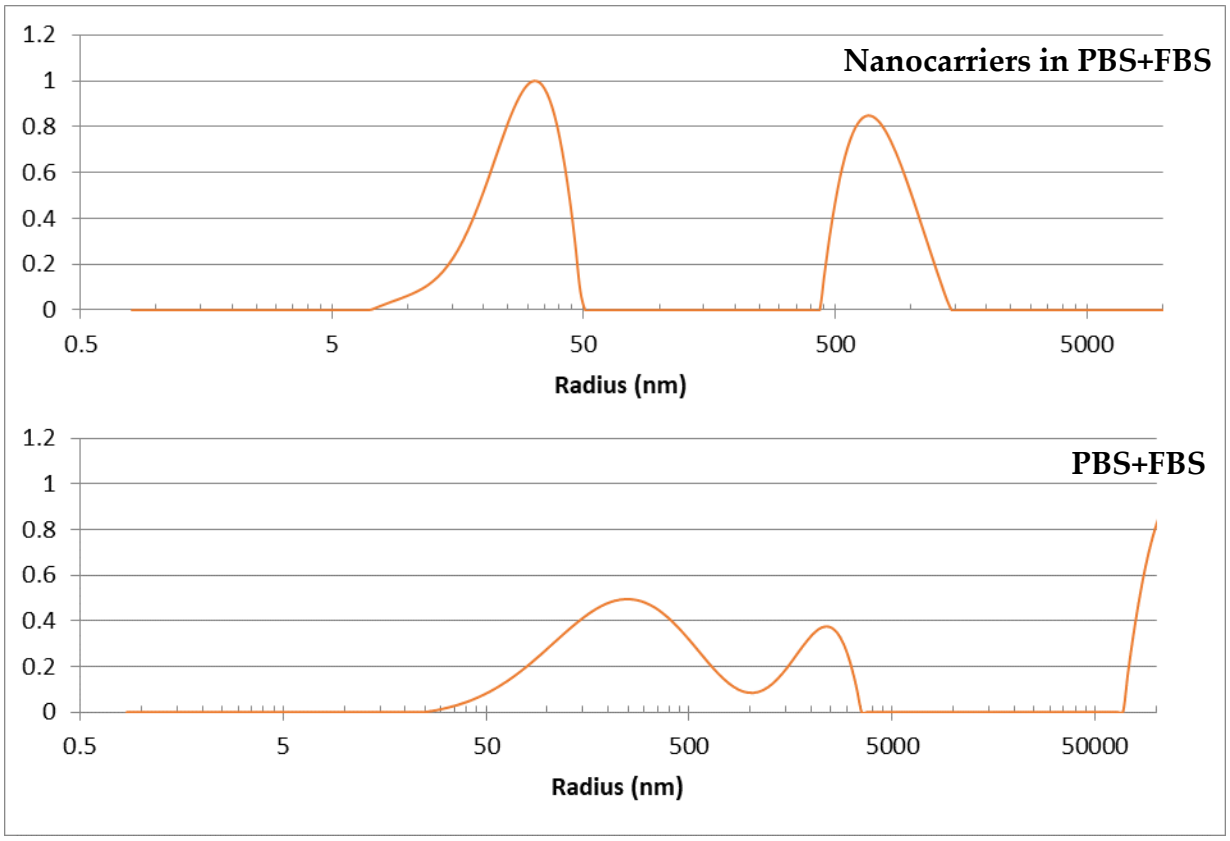


***Figure 3.19*** | *Comparison between intensity-weighted size distributions of sample with nanocarriers (above) and sample without (below) in solution of PBS+FBS.*

### *Gel electrophoresis*

The experiment on the samples from sucrose cushion centrifugation confirmed that in both resuspended pellet and supernatant solution the same corona-carrier complexes could be found after three centrifugation cycles. The results seemed to also confirm the biofouling properties of the polymer poly(2-oxazoline) since they indicated the presence of very few proteins [Figure 3.20]. The experiment should be repeated with more concentrated samples to have more clear results.

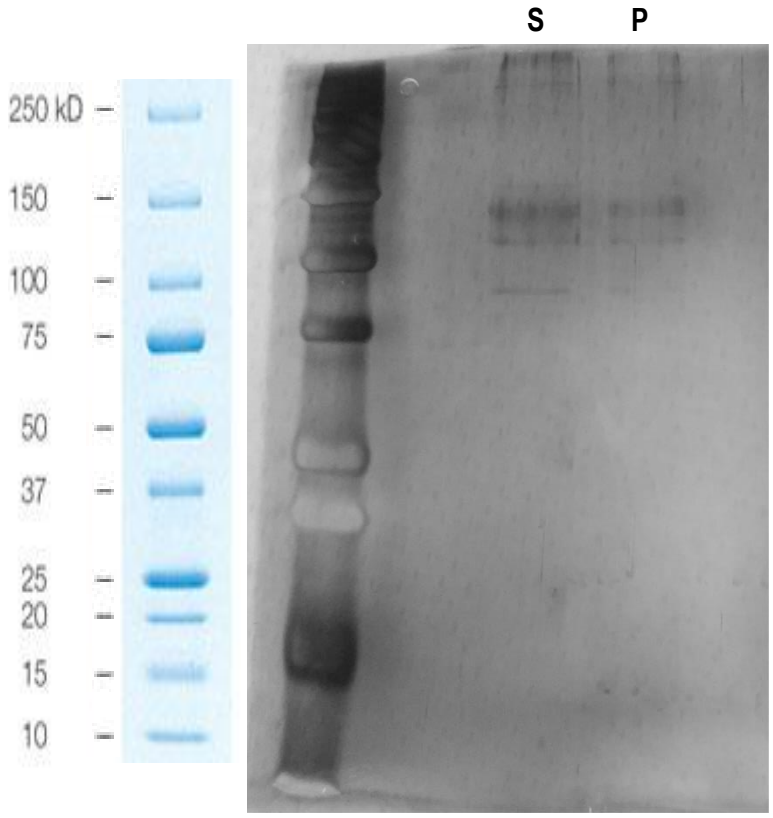


***Figure 3.20*** | *SDS-PAGE gel of the resuspended pellet solution (P) and the supernatant solution (S) after centrifugation of CmPhOx27:59 solution diluted with PBS+FBS. Since the marker was "burnt out" by the staining, a reference is reported on the left.*

Gel electrophoresis on the samples from sucrose gradient ultracentrifugation was carried out on the most interesting layers: for the sample with nano-objects from layer 11 to 3 (with the exception of layer 10, the volume of which wasn't enough for any analysis), while for the sample with only biological medium from layer 11 to 6. Most of the proteins seemed to be concentrated in both layers 11. Proteins bands typical of FBS were observed in layer 10 of the only FBS solution, while layer 9 of the two sample presented a discrepancy: a band was observed for the sample with the nanocarriers but not for the one with only FBS [Figure 3.21]. No other bands were observed in any other layer. These results show the accumulation of unbound proteins towards the surface of the solution and seem to suggest the occurred isolation of corona-carrier complexes.

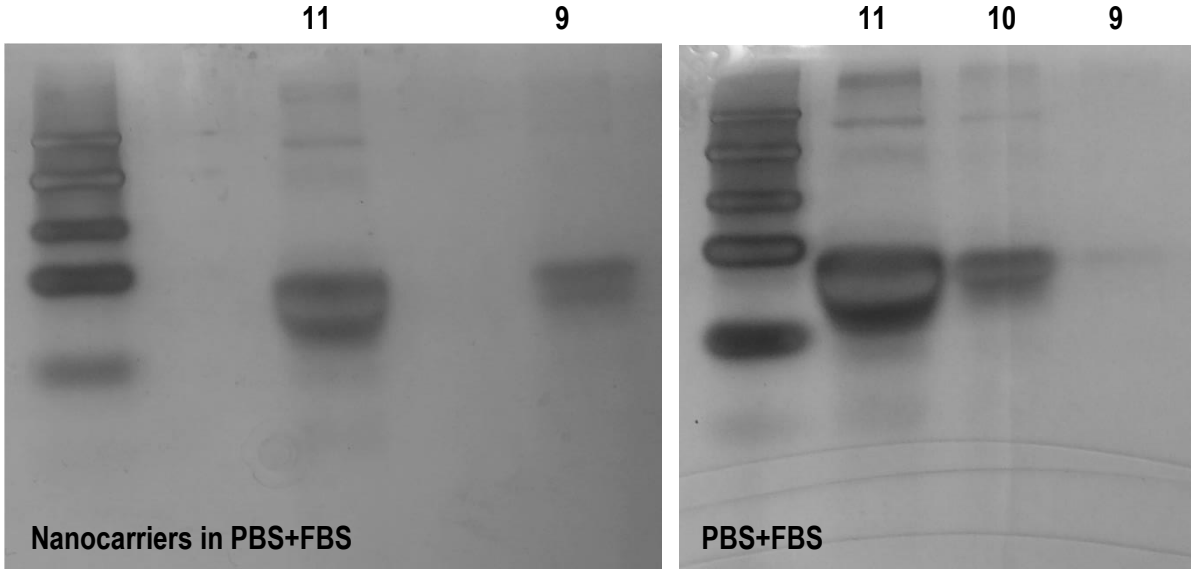


***Figure 3.21*** | *Comparison of SDS-PAGE gel of the layers from ultracentrifugation of CmPhOx27:59 solution diluted with PBS+FBS and of PBS+FBS only.*

The results obtained from this preliminary protein corona analysis are promising, however, additional more in depth analyses will be needed to better characterize the corona-carrier complexes and investigate the composition and the properties of the protein corona.

# 4. Conclusions and future developments

The aim of this thesis work was to assess the ability to form polymeric nanovectors of newly synthesised poly(2-oxazolines), depending on their composition and molecular weight, and characterize the obtained nano-systems with in mind their potential use for photodynamic therapy. This therapeutic modality for cancer suffers limitations that could be overcome by the use of nanocarriers to deliver a photosensitive compound to the desired target. The potential of polyoxazoline nanovectors for PDT has already been investigated [52] and this work aimed to expand the characterization of the objects also in presence of biological fluid. The three studied poly(2-oxazolines) formed varied self-assemblies with different sizes and morphologies which have been characterized by means of DLS and TEM respectively. The addition of a longer hydrophobic block to methyl-oxazoline affected the properties of the self-assemblies much more than increasing its molecular weight: TEM images of the nano-objects formed by the copolymer containing both phenyl and methyl-oxazoline groups showed the clear presence of two populations. Changing the method of formation of the self-assemblies also lead to different outcomes, as well as using differing solvents. Film rehydration method proved to be particularly promising given the formation of quite narrow distributions of nanosystems also observed in cryo-TEM pictures. Size and shape was again influenced by the choice of stabilizing polymer; a range of poly(alkyl methacrylates) was studied and two were respectively used to crosslink two of the amphiphilic polymers successfully.

One amphiphilic polymer was selected to conduct preliminary studies on the protein corona formation on the self-assemblies. The results were promising and suggested the formation of a small protein corona – thus confirming the biofouling properties of this type of poly(2-oxazoline) [69], succeeding in isolating corona-carrier complexes with

ultracentrifugation, and proved the stability of the objects (both the non-crosslinked and the crosslinked ones) in presence of 10% of fetal bovine serum.

Further characterization is necessary to confirm and refine these results: nanoparticle tracking analysis (NTA) could be employed to characterize the objects, and especially flow field flow fractionation (F-FFF) should be used to overcome the intrinsic weakness of DLS in analysing multi-population systems. After optimization of the isolation method of corona-carrier complexes, the same techniques could be used to better characterize them, while stability could be investigated on a longer period of time and in presence of a larger percentage of biological fluid. Characterization and protein corona analyses of the systems should be repeated also in presence of a photosensitizer, accompanied by UV-vis absorption spectroscopy and TEM to ensure the encapsulation of the PS, and by the examination of the kinetics of PS release. Finally, biological tests for the cytotoxicity and PDT efficiency could be carried out *in vitro*.

Great attention should be dedicated to the ideation of an optimized procedure to screen new poly(2-oxazolines) to identify the most promising compositions and molecular weights before proceeding with more in depth analyses.

# Appendix A - DLS

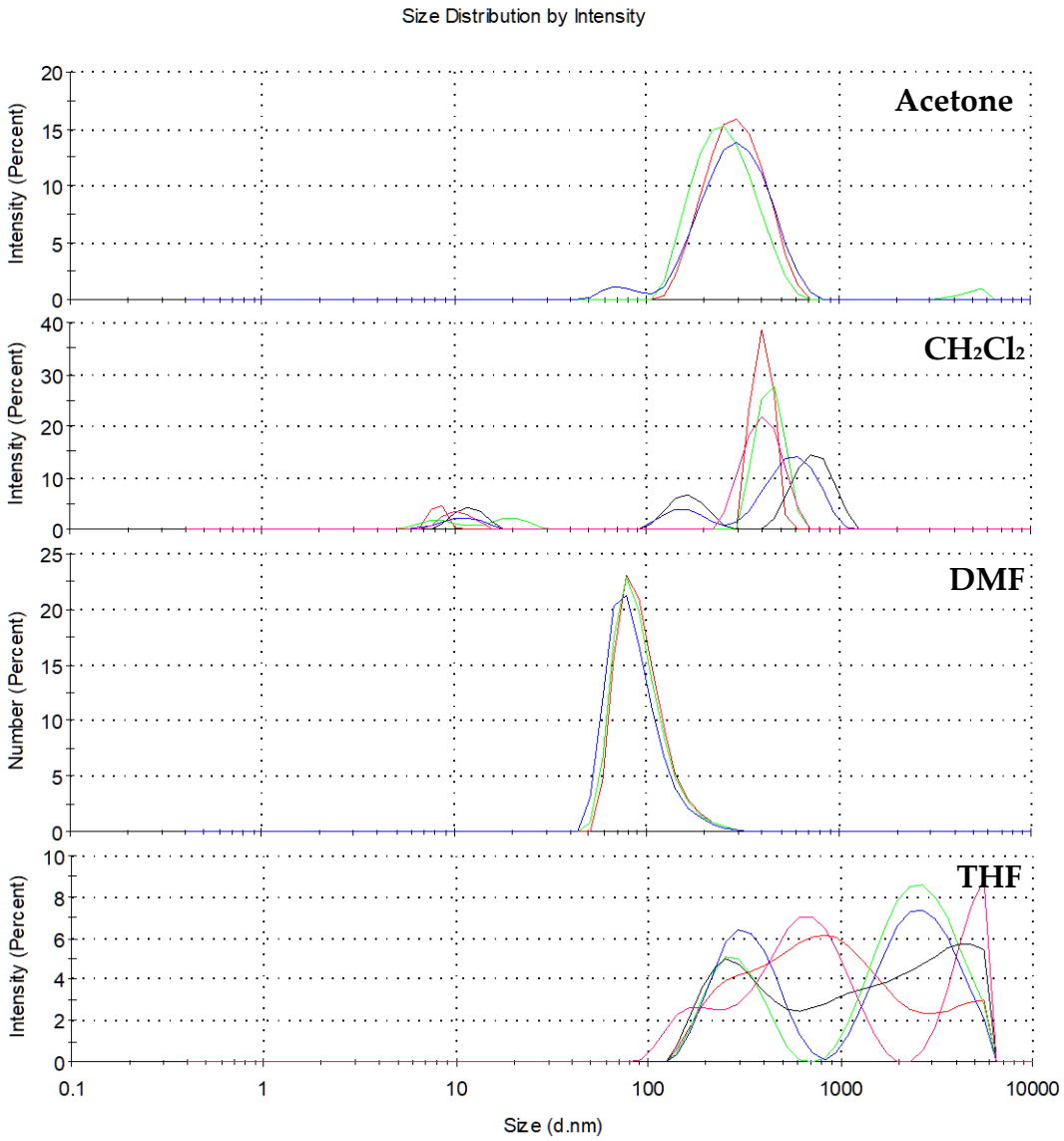


***Figure A.1*** | *Intensity-weighted size distribution for CmPOx15/CmPMMA self-assemblies prepared with different solvents.*

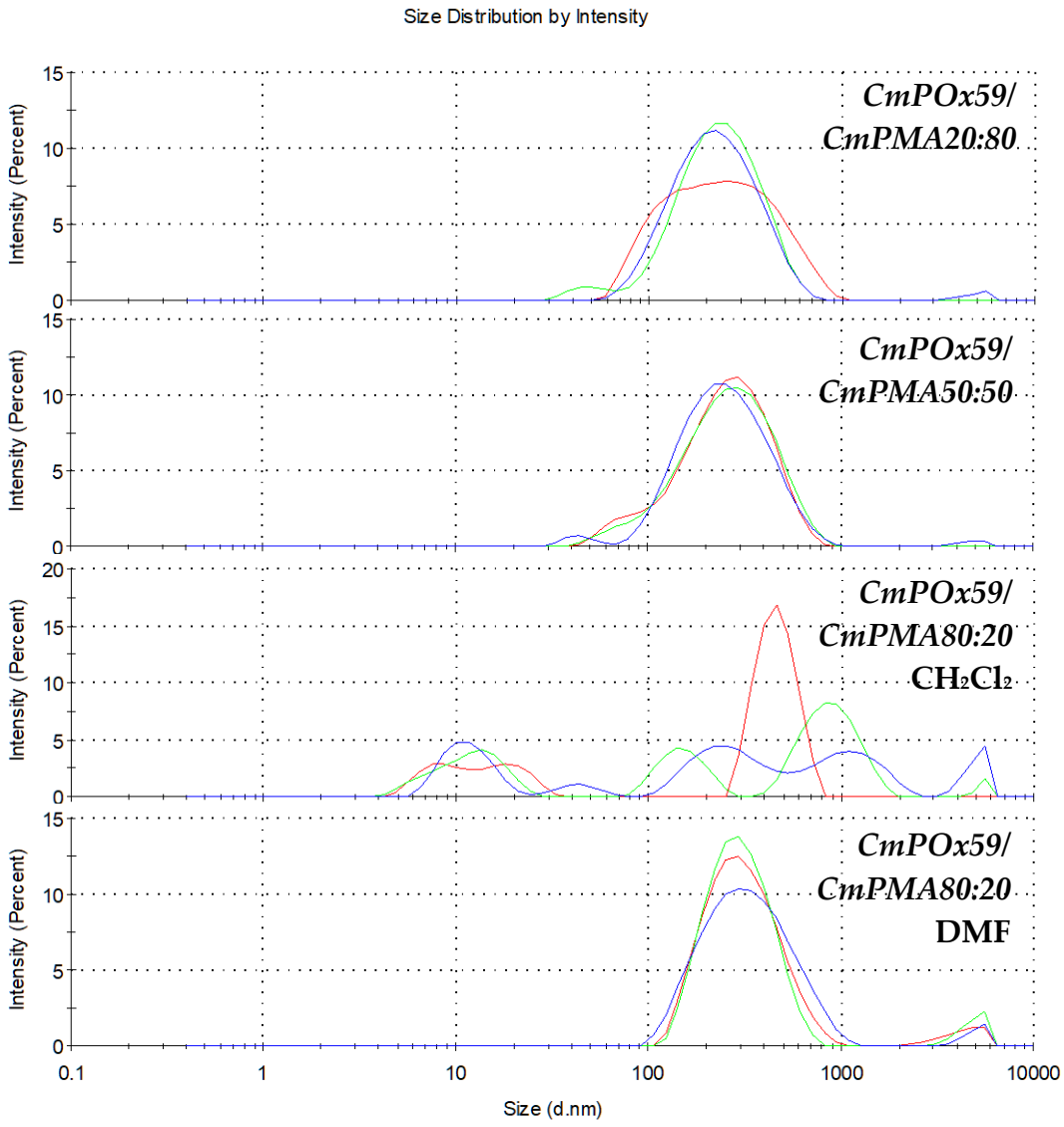


***Figure A.2*** | *Intensity-weighted size distribution for CmPOx59/CmPMA20:80, CmPOx59/CmPMA50:50 and CmPOx59/CmPMA80:20 self-assemblies.*

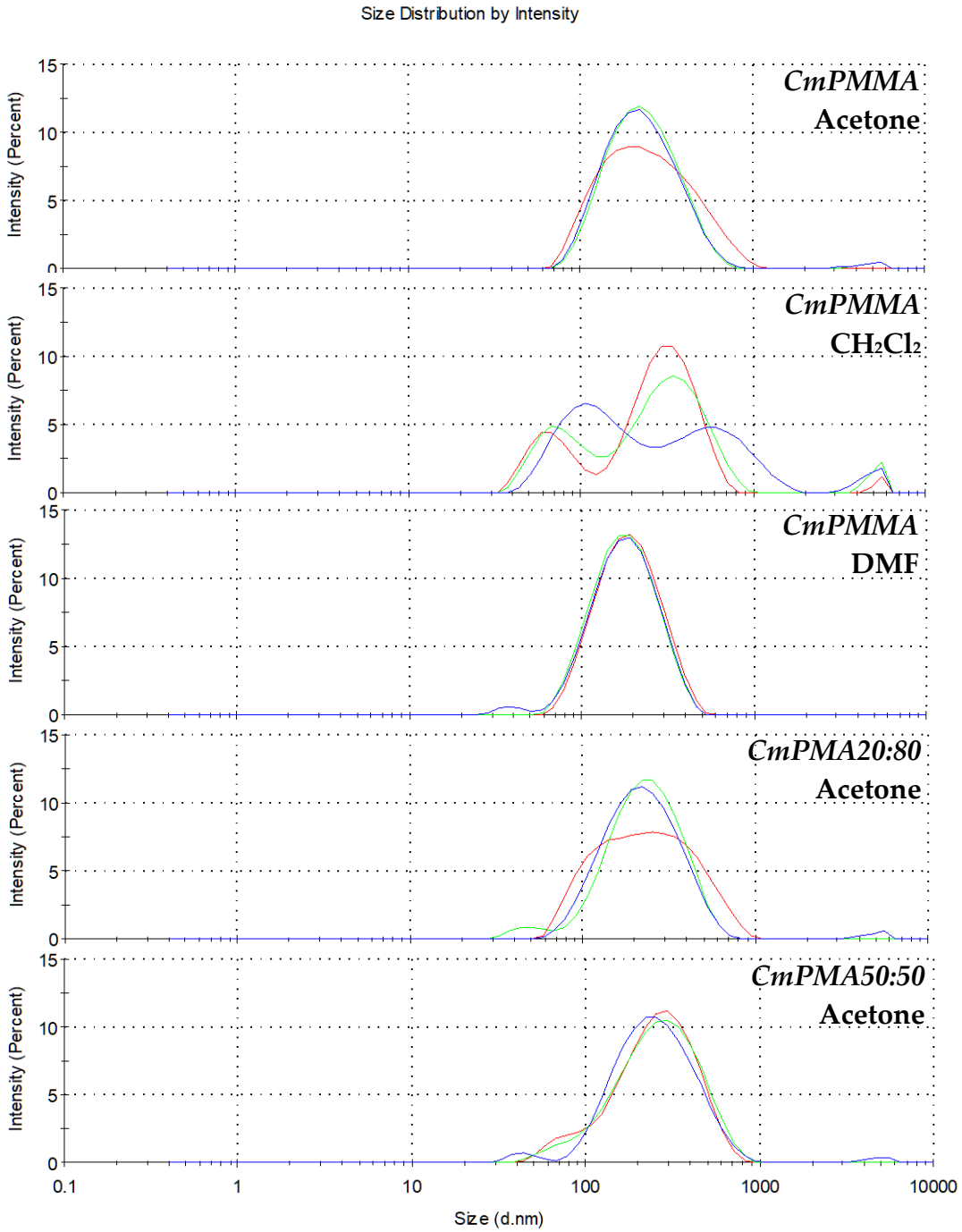


***Figure A.3*** | *Intensity-weighted size distribution for CmPhOx27:59/stabilizing polymer self-assemblies prepared with different solvents (CmPMMA dissolved in acetone, CH2Cl2 and DMF) and different stabilizing polymers (CmPMMA, CmPMA20:80 and CmPMA50:50).*

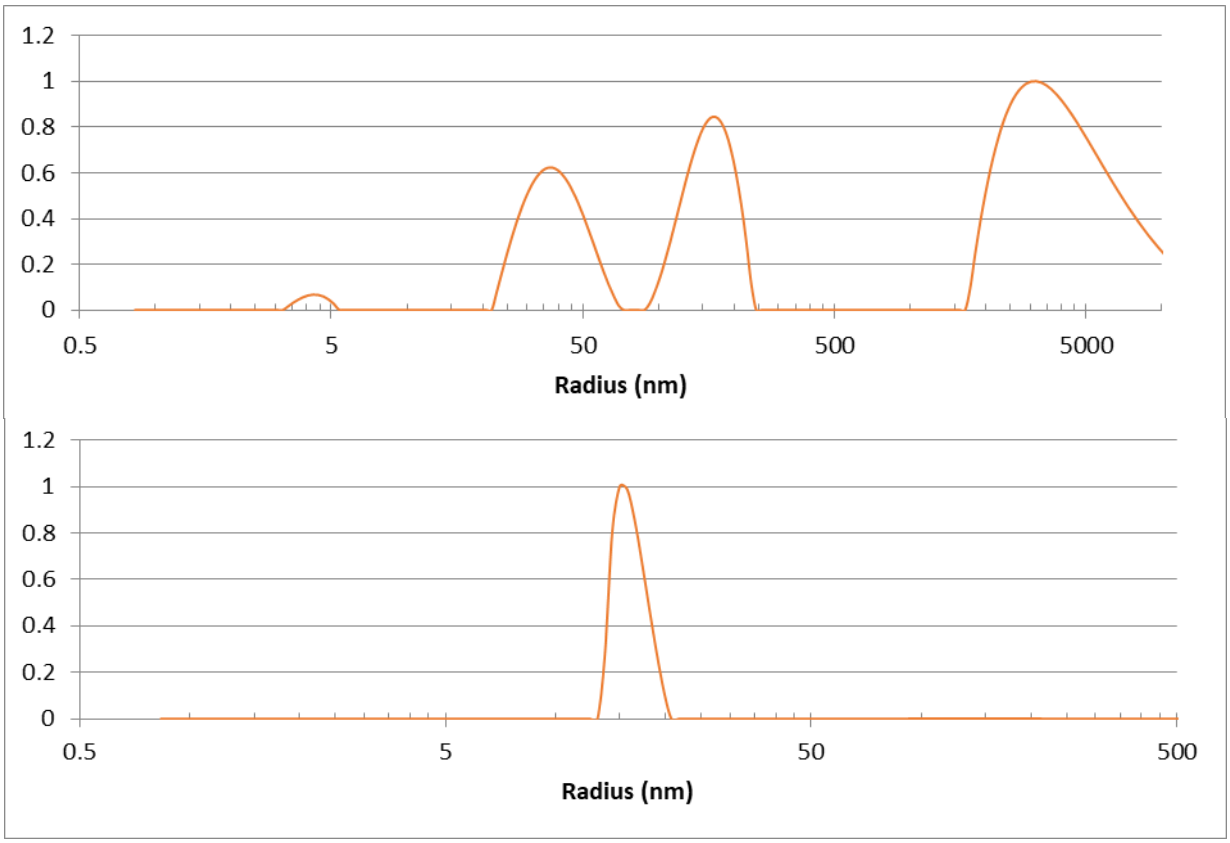


***Figure A.4*** | *Intensity-weighted (above) and number-weighted (below) size distribution for CmPhOx27:59/CmPMA50:50 self-assemblies prepared with film rehydration method using chloroform.*

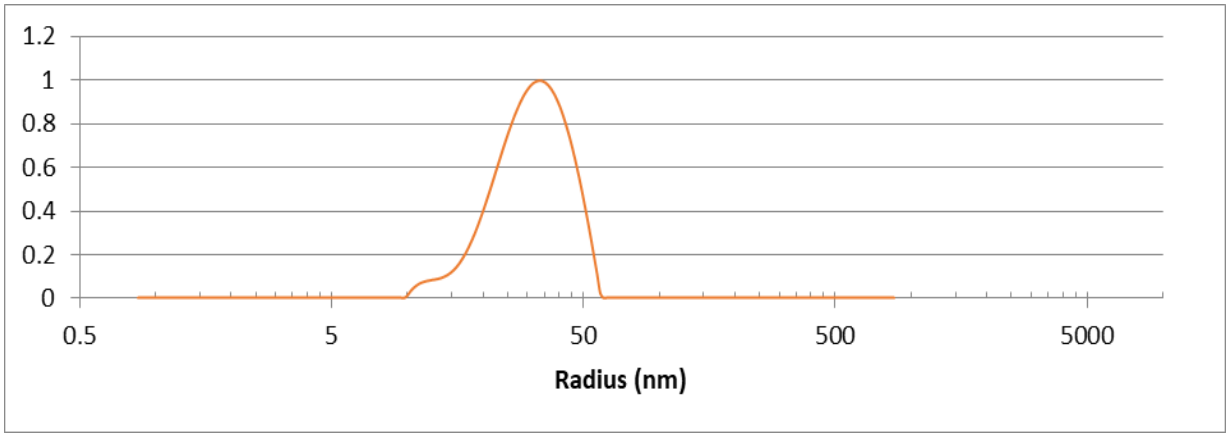


***Figure A.5*** | *Intensity-weighted size distribution for CmPhOx27:59 self-assemblies prepared with film rehydration method using chloroform.*

# Appendix B - TEM

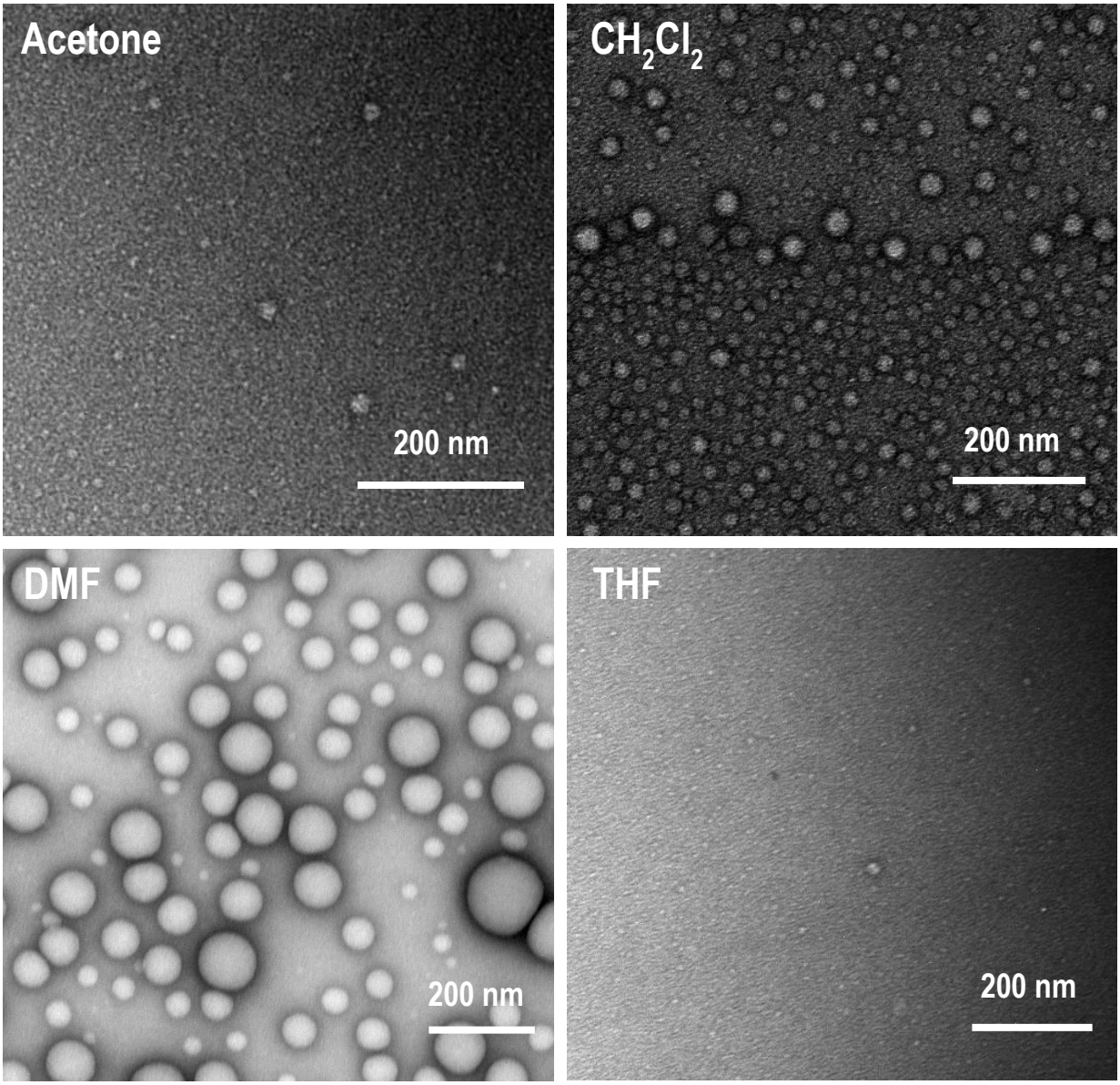


***Figure B.1*** | *TEM images of the solutions of CmPOx15/CmPMMA prepared with acetone (up left), prepared with $CH_2Cl_2$ (up right), prepared with DMF (bottom left) and prepared with THF (bottom right).*

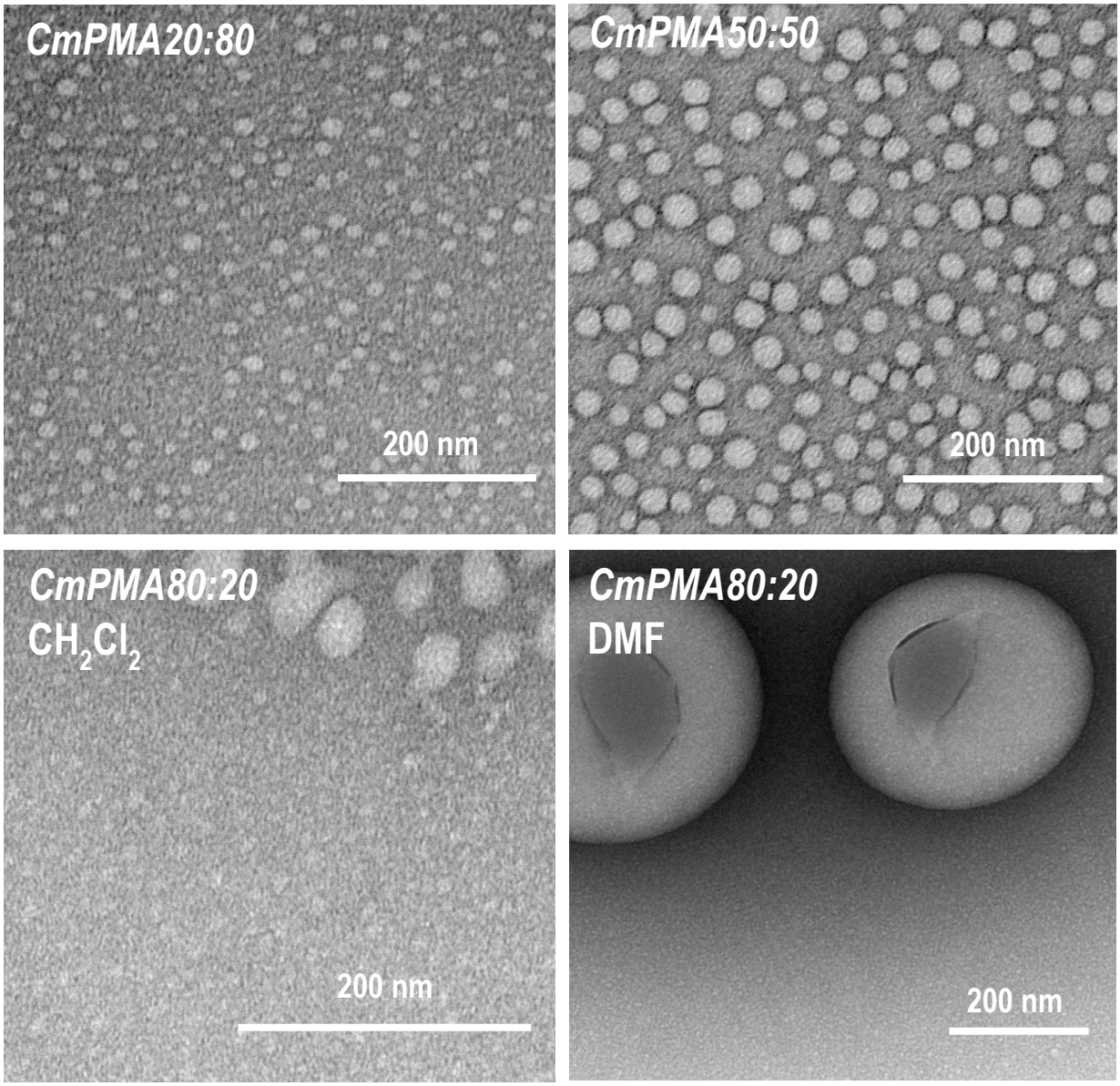


***Figure B.2*** | *TEM images of the solutions of CmPOx59/CmPMA20:80 (up left), of CmPOx59/CmPMA50:50 (up right), of CmPOx59/CmPMA80:20 prepared with $CH_2Cl_2$ (bottom left) and of CmPOx59/CmPMA80:20 prepared with DMF (bottom right).*

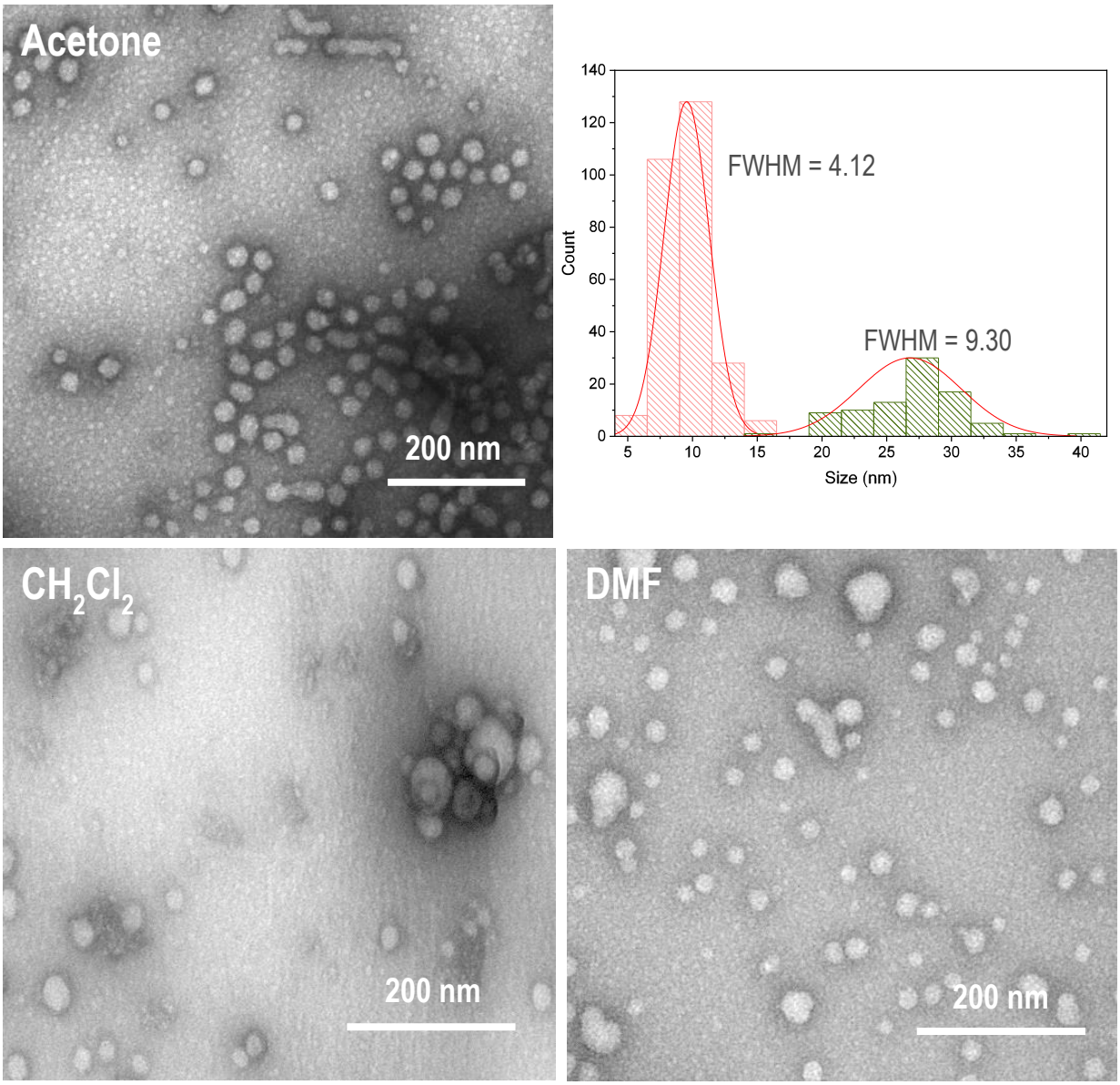


***Figure B.3*** | *TEM images of the solutions of CmPhOx27:59/CmPMMA prepared with acetone (up left), with $CH_2Cl_2$ (bottom left) and with DMF (bottom right). On the up right a typical statistical analysis of the size distribution of a solution of CmPhOx27:59/CmPMMA prepared with acetone. FWGH stands for Full Width Half Maximum.*

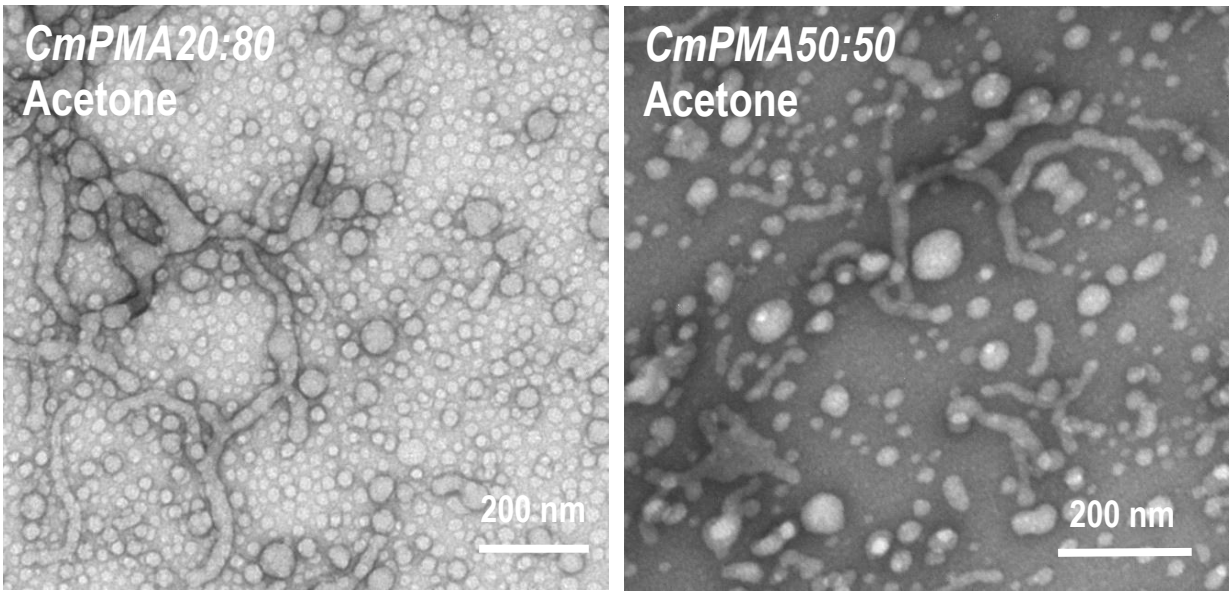


***Figure B.4*** | *TEM images of the solutions of CmPhOx27:59/CmPMA20:80 prepared with acetone (left) and of CmPhOx27:59/CmPMA50:50 prepared with acetone (right).*

# Ringraziamenti

Questa tesi non sarebbe divenuta realtà senza il contributo di tutte le persone che mi hanno supportato, spronato e sfidato in questi anni di università e in questi mesi intensi di lavoro e apprendimento.

Desidero ringraziare innanzitutto la mia relatrice professoressa Francesca Baldelli Bombelli per avermi offerto l'occasione di fare la tesi all'estero e di completarla nel suo laboratorio. Grazie per la pazienza e tutti i suggerimenti dal punto di vista scientifico e umano.

Un enorme ringraziamento alle mie co-supervisors a Tolosa, le professoresse Barbara Lonetti e Anne-Françoise Mingotaud, al direttore del laboratorio Christophe Mingotaud e al resto del team IDeAS del laboratorio IMRCP per avermi accolto così calorosamente. Grazie per avermi dato la possibilità di lavorare nel loro gruppo di ricerca e avermi guidato durante tutto il percorso dandomi nozioni e insegnamenti fondamentali per la stesura di questa tesi. E grazie per l'inestimabile supporto umano quando mi sono trovata bloccata lontana da casa durante una pandemia.

Ringrazio tutto il gruppo SupraBioNanoLab per i consigli e l'aiuto senza cui non avrei potuto completare questo periodo di ricerca come desideravo. Grazie per avermi accolto a lavorare assieme a voi.

Un immenso grazie ai miei genitori, per avermi sostenuto in ogni senso della parola in tutte le fasi della vita, soprattutto in questi ultimi anni e nei momenti di scoraggiamento. Mi avete sempre rincuorato spingendomi a non mollare e a provarci malgrado le difficoltà. Se ho raggiunto questo traguardo è gran parte merito del vostro sostegno, affetto e della vostra costante vicinanza.

Grazie a cugine e cugino, zie e zii e al resto della mia famiglia che mi sono stati vicini e mi hanno sempre spronato. Un grazie speciale ai miei nonni a cui questa tesi è dedicata.

Volevo ringraziare tutti gli amici senza i quali non sarei mai arrivata in fondo a questo percorso universitario. Marti e Vale, la mia superfamily, ho sempre meno parole per esprimere quanto vi voglio bene e quanto sono grata siate nella mia vita. Grazie mille a Sara, Marghe, Bea, Fabio, Teo, Elisa e tutti gli altri per le risate, gli attimi memorabili e anche il più piccolo consiglio che mi avete donato.

Ringrazio i miei maestri e tutti i compagni di scherma. Grazie per avermi permesso di "sfogarmi" su di voi e per avermi insegnato molto dal punto di vista sportivo e umano.

E infine grazie a me stessa, che ho fatto il resto.

# Bibliography

[1] R. L. Yanovsky, D. W. Bartenstein, G. S. Rogers, S. J. Isakoff, and S. T. Chen, "Photodynamic therapy for solid tumors: A review of the literature," *Photodermatology, Photoimmunology & Photomedicine*, vol. 35, no. 5, pp. 295-303, 2019.

[2] Y. Matoba, K. Banno, I. Kisu, and D. Aoki, "Clinical application of photodynamic diagnosis and photodynamic therapy for gynecologic malignant diseases: A review," *Photodiagnosis and Photodynamic Therapy*, vol. 24, pp. 52-57, 2018.

[3] P. Agostinis, K. Berg, K. A. Cengel, T. H. Foster, A. W. Girotti, S. O. Gollnick, S. M. Hahn, M. R. Hamblin, A. Juzeniene, D. Kessel, M. Korbelik, J. Moan, P. Mroz, D. Nowis, J. Piette, B. C. Wilson, and J. Golab, "Photodynamic therapy of cancer: An update," *CA: A Cancer Journal for Clinicians*, vol. 61, no. 4, pp. 250-281, 2011.

[4] Á Juarranz, P. Jaén, F. Sanz-Rodríguez, J. Cuevas, and S. González, "Photodynamic therapy of cancer. Basic principles and applications," *Clinical and Translational Oncology*, vol. 10, no. 3, pp. 148-154, 2008.

[5] B. M. Luby, C. D. Walsh, and G. Zheng, "Advanced Photosensitizer Activation Strategies for Smarter Photodynamic Therapy Beacons," *Angewandte Chemie International Edition*, vol. 58, no. 9, pp. 2558-2569, 2019.

[6] N. P. Brodin, C. Guha, and W. A. Tomé, "Photodynamic Therapy and Its Role in Combined Modality Anticancer Treatment," *Technology in Cancer Research & Treatment*, vol. 14, no. 4, pp. 355-368, 2015.

[7] I. S. Mfouo-Tynga, L. D. Dias, N. M. Inada, and C. Kurachi, "Features of third generation photosensitizers used in anticancer photodynamic therapy: Review," *Photodiagnosis and Photodynamic Therapy*, vol. 34, pp. 102091, 2021.

[8] J. Zhang, C. Jiang, J. P. Figueiró Longo, R. B. Azevedo, H. Zhang, and L. A. Muehlmann, "An updated overview on the development of new photosensitizers for anticancer photodynamic therapy," *Acta Pharmaceutica Sinica B*, vol. 8, no. 2, pp. 137-146, 2018.

[9] J. A. Figueira and V. C. Veltrini, "Photodynamic therapy in oral potentially malignant disorders—Critical literature review of existing protocols," *Photodiagnosis and Photodynamic Therapy*, vol. 20, pp. 125-129, 2017.

[10] S. H. Ibbotson, T. H. Wong, C. A. Morton, N. J. Collier, A. Haylett, K. E. McKenna, R. Mallipeddi, H. Moseley, L. E. Rhodes, D. C. Seukeran, K. A. Ward, M. F. M. Mustapa, and L. S. Exton, "Adverse effects of topical photodynamic therapy: a consensus review and approach to management," *British Journal of Dermatology*, vol. 180, no. 4, pp. 715-729, 2019.

[11] J. P. Celli, B. Q. Spring, I. Rizvi, C. L. Evans, K. S. Samkoe, S. Verma, B. W. Pogue, and T. Hasan, "Imaging and Photodynamic Therapy: Mechanisms, Monitoring, and Optimization," *Chemical Reviews*, vol. 110, no. 5, pp. 2795-2838, 2010.

[12] R. R. Allison and C. H. Sibata, "Oncologic photodynamic therapy photosensitizers: A clinical review," *Photodiagnosis and Photodynamic Therapy*, vol. 7, no. 2, pp. 61-75, 2010.

[13] X. Li, N. Kwon, T. Guo, Z. Liu, and J. Yoon, "Innovative Strategies for Hypoxic-Tumor Photodynamic Therapy," *Angewandte Chemie International Edition*, vol. 57, no. 36, pp. 11522-11531, 2018.

[14] L. Zhang, F. X. Gu, J. M. Chan, A. Z. Wang, R. S. Langer, and O. C. Farokhzad, "Nanoparticles in medicine: therapeutic applications and developments," *Clinical Pharmacology and Therapeutics*, vol. 83, no. 5, pp. 761-769, 2008.

[15] C. Zhang, L. Yan, X. Wang, S. Zhu, C. Chen, Z. Gu, and Y. Zhao, "Progress, challenges, and future of nanomedicine," *Nano Today*, vol. 35, pp. 101008, 2020.

[16] J. Wolfram and M. Ferrari, "Clinical cancer nanomedicine," *Nano Today*, vol. 25, pp. 85-98, 2019.

[17] S. F. Vencken and C. M. Greene, "Chapter 15 - A review of the regulatory framework for nanomedicines in the European Union," , pp. 641-679, 2018.

[18] Y. H. Choi and H. Han, "Nanomedicines: current status and future perspectives in aspect of drug delivery and pharmacokinetics," *Journal of Pharmaceutical Investigation*, vol. 48, no. 1, pp. 43-60, 2018.

[19] T. Lammers, S. Aime, W. E. Hennink, G. Storm, and F. Kiessling, "Theranostic Nanomedicine," *Accounts of Chemical Research*, vol. 44, no. 10, pp. 1029-1038, 2011.

[20] R. Zingg and M. Fischer, "The consolidation of nanomedicine," *Wiley Interdisciplinary Reviews: Nanomedicine and Nanobiotechnology*, vol. 11, pp. e1569, 2019.

[21] A. P. Dias, S. da Silva Santos, J. V. da Silva, R. Parise-Filho, E. Igne Ferreira, O. E. Seoud, and J. Giarolla, "Dendrimers in the context of nanomedicine," *International Journal of Pharmaceutics*, vol. 573, pp. 118814, 2020.

[22] M. Dionzou, A. Morère, C. Roux, B. Lonetti, J. -. Marty, C. Mingotaud, P. Joseph, D. Goudounèche, B. Payré, M. Léonetti, and A. -. Mingotaud, "Comparison of methods for the fabrication and the characterization of polymer self-assemblies: what are the important parameters?" *Soft Matter*, vol. 12, no. 7, pp. 2166-2176, 2016.

[23] D. Peer, J. M. Karp, S. Hong, O. C. Farokhzad, R. Margalit, and R. Langer, "Nanocarriers as an emerging platform for cancer therapy," *Nature Nanotechnology*, vol. 2, no. 12, pp. 751-760, 2007.

[24] E. Larrañeta and R. F. Donnelly, "Chapter 18 Bioadhesive Polymers for Drug Delivery," , pp. 559-601, 2017.

[25] N. D. Donahue, H. Acar, and S. Wilhelm, "Concepts of nanoparticle cellular uptake, intracellular trafficking, and kinetics in nanomedicine," *Advanced Drug Delivery Reviews*, vol. 143, pp. 68-96, 2019.

[26] J. Coty and C. Vauthier, "Characterization of nanomedicines: A reflection on a field under construction needed for clinical translation success," *Journal of Controlled Release*, vol. 275, pp. 254-268, 2018.

[27] C. Fornaguera and C. Solans, "Analytical Methods to Characterize and Purify Polymeric Nanoparticles," *International Journal of Polymer Science*, vol. 2018, pp. e6387826, 2018.

[28] A. A. Khorasani, J. L. Weaver, and C. Salvador-Morales, "Closing the gap: accelerating the translational process in nanomedicine by proposing standardized characterization techniques," *International Journal of Nanomedicine*, vol. 9, no. 1, pp. 5729-5751, 2014.

[29] M. Klein, M. Menta, T. G. Dacoba, J. Crecente-Campo, M. J. Alonso, D. Dupin, I. Loinaz, B. Grassl, and F. Séby, "Advanced nanomedicine characterization by DLS and AF4-UV-MALS: Application to a HIV nanovaccine," *Journal of Pharmaceutical and Biomedical Analysis*, vol. 179, pp. 113017, 2020.

[30] R. Cai and C. Chen, "The Crown and the Scepter: Roles of the Protein Corona in Nanomedicine," *Advanced Materials*, vol. 31, no. 45, pp. 1805740, 2019.

[31] X. Lu, P. Xu, H. Ding, Y. Yu, D. Huo, and Y. Ma, "Tailoring the component of protein corona via simple chemistry," *Nature Communications*, vol. 10, no. 1, pp. 1-14, 2019.

[32] L. Zeng, J. Gao, Y. Liu, J. Gao, L. Yao, X. Yang, X. Liu, B. He, L. Hu, J. Shi, M. Song, G. Qu, and G. Jiang, "Role of protein corona in the biological effect of nanomaterials: Investigating methods," *TrAC Trends in Analytical Chemistry*, vol. 118, pp. 303-314, 2019.

[33] R. Cagliani, F. Gatto, and G. Bardi, "Protein Adsorption: A Feasible Method for Nanoparticle Functionalization?" *Materials (Basel, Switzerland)*, vol. 12, no. 12, 2019.

[34] P. C. Ke, S. Lin, W. J. Parak, T. P. Davis, and F. Caruso, "A Decade of the Protein Corona," *ACS Nano*, vol. 11, no. 12, pp. 11773-11776, 2017.

[35] L. Digiacomo, D. Pozzi, S. Palchetti, A. Zingoni, and G. Caracciolo, "Impact of the protein corona on nanomaterial immune response and targeting ability," *WIREs Nanomedicine and Nanobiotechnology*, vol. 12, no. 4, pp. e1615, 2020.

[36] T. Yeo, P. N. Manghnani, E. Middha, Y. Pan, H. Chen, C. T. Lim, and B. Liu, "Mechanistic Understanding of the Biological Responses to Polymeric Nanoparticles," *ACS Nano*, vol. 14, no. 4, pp. 4509-4522, 2020.

[37] L. Böhmert, L. Voß, V. Stock, A. Braeuning, A. Lampen, and H. Sieg, "Isolation methods for particle protein corona complexes from protein-rich matrices," *Nanoscale Advances*, vol. 2, no. 2, pp. 563-582, 2020.

[38] D. Docter, U. Distler, W. Storck, J. Kuharev, D. Wünsch, A. Hahlbrock, S. K. Knauer, S. Tenzer, and R. H. Stauber, "Quantitative profiling of the protein coronas that form around nanoparticles," *Nature Protocols*, vol. 9, no. 9, pp. 2030-2044, 2014.

[39] D. D. Silvio, N. Rigby, B. Bajka, A. Mayes, A. Mackie, and F. B. Bombelli, "Technical tip: high-resolution isolation of nanoparticle–protein corona complexes from physiological fluids," *Nanoscale*, vol. 7, no. 28, pp. 11980-11990, 2015.

[40] A. Master, M. Livingston, and A. Sen Gupta, "Photodynamic nanomedicine in the treatment of solid tumors: Perspectives and challenges," *Journal of Controlled Release*, vol. 168, no. 1, pp. 88-102, 2013.

[41] K. Shanmugapriya and H. W. Kang, "Engineering pharmaceutical nanocarriers for photodynamic therapy on wound healing: Review," *Materials Science and Engineering: C*, vol. 105, pp. 110110, 2019.

[42] J. Chen, T. Fan, Z. Xie, Q. Zeng, P. Xue, T. Zheng, Y. Chen, X. Luo, and H. Zhang, "Advances in nanomaterials for photodynamic therapy applications: Status and challenges," *Biomaterials*, vol. 237, pp. 119827, 2020.

[43] S. S. Lucky, K. C. Soo, and Y. Zhang, "Nanoparticles in Photodynamic Therapy," *Chemical Reviews*, vol. 115, no. 4, pp. 1990-2042, 2015.

[44] B. Yang, Y. Chen, and J. Shi, "Reactive Oxygen Species (ROS)-Based Nanomedicine," *Chemical Reviews*, vol. 119, no. 8, pp. 4881-4985, 2019.

[45] D. Gao and P. Lo, "Polymeric micelles encapsulating pH-responsive doxorubicin prodrug and glutathione-activated zinc(II) phthalocyanine for combined chemotherapy and photodynamic therapy," *Journal of Controlled Release*, vol. 282, pp. 46-61, 2018.

[46] L. Gibot, A. Lemelle, U. Till, B. Moukarzel, A. Mingotaud, V. Pimienta, P. Saint-Aguet, M. Rols, M. Gaucher, F. Violleau, C. Chassenieux, and P. Vicendo, "Polymeric Micelles Encapsulating Photosensitizer: Structure/Photodynamic Therapy Efficiency Relation," *Biomacromolecules*, vol. 15, no. 4, pp. 1443-1455, 2014.

[47] U. Till, L. Gibot, P. Vicendo, M. Rols, M. Gaucher, F. Violleau, and A. Mingotaud, "Crosslinked polymeric self-assemblies as an efficient strategy for photodynamic therapy on a 3D cell culture," *RSC Advances*, vol. 6, no. 74, pp. 69984-69998, 2016.

[48] U. Till, L. Gibot, C. Mingotaud, P. Vicendo, M. Rols, M. Gaucher, F. Violleau, and A. Mingotaud, "Self-assembled polymeric vectors mixtures: characterization of the polymorphism and existence of synergistic effects in photodynamic therapy," *Nanotechnology*, vol. 27, no. 31, pp. 315102, 2016.

[49] K. Knop, A. Mingotaud, N. El-Akra, F. Violleau, and J. Souchard, "Monomeric pheophorbide(a)-containing poly(ethyleneglycol-b-ε-caprolactone) micelles for photodynamic therapy," *Photochemical & Photobiological Sciences*, vol. 8, no. 3, pp. 396-404, 2009.

[50] T. T. Hoang Thi, E. Pilkington, D. H. Nguyen, J. S. Lee, K. Park, and N. Truong Phuoc, "The Importance of Poly(ethylene glycol) Alternatives for Overcoming PEG Immunogenicity in Drug Delivery and Bioconjugation," *Polymers*, vol. 12, pp. 298, 2020.

[51] A. Ahmed Sebak, "Limitations of PEGylated Nanocarriers: Unfavourable Physicochemical Properties, Biodistribution Patterns and Cellular and Subcellular Fates," *International Journal of Applied Pharmaceutics*, vol. 10, 2018.

[52] A. Oudin, J. Chauvin, L. Gibot, M. Rols, S. Balor, D. Goudounèche, B. Payré, B. Lonetti, P. Vicendo, A. Mingotaud, and V. Lapinte, "Amphiphilic polymers based on polyoxazoline as relevant nanovectors for photodynamic therapy," *Journal of Materials Chemistry B*, vol. 7, no. 32, pp. 4973-4982, 2019.

[53] C. J. Martínez Rivas, M. Tarhini, W. Badri, K. Miladi, H. Greige-Gerges, Q. A. Nazari, S. A. Galindo Rodríguez, R. Á Román, H. Fessi, and A. Elaissari, "Nanoprecipitation process: From encapsulation to drug delivery," *International Journal of Pharmaceutics*, vol. 532, no. 1, pp. 66-81, 2017.

[54] L. Korchia, C. Bouilhac, V. Lapinte, C. Travelet, R. Borsali, and J. Robin, "Photodimerization as an alternative to photocrosslinking of nanoparticles: proof of concept with amphiphilic linear polyoxazoline bearing coumarin unit," *Polymer Chemistry*, vol. 6, no. 33, pp. 6029-6039, 2015.

[55] S. Emami and S. Dadashpour, "Current developments of coumarin-based anti-cancer agents in medicinal chemistry," *European Journal of Medicinal Chemistry*, vol. 102, pp. 611-630, 2015.

[56] J. Stetefeld, S. A. McKenna, and T. R. Patel, "Dynamic light scattering: a practical guide and applications in biomedical sciences," *Biophysical Reviews*, vol. 8, no. 4, pp. 409-427, 2016.

[57] S. Bhattacharjee, "DLS and zeta potential – What they are and what they are not?" *Journal of Controlled Release*, vol. 235, pp. 337-351, 2016.

[58] J. P. Patterson, M. P. Robin, C. Chassenieux, O. Colombani, and R. K. O'Reilly, "The analysis of solution self-assembled polymeric nanomaterials," *Chemical Society Reviews*, vol. 43, no. 8, pp. 2412-2425, 2014.

[59] A. G. Mailer, P. S. Clegg, and P. N. Pusey, "Particle sizing by dynamic light scattering: non-linear cumulant analysis," *Journal of Physics: Condensed Matter*, vol. 27, no. 14, pp. 145102, 2015.

[60] L. Gibot, A. Lemelle, U. Till, B. Moukarzel, A. Mingotaud, V. Pimienta, P. Saint-Aguet, M. Rols, M. Gaucher, F. Violleau, C. Chassenieux, and P. Vicendo, "Polymeric Micelles Encapsulating Photosensitizer: Structure/Photodynamic Therapy Efficiency Relation," *Biomacromolecules*, vol. 15, no. 4, pp. 1443-1455, 2014.

[61] G. H. Michler and W. Lebek, "Chapter 3 - Electron Microscopy of Polymers," , pp. 2199b-5h, 2016.

[62] J. Kuntsche, J. Horst, and H. Bunjes, "Cryogenic transmission electron microscopy (cryo-TEM) for studying the morphology of colloidal drug delivery systems," *International journal of pharmaceutics*, vol. 417, pp. 120-37, 2011.

[63] J. H. F. Bothwell and J. L. Griffin, "An introduction to biological nuclear magnetic resonance spectroscopy," *Biological Reviews*, vol. 86, no. 2, pp. 493-510, 2011.

[64] V. Mirshafiee, R. Kim, M. Mahmoudi, and M. L. Kraft, "The importance of selecting a proper biological milieu for protein corona analysis in vitro: Human plasma versus human serum," *The International Journal of Biochemistry & Cell Biology*, vol. 75, pp. 188-195, 2016.

[65] U. K. Laemmli, "Cleavage of Structural Proteins during the Assembly of the Head of Bacteriophage T4," *Nature*, vol. 227, no. 5259, pp. 680-685, 1970.

[66] C. Wang, Z. Wang, and L. Dong, "Translating Current Bioanalytical Techniques for Studying Corona Activity," *Trends in Biotechnology*, vol. 36, no. 7, pp. 661-672, 2018.

[67] L. Guerrini, R. A. Alvarez-Puebla, and N. Pazos-Perez, "Surface Modifications of Nanoparticles for Stability in Biological Fluids," *Materials (Basel, Switzerland)*, vol. 11, no. 7, 2018.

[68] S. Lazzari, D. Moscatelli, F. Codari, M. Salmona, M. Morbidelli, and L. Diomede, "Colloidal stability of polymeric nanoparticles in biological fluids," *Journal of Nanoparticle Research*, vol. 14, no. 6, pp. 1-10, 2012.

[69] T. Lorson, M. M. Lübtow, E. Wegener, M. S. Haider, S. Borova, D. Nahm, R. Jordan, M. Sokolski-Papkov, A. V. Kabanov, and R. Luxenhofer, "Poly(2-oxazoline)s based biomaterials: A comprehensive and critical update," *Biomaterials*, vol. 178, pp. 204-280, 2018.